

# UC Merced

## UC Merced Electronic Theses and Dissertations

### Title

Insights into Quantum Gravity: from Quantum Optics to Black Holes

### Permalink

<https://escholarship.org/uc/item/51k4w229>

### Author

Thompson, Johnathon James

### Publication Date

2019

Peer reviewed|Thesis/dissertation

UNIVERSITY OF CALIFORNIA, MERCED

Insights into Quantum Gravity: from Quantum Optics to Black Holes

A Dissertation submitted in partial fulfillment of the  
requirements for the degree of  
Doctor of Philosophy  
in

Physics

by

Johnathon James Thompson

August 2019

Portion of Chapter 4:

© Physical Review

All other chapters: © Johnathon James Thompson 2019

All Rights Reserved

The dissertation of Johnathon James Thompson, titled Insights into Quantum Gravity: from Quantum Optics to Black Holes, is approved, and it is acceptable in quality and form for publication.

---

(Professor Raymond Y. Chiao)   Principal Co-Adviser

---

Date

---

(Professor Jay E. Sharping)   Principal Co-Adviser

---

Date

---

(Professor Lin Tian)   Committee Chair

---

Date

---

(Professor Gerardo Muñoz)   Committee Member

---

Date

University of California, Merced  
2019

This dissertation is dedicated to my son, Johnathon Alexander Thompson, for being the reason to work so hard for a brighter future.

# Acknowledgments

I would like to thank my wife, Yesenia Thompson, for her tireless support in this endeavor, for keeping me sane, and for encouraging me to live up to the version of me that she sees.

I would like to thank my advisors Dr. Chiao and Dr. Sharping for allowing me to grow under their guidance, for being role models, and always encouraging me to do work that is important even if it may seem controversial. I would like to thank Dr. Muñoz and Dr. Singleton for enlightening discussions, for really giving me the foundation that I needed to succeed as a PhD student, and for being the referees for all of my bad ideas. I would like to acknowledge Nader Inan, Luis Martinez, Al Castelli, and Alison Huff for their help and guidance as senior graduate students when I first entered the PhD program, they helped to make things less intimidating.

This dissertation was funded in part by the University of California, Merced Physics Graduate Student Summer Fellowship 2015, 2017, and 2018, as well as the Department of Defense DSO Grant 2016-2017, the University of California Merced Fletcher Jones Fellowship from 2018-2019, and SLS GR LLC Summer 2016.

# Johnathon J. Thompson

*Address* 2222 Huntington Dr. Apt. F16, Duarte CA, 91010  
*Phone* (559) 303-7861  
*Mail* Jthompson29@ucmerced.edu  
*Linkedin* www.linkedin.com/in/johnathonthompson

## RESEARCH INTERESTS

---

Quantum Optics, Optomechanics, Quantum Computing, Gravitational Waves, Black Holes, Quantum Gravity

## EDUCATION

---

**Ph.D. Physics** 2014-Present

*University of California, Merced*

GPA: 4.0

Expected Graduation in 2019

**M.S. Physics** 2011-2014

*California State University, Fresno*

Thesis: Black Holes in Nonlinear Electrodynamics

**B.S. Physics** 2007-2011

*California State University, Fresno*

## PROFESSIONAL POSITIONS

---

**Teaching Assistant** 2014-2018

*University of California Merced*

Courses: General Physics, Discussion and Laboratory

**Teaching Associate** 2011-2014

*California State University, Fresno*

Courses: 21 Total, General Physics, Laboratory and Instructor of Record

**Senator, College of Science and Mathematics** 2009-2010

*California State University, Fresno*

Worked with other senators to make policies and decisions that affected the entire campus.

**Member, Instructionally Related Activities Committee** 2010-2011

*California State University, Fresno*

Responsible for allocating nearly one million dollars to various projects on campus.

## SKILLS

---

<i>Low-Temp Measurements</i>	Dilution Refrigerator Maintenance and Repair, 4 wire and Ring Down
<i>Machining</i>	Training on Lathe, Mill, CNC, and Soldering
<i>Software</i>	MATHEMATICA, L <sup>A</sup> T <sub>E</sub> X, MS-Office, LABVIEW, C++
<i>Additional</i>	Sputtering, PID Frequency Control

## RESEARCH EXPERIENCE

---

**Graduate Researcher** 2014-Present

*University of California Merced*

Project: Unphysical Anomalies in Spacetime

- Investigated the Information Paradox, Cauchy Problem, and Naked Singularities.
- Showed that Naked Singularities cannot form even in theory. Applied QED to resolve the Cauchy Problem.

Project: Generation and Amplification of Gravitational Waves for Military Communication.

- Helped develop formalism for modeling quantum matter-gravitational wave interactions.
- Studied the Meissner effect for gravitational waves.

Project: Generation and frequency conversion of quantum states in high Q SRF parametric oscillators.

- Devised method for calculating photon number and squeezing parameter for SRF cavities with oscillating boundaries.
- Created software and hardware for controlling the resonant frequency of SRF cavities.
- Repaired and maintained the dilution refrigerators.

**Graduate Researcher**

2012-2014

*California State University, Fresno*

Project: Nonsingular Black Holes From Nonlinear Electrodynamics.

- Used black holes coupled to nonlinear electrodynamics to study regular black holes.
- Constructed the mathematical formalism to develop the lagrangian density for matter from the metric for any black hole.
- Developed a first order QED correction to the Reissner Nordstrom black hole.
- Calculated the acceleration of test particles and equilibrium conditions.

**Research Assistant**

2008-2010

*Strongly Correlated Electron Laboratory, California State University, Fresno*

Project: Low Temperature Tests of Type II Superconductors

- Built a multiplexer for cryogenic experiments which allowed for multiple sample testing during a single run using LABVIEW.
- Worked on a susceptometer and built a calorimeter and resistivity probes for low temperature experiments.

## **PUBLICATIONS**

---

**J. Thompson**, “Dynamical Casimir Effect, Squeezing, and Parametric Processes in Cavities- a Toolkit.” (in preparation)

**J. Thompson**, G. Munoz, “Chronology Protection of Black Holes.” (In Review PRL)

Alison Huff, **J. Thompson**, J. Pate, H. Kim, R. Chiao, and J. Sharping, “A parametric oscillator for classroom demonstration or student laboratory.” (Accepted to EJP)

J. M. Pate, L. A. Martinez, **J. J. Thompson**, R. Y. Chiao, and J. E. Sharping, “Electrostatic tuning of mechanical and microwave resonances in 3D superconducting radio frequency cavities.” AIP Advances **8** 115223 (2018)

**J. Thompson**, G. Munoz, “Charged Black Hole Horizons and QED Effects” Phys. Rev. D **96** 064001 (2017)

R.Y. Chiao, J.S. Sharping, L.A. Martinez, B.S. Kang, A. Castelli, N.A. Inan, **J.J. Thompson**, “Dynamical Casimir Effect and the Possibility of Laser-like Generation of Gravitational Radiation.” JBIS **70** 10/11 (2017)

N.A. Inan, **J.J. Thompson**, R.Y. Chiao, “Interaction of Gravitational Waves with Superconductors.” Fortschr. Phys. (2016)

**J. Thompson**, U. Urbina, Faculty Advisor: P.C. Ho, “Constructing a Multiplexer (Scanner).” Proceedings on National Conference on Undergraduate Research. (2010)



## **CONFERENCES AND WORKSHOPS**

---

Advanced Propulsion Workshop, Estes Park, CO (2018) “ QED Black Holes and Electrons”

Advanced Propulsion Workshop, The Aerospace Corporation, El Segundo, CA (2017)

APS March Meeting, New Orleans, LA (2017) “Feasibility of Detecting the Dynamical Casimir Effect in High Q SRF Cavities”

Cavity Optomechanics Workshop: Fundamentals and Applications of Controlling and Measuring Nano- and Micro-mechanical Oscillators with Lasers, CLEO Conference, San Jose, CA (2017)

APS Far West, University of California Davis, Davis CA (2016) “Lack of Cauchy Horizon for QED Black Holes”

National Conference on Undergraduate Research, University of Montana, Missoula, MO (2010) “Constructing a Multiplexer”

Twenty-Fourth Annual California State University Student Research Competition, California State University, San Jose, CA (2010) “Constructing a Multiplexer”

## **FELLOWSHIPS AND AWARDS**

---

Fletcher Jones Fellowship (2018-2019)

UC Merced Summer Fellowship (2015-2018)

UC Merced Travel Grant (2016-2018)

Teaching Associate of the Year Award (2014)

Teaching Associate of the Year Award (2013)

Hands On Networking Scholarship (2010)

Undergraduate Research Award (2010)

Faculty Sponsored Student Research Award (2010)

# Abstract

Insights into Quantum Gravity: from Quantum Optics to Black Holes

by

Johnathon James Thompson

Doctor of Philosophy in Physics

University of California, Merced

Professor Lin Tian, Chair

Although this dissertation has several themes, the central question being asked is, what insights can we gain into quantum gravity without fully quantizing gravity, and whether any experiments can be done to probe the interface between quantum mechanics and general relativity. During the process of asking this question we explored quantum optics, optomechanics, gravitational waves, and black holes. We found that the dynamical Casimir effect in our superconducting radio frequency cavities will have a threshold too high for the observation of squeezed vacuum. This is true whether we assume the vacuum is composed of gravitons or photons. We found that gravitational waves do interact with quantum macroscopic states differently than for normal matter, but this does not at present lead to any observable effect. We found that in general, the unphysical anomalies in classical spacetimes are removed when quantum mechanics is applied. We showed that Cauchy horizons which lead to mass inflation, and naked singularities which lead to issues with causality, are removed if the problems are treated correctly. By correctly, we mean applying quantum mechanics when it is non negligible, and applying the quantum mechanical idea of intrinsic mass to gravitating matter.

# Contents

<b>Acknowledgments</b>	<b>v</b>
<b>Curriculum Vitae</b>	<b>vi</b>
<b>Abstract</b>	<b>ix</b>
<b>1 Introduction</b>	<b>1</b>
<b>2 Quantum Optomechanics</b>	<b>4</b>
2.1 Materials & Methods . . . . .	4
2.2 Optomechanical Hamiltonian . . . . .	6
2.3 Dynamical Casimir Effect . . . . .	7
2.3.1 Single Cavity DCE . . . . .	8
2.3.2 Double Cavity DCE . . . . .	13
2.3.3 Power Thresholds . . . . .	24
2.3.4 DCE Conclusion . . . . .	31
2.4 Quadrature Squeezing . . . . .	31
2.5 Conclusion . . . . .	34
2.6 Recent Research . . . . .	37
2.6.1 DCE with Forcing . . . . .	37
2.6.2 2 Photon Raman-DCE . . . . .	38
2.7 Our Lab Values . . . . .	40
<b>3 Gravitational Waves</b>	<b>41</b>

<b>4</b>	<b>Black Holes</b>	<b>45</b>
4.1	Black Holes and Their Problems . . . . .	46
4.1.1	The Cause of the Problems . . . . .	48
4.2	QED Blackholes . . . . .	51
4.2.1	Introduction . . . . .	51
4.2.2	QED-corrected Schwarzschild metric . . . . .	53
4.2.3	Horizons . . . . .	55
4.2.4	Surface gravity and Hawking temperature . . . . .	59
4.2.5	Black hole Evolution . . . . .	61
4.2.6	Discussion . . . . .	67
4.2.7	Conclusion . . . . .	69
4.3	Chronology Protecting Black Holes . . . . .	70
4.3.1	Introduction . . . . .	70
4.3.2	The Gravitating Mass of Coulomb Fields . . . . .	70
4.3.3	Adding Angular Momentum . . . . .	72
4.3.4	Naked Singularity Criteria . . . . .	76
4.3.5	Conclusion . . . . .	78
4.4	Application of QED To Modified Mass . . . . .	78
<b>5</b>	<b>Conclusions and Future Direction</b>	<b>90</b>
5.1	Future Direction . . . . .	91
5.1.1	Double Cavity 2 Photon Raman-DCE . . . . .	91
5.1.2	Noise from Gravitational Wave Signals . . . . .	92
5.1.3	A Comment on “Zero” Mass Black Holes . . . . .	93
<b>A</b>	<b>Lagrangian Analysis</b>	<b>94</b>
A.1	Lagrangian Validity Analysis . . . . .	94
A.1.1	Units . . . . .	95
A.1.2	The leading terms in each piece of the Lagrangian . . . . .	97
A.1.3	The inequalities . . . . .	98
A.1.4	$\mathcal{L}' \ll \mathcal{L}_{EM}$ . . . . .	98
A.1.5	$\mathcal{L}_a \ll \mathcal{L}_{EM}$ . . . . .	98

A.1.6	$\mathcal{L}_g \ll \mathcal{L}_a$	98
A.1.7	$\mathcal{L}' \ll \mathcal{L}_a$	98
<b>B</b>	<b>QED Analysis</b>	<b>100</b>
B.1	First and Second Order QED	100
	<b>Bibliography</b>	<b>110</b>
	Bibliography	110

# List of Tables

2.1	Dynamical Casimir Effect Single Cavity Thresholds . . . . .	34
2.2	Dynamical Casimir Effect Single Cavity, Our Lab Thresholds . . . . .	35
2.3	Dynamical Casimir Effect Double Cavity Thresholds . . . . .	36
2.4	Dynamical Casimir Effect Double Cavity, Our Lab Thresholds . . . . .	37

# List of Figures

2.1	Double cavity scheme for producing degenerate signal and idler photons	4
2.2	Triple cavity scheme for producing non-degenerate signal and idler photons . . . . .	5
2.3	Detection scheme for observing squeezed RF output. . . . .	5
2.4	Simplified diagram of our system as a single cavity with a membrane for one end . . . . .	6
2.5	The cavity frequencies $f_{\pm}$ vs. the detuning $f_2 - f_1$ . $f_1 = 10$ Hz and $j_0 = 2\pi \times 10^{-1}$ Hz. . . . .	14
2.6	Energy level diagrams for the double cavity in the case $\omega_d = \omega_2 - \omega_1$ .	16
2.7	Energy level diagrams for Raman effect. . . . .	18
2.8	Schematic of Reece's double cavity experiment. [21] . . . . .	19
2.9	Results from Reece's double cavity experiment. Observation of Parametric Conversion. [21] . . . . .	20
2.10	Number of photons with $\omega_1$ in the cavity vs. input power. . . . .	22
2.11	Number of photons with $\omega_2$ in the cavity vs. input power. . . . .	22
2.12	Number of phonons with $\omega_m$ in the membrane vs. input power. . . . .	23
2.13	Number of photons with $\omega_1$ leaving the cavity per second vs. input power. . . . .	23
2.14	Force acting on the membrane vs. time . . . . .	30
2.15	Oscillation of the membrane vs. time . . . . .	30
2.16	Energy level diagram for 2 photon driving DCE [28]. . . . .	39
4.1	Evolution rates and % difference in evolution rates of a $Q = 10^{-18}M$ black hole . . . . .	63

4.2	Evolution of a $150 \times 10^6 M_\odot$ black hole with $Q^2/M^2 = 0.1$ . . . . .	64
4.3	% difference in evolution rates of a $Q = M$ black hole. . . . .	65
4.4	Evolution of near extremal black holes. Notice, the difference is indistinguishable for the $20 \times 10^6 M_\odot$ and $50 \times 10^6 M_\odot$ black holes. . . . .	66
4.5	Plot of the horizons vs. $Q$ for $M_0 = 10^9 m$ and $J = 0$ . The dashed line is $r_H$ and the solid line is $r_-$ . . . . .	74
4.6	Plot of the horizons vs. $J$ for $M_0 = 10^9 m$ and $Q = 0$ . The dashed line is $r_H$ and the solid line is $r_-$ . . . . .	75
4.7	Plot of the horizons vs. $Q$ for $M_0 = 10^9 m$ and $J = 10^{18} m^2$ . The dashed line is $r_H$ and the solid line is $r_-$ . . . . .	75
4.8	Plot of $a^{*2} + \sigma^2$ vs. $Q$ for $M_0 = 10^9 m$ and $J = 0$ . . . . .	76
4.9	Plot of $a^{*2} + \sigma^2$ vs. $J$ for $M_0 = 10^9 m$ and $Q = 0$ . . . . .	77
4.10	Plot of $a^{*2} + \sigma^2$ vs. $J$ for $M_0 = 10^9 m$ and $Q = 10^9 m$ . . . . .	77
4.11	Plot of the roots of $f(r)$ in meters vs. $\frac{Q}{M_0}$ for $M_0 = 2.5 \times 10^3 M_\odot$ . . .	80
4.12	Plot of invalid regions as a $\log(r)$ vs $\sigma$ plot for a $M_0 = 2.5 \times 10^3 M_\odot$ blackhole. Here we chose $2.5 \times 10^3 M_\odot$ because at only $10^3 M_\odot$ , $r_H$ becomes invalid at $\sigma > 1$ . The regions $\mathcal{L}_g > \mathcal{L}_a$ and $\mathcal{L}' > \mathcal{L}_a$ are outside of this plot window. . . . .	81
4.13	Plot of the roots of $f(r)$ in meters vs. $\frac{Q}{M_0}$ for $M_0 = 10^6 M_\odot$ . . . . .	82
4.14	Zoomed in version of the Plot of invalid regions as a $\log(r)$ vs $\sigma$ plot for a $M_0 = 10^6 M_\odot$ black hole. Here $A = 0$ . The regions $\mathcal{L}_g > \mathcal{L}_a$ and $\mathcal{L}' > \mathcal{L}_a$ are outside of this plot window. . . . .	83
4.15	Zoomed in version of the Plot of invalid regions as a $\log(r)$ vs $\sigma$ plot for a $M_0 = 10^6 M_\odot$ black hole. The regions $\mathcal{L}_g > \mathcal{L}_a$ and $\mathcal{L}' > \mathcal{L}_a$ are outside of this plot window. . . . .	84
4.16	Zoomed in version of the Plot of invalid regions as a $\log(r)$ vs $\sigma$ plot for a $M_0 = 10^6 M_\odot$ black hole. The regions $\mathcal{L}_g > \mathcal{L}_a$ and $\mathcal{L}' > \mathcal{L}_a$ are outside of this plot window. . . . .	85
4.17	Plot of $\frac{Q}{M_g}$ vs. $\frac{Q}{M_0}$ for $M_0 = 10^4 M_\odot$ . $a = A = 0$ in Red, $A = 0$ in Blue, and $a, A \neq 0$ in Black. . . . .	87



4.18	Plot of $\frac{Q}{M_g}$ vs. $\frac{Q}{M_0}$ for $M_0 = 2.5 \times 10^3 M_\odot$ . $a = A = 0$ in Red, $A = 0$ in Blue, and $a, A \neq 0$ in Black. . . . .	87
4.19	Plot of $\frac{Q}{M_g}$ vs. $\frac{Q}{M_0}$ for $M_0 = 2.5 \times 10^3 M_\odot$ . $a = A = 0$ in Red, $A = 0$ in Blue, and $a, A \neq 0$ in Black. . . . .	88
4.20	Plot of $\frac{Q}{M_g}$ vs. $\frac{Q}{M_0}$ for $M_0 = 10^{-6} M_\odot$ . $a = A = 0$ in Red, $A = 0$ in Blue, and $a, A \neq 0$ in Black. . . . .	88
A.1	Plot of invalid regions as a $\log(r)$ vs $\sigma$ plot for a $M_0 = 10^6 M_\odot$ blackhole. Here $r_H = 2M_0$ . The region where our analysis is valid is the unshaded region. . . . .	99
B.1	Plot of $e(r)$ vs. $r$ for $a = A = 0$ in red, $A = 0$ in blue, and $a, A \neq 0$ in black, for $Q = 1m$ . . . . .	101
B.2	Plot of $e(r)$ vs. $r$ for $a = A = 0$ in red, $A = 0$ in blue, and $a, A \neq 0$ in black, for $Q = 1m$ . . . . .	102
B.3	Plot of $e(r)$ vs. $r$ for $a = A = 0$ in red, $A = 0$ in blue, and $a, A \neq 0$ in black, for $Q = 1m$ . . . . .	102
B.4	Plot of $e(r)$ vs. $r$ for $a, A \neq 0$ in black only. For $Q = 1m$ . . . . .	103
B.5	Plot of invalid regions as a $\log(r)$ vs. $\sigma$ plot for a $M = 10^2 M_\odot$ black hole. Roots of $f(r)$ solved numerically using QED. The regions $\mathcal{L}' > \mathcal{L}_{EM}$ , $\mathcal{L}_g > \mathcal{L}_a$ and $\mathcal{L}' > \mathcal{L}_a$ are outside of this plot window. . . . .	104
B.6	Plot of invalid regions as a $\log(r)$ vs. $\sigma$ plot for a $M = 10^3 M_\odot$ black hole. Roots of $f(r)$ solved numerically using QED. The regions $\mathcal{L}' > \mathcal{L}_{EM}$ , $\mathcal{L}_g > \mathcal{L}_a$ and $\mathcal{L}' > \mathcal{L}_a$ are outside of this plot window. . . . .	105
B.7	Plot of invalid regions as a $\log(r)$ vs. $\sigma$ plot for a $M = 2.5 \times 10^3 M_\odot$ black hole. Roots of $f(r)$ solved numerically using QED. The regions $\mathcal{L}' > \mathcal{L}_{EM}$ , $\mathcal{L}_g > \mathcal{L}_a$ and $\mathcal{L}' > \mathcal{L}_a$ are outside of this plot window. . . . .	106
B.8	Plot of invalid regions as a $\log(r)$ vs. $\sigma$ plot for a $M = 10^4 M_\odot$ black hole. Roots of $f(r)$ solved numerically using QED. The regions $\mathcal{L}' > \mathcal{L}_{EM}$ , $\mathcal{L}_g > \mathcal{L}_a$ and $\mathcal{L}' > \mathcal{L}_a$ are outside of this plot window. . . . .	107
B.9	Roots of $f(r)$ for a $M = 10^3 M_\odot$ black hole. . . . .	108
B.10	Roots of $f(r)$ for a $M = 10^6 M_\odot$ black hole. . . . .	108

B.11 Roots of $f(r)$ for a $M = 10^{10}M_{\odot}$ black hole. . . . .	109
---	-----

# Chapter 1

## Introduction

This dissertation is a combination of work done in both quantum optomechanics and general relativity. One of my main interests is how principles in general relativity can be applicable in the context of quantum mechanics, and how principles of quantum mechanics are applicable in the context of general relativity. While the complete merger of the two fields is not the topic of this dissertation, we do seek to gain insights into quantum gravity.

One of the most compelling thought experiments that explains why gravity must be quantized is actually based in quantum optomechanics. This was a thought experiment proposed by both Eppley and Hannah [1] and Page and Geilker [2] and goes as follows. Imagine a mechanical oscillator, for example a membrane, has been prepared in a state with minimum uncertainty in momentum. The uncertainty principle,  $\Delta p \Delta x \geq \frac{1}{2}\hbar$ , tells us that the uncertainty in the position  $x$  must therefore be large. Now imagine that we use a superposition of very high frequency classical gravitational waves to measure the position of the membrane. Using a classical GR wave instead of a laser allows for an arbitrarily precise measurement of position, because classically the gravitational wave frequency can be arbitrarily high without adding momentum to the wave. When the position is measured with an arbitrarily large degree of accuracy, this leads to an instantaneous change in the uncertainty of the momentum, violating momentum conservation. Conservation of momentum in this case seems to suggest that gravitational waves must be quantized.

Additionally, there is another good example of quantum mechanics and gravity interacting in an interesting way. General relativity says that all energy gravitates. A quantum physicist might ask, “But there are particles such as a photon with energy and no mass, do these have a gravitational interaction?” The answer to that is yes. But whether two beams of photons attract, repel, or neither depends on their orientation [3], [4]. The answer is very nonintuitive, two beams of photons going in the same direction will not repel or attract, but two beams of photons going in opposite directions will have an attraction that is four times the attraction that is expected from equating their energies to gravitating mass naively. This is because the whole stress energy momentum tensor  $T^{\mu\nu}$  matters in Einstein’s equations,  $G^{\mu\nu} = \kappa T^{\mu\nu}$ .

These types of questions that are on the border of quantum mechanics and gravity was what interested me in the Chiao-Sharping group at the University of California. The two original central problems that we were trying to solve were, “What interaction, if any, does a gravitational wave have with a superconductor?” and “If superconductors serve as mirrors to gravitational waves, can we parametrically amplify gravitons via the dynamical Casimir effect (DCE) in a superconducting radio frequency cavity by modulating one of the walls of the cavity?” Although I spent hundreds of hours working on these questions, this was primarily the work of a fellow graduate student, Nathan Inan [5], who undoubtedly spent thousands of hours working on this question. Chapter 3 is a brief summary of the main conclusions from this work.

If we were to perform a graviton dynamical Casimir effect, then surely we should be able to first perform a photon dynamical Casimir effect. Most of my independent work was on calculating thresholds for parametric processes in a cylindrical cavity system with a membrane as one end. This is the topic of Chapter 2. The dynamical Casimir effect is the creation of particles out of vacuum due to the motion of a mirror which serves as a boundary condition for the specific particles fields [6]. You will get a creation of particles whenever the mirror moves so fast that the field cannot adiabatically adapt to the motion of the mirror, creating a mismatch in the modes. Because this work yielded very high thresholds for the DCE of photons, it is expected that the graviton DCE will not be possible.

Since the calculated thresholds were high, our lab began to look at other ways of doing an experiment with gravitational waves. Professor Ray Chiao started playing with the idea of using superconducting junctions to measure and generate gravitational waves [7]. I am not so involved in his new work on this, but one of these discussions with him got me thinking about the role of quantum mechanics in general relativity. Specifically the questions of instantaneity, what is mass, and the ideas of proper time and local time. These are all inconsistencies between the two fields of study. I zeroed in on the interpretation of mass. Specifically, because in GR the effective mass of a black hole is allowed to become negative in the interior of the black hole which leads to interesting problems that will be discussed in Chapter 4. Quantum mechanics says that there is intrinsic mass, so you have some minimum energy that cannot be extracted. I saw this interpretation as a way to possibly solve one of the problems with black holes. This train of thought led to two papers where we solved two major problems facing black hole physics, namely, the Cauchy problem and the naked singularity problem. Both of these are discussed in detail in Chapter 4.

# Chapter 2

## Quantum Optomechanics

### 2.1 Materials & Methods

Most of the planned experiments in our lab utilize high Q superconducting radio frequency cavities [8], [9]. We can use both double (degenerate) and triple (non-degenerate) cavities, see Figures 2.1 and 2.2. The double cavity is used to generate the dynamical Casimir effect, and below threshold vacuum squeezing. The triple cavity is used to generate stimulated Raman and to investigate possible graviton production.

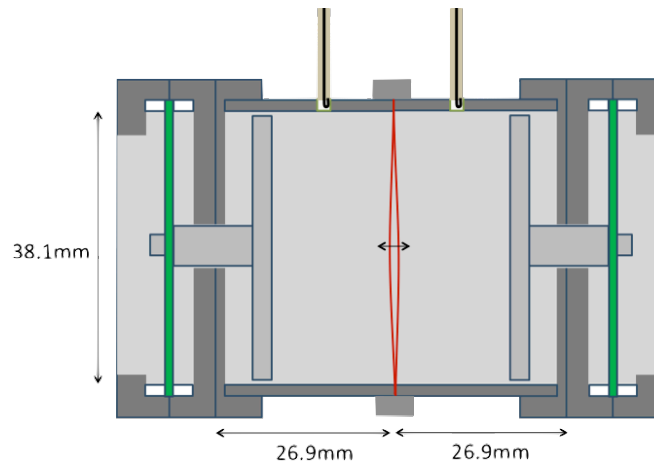


Figure 2.1: Double cavity scheme for producing degenerate signal and idler photons

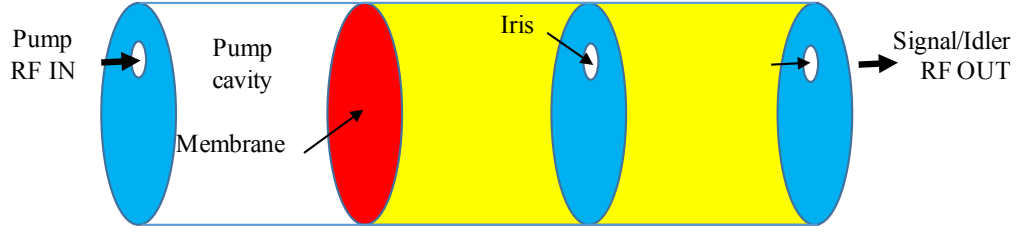


Figure 2.2: Triple cavity scheme for producing non-degenerate signal and idler photons

Figure 2.1 is shown in more detail than Figure 2.2 in order to show how we tune the frequency of the cavities. Tuning is accomplished by using PZTs (in green) to move the end wall of the cavity. To Lock frequencies, we use a PID control loop in LabView.

To decrease thermal noise and to increase the quality factors of our cavities, we put the cavities at the bottom stage of our dilution refrigerator which has a steady state cooling power of  $250 \mu\text{W}$  at 30 mK. The design of our dilution refrigerator's homodyne and heterodyne detection schemes to measure the amount of squeezing in our cavities is shown in Figure 2.3.

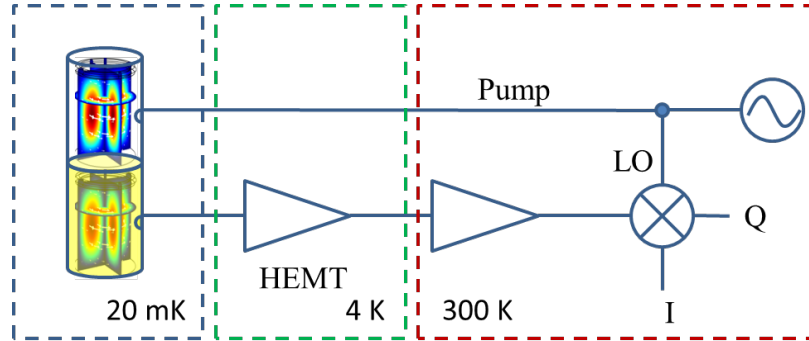


Figure 2.3: Detection scheme for observing squeezed RF output.

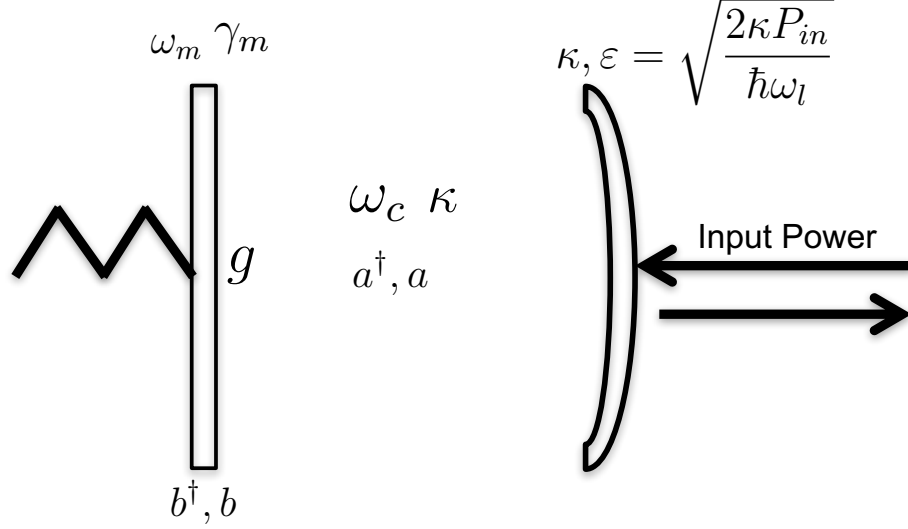


Figure 2.4: Simplified diagram of our system as a single cavity with a membrane for one end

## 2.2 Optomechanical Hamiltonian

The easiest way to study our system is to begin with the Hamiltonian. If we only concern ourselves with a single cavity with a membrane on one end, our Hamiltonian looks like,

$$H = \hbar\omega_c a^\dagger a + \hbar\omega_m b^\dagger b - \frac{1}{2}\hbar g (2a^\dagger a - a^2 - a^{\dagger 2}) (b + b^\dagger) + i\hbar\varepsilon(a^\dagger e^{-i\omega_l t} - a e^{i\omega_l t}), \quad (2.1)$$

where  $b^\dagger$  and  $b$  are the creation and annihilation operators for the membrane,  $a^\dagger$  and  $a$  are the creation and annihilation operators for the cavity,  $\omega_c$  is the cavity resonance,  $\omega_m$  is the membrane resonance,  $\omega_l$  is the frequency of the laser input,  $g$  is the coupling between the membrane and the cavity, and  $\varepsilon = \sqrt{\frac{2\kappa P_{in}}{\hbar\omega_l}}$  where  $P_{in}$  is the power of the laser and  $\kappa$  is the decay rate of the cavity. The first two terms are the bare energy of the cavity photons and membrane phonons. The third term is the phonon-photon interaction, and the last term is the power input into the cavity [10].



The coupling constant  $g = g_0 \sqrt{\frac{\hbar}{2m\omega_m}} \equiv g_0 x_{zpf}$  is related to the frequency change due to moving an element that is coupled to the cavity. For example, we can define the cavity frequency as,

$$\omega_c(x) = \omega_0 - g_0 x. \quad (2.2)$$

$g_0$  tells you how much the frequency changes when you change a boundary of the system. For a simple Fabry-Perot system, where the membrane changes the length  $L$  of the cavity,  $\omega(x) = \frac{n\pi c}{L+x} \approx \frac{n\pi c}{L} \left(1 - \frac{x}{L}\right)$ . So in the case of a Fabry-Perot system,  $g_0 = \frac{\omega_0}{L}$ . To find the dynamics of the system we use the Heisenberg equation of motion. For an operator  $A$ ,

$$\frac{dA}{dt} = \frac{i}{\hbar} [H, A]. \quad (2.3)$$

Energy loss in the membrane and cavity ( $\gamma_m, \kappa$ ) as well as the associated noise operators ( $a_{in}, \xi$ ) are added to the right hand side of the equation of motion.

$$\frac{dA}{dt} = \frac{i}{\hbar} [H, A] - \kappa A + \sqrt{2\kappa} A_{in} \quad (2.4)$$

When  $\kappa$  is introduced like this, it represents the losses of the field and not the energy, so  $\kappa = \frac{\omega}{2Q}$

## 2.3 Dynamical Casimir Effect

The surprising thing about quantum mechanics is the prediction that the pure vacuum has energy  $\frac{1}{2}\hbar\omega$  due to virtual particles coming into and out of existence. These virtual particles give rise to many interesting effects such as the dynamical Casimir effect. The dynamical Casimir effect is a dynamic version of the static Casimir effect. The static Casimir effect is a force generated by the presence of vacuum fluctuations acting on two parallel mirrors. The effect can be explained in the following intuitive manner. Vacuum fluctuations exist on the inside and outside of the mirrors. The boundary conditions of the mirrors have to be satisfied by the vacuum fluctuations and this limits the modes that exist on the inside of the mirrors. All modes of vacuum

fluctuations can exist on the outside. This difference in mode density leads to pressure on the plates.

The dynamical Casimir effect is the production of real observable photons by amplifying the vacuum fluctuations by accelerating one of the mirrors [6]. This can also be achieved by rapidly changing the effective geometry of the cavity. The DCE was first detected in 2011 using this method in a superconducting circuit [11].

We seek to achieve DCE in our cavities by parametrically amplifying the vacuum with an oscillating membrane. In our system, power is input into the pump cavity which causes the membrane to oscillate. This oscillation changes the length of the signal and idler cavity. If the oscillation is above threshold, this will create signal and idler photons. The threshold power is important, because we are limited by the  $250 \mu\text{W}$  cooling power of the dilution refrigerator.

### 2.3.1 Single Cavity DCE

The simplest dynamical Casimir effect is the amplification of a single cavity mode. For our system we will consider the signal/idler cavity. As a first step, in order to compare with accepted results in the literature [12], [13], [14], [15], we treat the membrane as a non-dynamical variable and ignore losses. We prescribe the membrane motion to be,

$$x(t) = \frac{\epsilon}{2i} (e^{i\omega_d t} - e^{-i\omega_d t}), \quad (2.5)$$

where  $\omega_d$  is the driving frequency of the membrane and  $\epsilon$  is the amplitude of oscillation of the membrane <sup>1</sup>. Using this prescribed motion, we can write the Hamiltonian of the system as,

$$H = \hbar\omega_c a^\dagger a - \frac{1}{2}\hbar g_0 (2a^\dagger a - a^2 - a^{\dagger 2}) \frac{\epsilon}{2i} (e^{i\omega_d t} - e^{-i\omega_d t}). \quad (2.6)$$

Now we go to a frame rotating at half the frequency of the drive  $R = e^{i\frac{\omega_d}{2} a^\dagger a t}$ . Since our optomechanical coupling is weak compared to the resonances of the cavity and

---

<sup>1</sup>We use  $\epsilon$  as the amplitude of oscillation. In the literature  $\epsilon$  is a dimensionless amplitude that has been scaled by the length of the cavity. The conversion is  $\epsilon' \rightarrow \epsilon L_z$  where unprimed denotes the notation used in the literature.

membrane,  $g \ll \omega_c, \omega_m$ , we may ignore non-resonant terms. We may ignore these terms because they represent only a small correction to the energy. The Hamiltonian after rotation and dropping oscillating terms becomes,

$$H = \hbar \left( \omega_c - \frac{\omega_d}{2} \right) a^\dagger a + \frac{1}{4i} \hbar g_0 \epsilon (a^2 - a^{\dagger 2}). \quad (2.7)$$

The equations of motion for  $a$  and  $a^\dagger$  are,

$$\frac{da}{dt} = -i \left( \omega_c - \frac{\omega_d}{2} \right) a + \frac{\epsilon}{2} g_0 a^\dagger, \quad (2.8)$$

and

$$\frac{da^\dagger}{dt} = i \left( \omega_c - \frac{\omega_d}{2} \right) a^\dagger + \frac{\epsilon}{2} g_0 a. \quad (2.9)$$

If we assume that the membrane is driven at twice the cavity resonance,  $\omega_d = 2\omega_c$ , then the solution to the equations of motion are,

$$a(t) = \cosh \left( \frac{\epsilon g_0 t}{2} \right) a_0 + \sinh \left( \frac{\epsilon g_0 t}{2} \right) a_0^\dagger, \quad (2.10)$$

and

$$a^\dagger(t) = \sinh \left( \frac{\epsilon g_0 t}{2} \right) a_0 + \cosh \left( \frac{\epsilon g_0 t}{2} \right) a_0^\dagger. \quad (2.11)$$

Since  $\langle N(t) \rangle = \langle 0 | a^\dagger(t) a(t) | 0 \rangle$ , then

$$N(t) = \sinh^2 \left( \frac{\epsilon g_0 t}{2} \right). \quad (2.12)$$

To find the coupling constant  $g_0$  for the cylindrical cavity we may employ the same method as we did in the Fabry-Perot case. We will be using the transverse electric (TE) modes of the cavity which have a resonant frequency defined by,

$$\omega_{mnp} = \frac{c \chi'_{mn}}{R} \sqrt{1 + \left( \frac{p\pi R}{\chi'_{mn} L} \right)^2}, \quad (2.13)$$

where  $R$  is the radius of the cavity,  $L$  is the length of the cavity,  $p$  is the longitudinal mode number, and  $\chi'_{mn}$  is the  $n$ th zero of the derivative of the  $m$ th modified Bessel function  $\mathcal{J}'_m(x)$ . We replace  $L$  with  $x + L$  and expand to first order in  $x$ .

$$\omega_{mnp}(x) = \omega_0 - \frac{p^2 c^2 \pi^2}{\omega_0 L^3} x \quad (2.14)$$

For the cylindrical cavities TE modes, driven by changing the length  $L$ , the coupling constant is,

$$g_0 = \frac{p^2 c^2 \pi^2}{\omega_0 L^3}. \quad (2.15)$$

These results agree with the calculation by Martin Crocce and others [12], [13], [14], [15], who found the dynamical Casimir effect using a different method. They do not define a coupling constant and do not include losses, and arrive at,

$$N(t) = \sinh^2 \left( \frac{p^2 c^2 \pi^2 \epsilon}{2 \omega L_z^3} t \right). \quad (2.16)$$

To solve for the threshold condition for the onset of amplification, we must include losses in the equations of motion.

$$\frac{da}{dt} = -i \left( \omega_c - \frac{\omega_d}{2} \right) a + \frac{\epsilon}{2} g_0 a^\dagger - \kappa a \quad (2.17)$$

$$\frac{da^\dagger}{dt} = i \left( \omega_c - \frac{\omega_d}{2} \right) a^\dagger + \frac{\epsilon}{2} g_0 a - \kappa a^\dagger \quad (2.18)$$

Again, we assume we are driving on resonance ( $\omega_d = 2\omega_c$ ), then,

$$a(t) = e^{-\kappa t} \left( \cosh \left( \frac{\epsilon g_0 t}{2} \right) a_0 + \sinh \left( \frac{\epsilon g_0 t}{2} \right) a_0^\dagger \right), \quad (2.19)$$

$$a^\dagger(t) = e^{-\kappa t} \left( \sinh \left( \frac{\epsilon g_0 t}{2} \right) a_0 + \cosh \left( \frac{\epsilon g_0 t}{2} \right) a_0^\dagger \right), \quad (2.20)$$

and

$$N(t) = e^{-2\kappa t} \sinh^2 \left( \frac{p^2 c^2 \pi^2 \epsilon}{2 \omega L_z^3} t \right) = -\frac{1}{2} e^{-2\kappa t} + \frac{1}{4} e^{(\epsilon g_0 - 2\kappa)t} + \frac{1}{4} e^{-(\epsilon g_0 + 2\kappa)t}. \quad (2.21)$$

In order to get an increase in photons it is clear that we must demand that  $\epsilon g_0 > 2\kappa$  or,

$$Q\epsilon g_0 > \omega_c \rightarrow \epsilon > \frac{\omega_c}{Q_c g_0}. \quad (2.22)$$

This condition is important, because it is general and applies to any cavity system where we implement a dynamic element that oscillates at twice the resonant frequency and changes the resonant frequency. In principle,  $g_0$  can be measured by experiment. This condition is powerful because for some cavity systems no analytic solution for the resonance exists. If you want to figure out if a cavity/membrane system is a good candidate to observe the DCE, you just need to measure  $g_0$ ,  $\omega_c$ , and  $Q_c$  for your system. For a Fabry-Perot system where  $g_0 = \omega_c/L$  and  $\omega_c = n\pi c/L$  we get the following threshold condition.

$$Q_c \omega_d \epsilon = Q_c v_m > 2\pi n c \quad (2.23)$$

If we use the results from a cylindrical cavity, we arrive at the following threshold condition for the amplitude of the oscillating membrane.

$$Q_c \omega_d \epsilon > \frac{2\pi c}{p^2} \left( \frac{L_z}{\mathcal{L}_{eff}} \right)^3 \gtrsim c \quad (2.24)$$

where  $\mathcal{L}_{eff} = \frac{\pi c}{\omega}$ . These amplitude thresholds compare nicely with [16], if you replace the amplitude here with the driving force required to obtain that amplitude. See Section 2.3.3 for the force required for specific membrane motion. The threshold written just in terms of the amplitude is,

$$\epsilon > \frac{\omega_c^2 L_z^3}{Q_c p^2 \pi^2 c^2}. \quad (2.25)$$

For our cavity values,  $\omega_c = 2\pi \times 10$  GHz,  $Q_c = 10^9$ ,  $L = 2.7$  cm we will need  $\epsilon > 8.75 \times 10^{-11}$  m.

### Off Resonant Excitation

Here we will look at off resonant motion exciting the cavity mode. Instead of looking at the process of one phonon becoming two photons,  $\omega_m = 2\omega_c$ , we will look at the process of  $k$  phonons becoming two photons,  $k\omega_m = 2\omega_c$  [17]. This will allow us to drive the system at a lower frequency. This is important because finding a material with a natural resonance at 20 GHz is difficult. Our membranes have a resonant frequency around 6 kHz, so this process would have to involve  $k \sim 10^6$ . This off resonant driving can be studied with Equations 2.19 and 2.20. Here we will solve for  $N(t)$  generally without using the condition  $\omega_m = 2\omega_c$ .

$$N(t) = \frac{\epsilon^2 g_0^2}{\epsilon^2 g_0^2 - (\omega_d - 2\omega_c)^2} e^{-2\kappa t} \sinh^2 \left( \frac{1}{2} \sqrt{\epsilon^2 g_0^2 - (\omega_d - 2\omega_c)^2} t \right) \quad (2.26)$$

This leads to a threshold condition for the amplitude in general of,

$$Q_c \epsilon g_0 \geq \omega_c \sqrt{1 + Q_c^2 \left( \frac{\omega_d}{\omega_c} - 2 \right)^2}, \quad (2.27)$$

and for our cylindrical cavity,

$$\epsilon \geq \frac{\omega_c^2 L^3}{Q_c \pi^2 c^2} \sqrt{1 + Q_c^2 \left( \frac{\omega_d}{\omega_c} - 2 \right)^2}. \quad (2.28)$$

If we plug in the values for the cavities in our lab, and we assume that we are driving at the 6 kHz resonance of our membrane, then this amplitude threshold expression tells us that we need the membrane to move with an amplitude of 17.5 cm. Even if we can find a material with a 10 GHz resonance, the amplitude needed would be 8.75 cm. Both of these amplitudes are larger than the length of the cavity  $L_z$ . According to the amplitude threshold expression you need your resonance to be within a line width of  $2\omega_c$  in order to have a reasonable threshold.

### 2.3.2 Double Cavity DCE

In this section we look at parametric amplification of vacuum fluctuations in a double cavity. Our setup is shown in Figure 2.2. The two cavities on the right side of Figure 2.2 are coupled together by an iris that allows the fields of each cavity to interact. The part of the Hamiltonian which describes this interaction looks like  $H_I = \hbar j_0(a_1^\dagger a_2 + a_1 a_2^\dagger)$ , where  $a_1$  and  $a_2$  represent the 2 different cavity annihilation operators.  $j_0$  is the coupling between the two cavities.  $j_0$  can be found experimentally by measuring the avoided crossing of the two cavity modes. This can be done by changing the resonance of one of the cavities. The minimum splitting in the avoided crossing will be twice the coupling constant,  $\Delta\omega_{min} = 2j_0$ . If we neglect the effect of the membrane on the system, the observed resonant frequencies can be written in terms of the bare resonance and the cavity-cavity coupling [18].

$$\omega_{\pm} = \frac{\omega_1 + \omega_2 \pm \sqrt{(\omega_1 + \omega_2)^2 - 4(\omega_1\omega_2 - j_0^2)}}{2} \quad (2.29)$$

In Figure 2.5, we plot Equation 2.29 as we change the bare resonance  $\omega_2$  to show the avoided crossing. The complete Hamiltonian for this system is,

$$H = \hbar \left( \omega_1 - \frac{\omega_d}{2} \right) a_1^\dagger a_1 + \hbar \left( \omega_2 - \frac{\omega_d}{2} \right) a_2^\dagger a_2 + \frac{1}{4i} \hbar g_0 \epsilon_0 \left( a_1^2 - a_1^{\dagger 2} \right) + \hbar j_0 (a_1^\dagger a_2 + a_1 a_2^\dagger). \quad (2.30)$$

Here we have prescribed the motion to the membrane, and we have already moved to a frame rotating at the drive frequency. In general the equations of motion are,

$$\frac{da_1}{dt} = -i \left( \omega_1 - \frac{\omega_d}{2} \right) a_1 + \frac{\epsilon_0}{2} g_0 a_1^\dagger - \kappa a_1 - i j_0 a_2, \quad (2.31)$$

$$\frac{da_1^\dagger}{dt} = i \left( \omega_1 - \frac{\omega_d}{2} \right) a_1^\dagger + \frac{\epsilon_0}{2} g_0 a_1 - \kappa a_1^\dagger + i j_0 a_2^\dagger, \quad (2.32)$$

$$\frac{da_2}{dt} = -i \left( \omega_2 - \frac{\omega_d}{2} \right) a_2 - \kappa a_2 - i j_0 a_1, \quad (2.33)$$

and

$$\frac{da_2^\dagger}{dt} = i \left( \omega_2 - \frac{\omega_d}{2} \right) a_2^\dagger - \kappa a_2^\dagger + i j_0 a_1^\dagger. \quad (2.34)$$

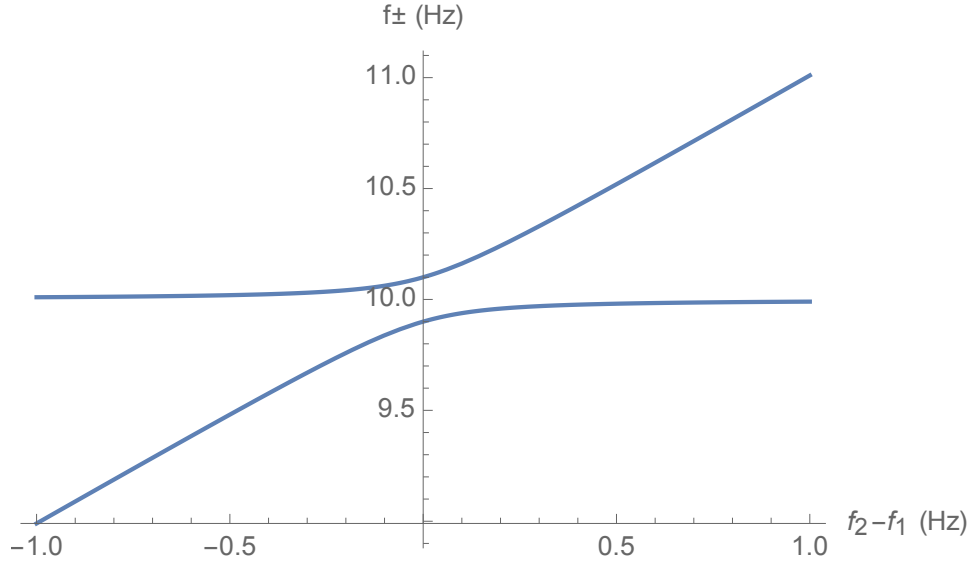


Figure 2.5: The cavity frequencies  $f_{\pm}$  vs. the detuning  $f_2 - f_1$ .  $f_1 = 10$  Hz and  $j_0 = 2\pi \times 10^{-1}$  Hz.

The double cavity setup gives us several ways to amplify vacuum fluctuations. The first and most obvious is to pump at the addition frequency of the modes,  $\omega_d = \omega_1 + \omega_2$ . In this case, one phonon becomes two coupled cavity photons, one for each cavity. For this case we substitute,  $\omega_2 \rightarrow \omega_d - \omega_1$ , and in this case, the equations of motion are,

$$\frac{da_1}{dt} = -i \left( \omega_1 - \frac{\omega_d}{2} \right) a_1 + \frac{\epsilon_0}{2} g_0 a_1^\dagger - \kappa a_1 - i j_0 a_2, \quad (2.35)$$

$$\frac{da_1^\dagger}{dt} = i \left( \omega_1 - \frac{\omega_d}{2} \right) a_1^\dagger + \frac{\epsilon_0}{2} g_0 a_1 - \kappa a_1^\dagger + i j_0 a_2^\dagger, \quad (2.36)$$

$$\frac{da_2}{dt} = -i \left( \omega_d - \omega_1 - \frac{\omega_d}{2} \right) a_2 - \kappa a_2 - i j_0 a_1, \quad (2.37)$$

and

$$\frac{da_2^\dagger}{dt} = i \left( \omega_d - \omega_1 - \frac{\omega_d}{2} \right) a_2^\dagger - \kappa a_2^\dagger + i j_0 a_1^\dagger. \quad (2.38)$$

The solution to this set of coupled equations takes up several lines, so we will not show it here. But they lead to the following amplitude threshold for amplification of



the fields  $a_1$  and  $a_2$ .

$$\epsilon \geq \frac{4j_0^2 + 4\kappa^2 + (\omega_d - 2\omega_1)^2}{g_0 \sqrt{4\kappa^2 + (\omega_d - 2\omega_1)^2}} \quad (2.39)$$

If the cavity-cavity coupling,  $j_0 \rightarrow 0$ , then we recover the amplitude threshold from the single cavity case. This tells us that the best threshold in this specific double cavity case will be when the coupling between the cavities is very small. This will put the two cavity resonances very close together. This case is not feasible experimentally because it will require  $\omega_d = \omega_m \sim 20$  GHz. The amplitude needed for amplification given in Equation 2.39, using our cavity values of  $\omega_1 = 2\pi \times 10$  GHz,  $Q_c = 10^9$ ,  $L = 2.7$  cm, and  $j_0 = 2\pi \times 1$  kHz is  $3.5 \times 10^{-8}$  m. For any given  $j_0$ , the threshold amplitude is minimized when  $\omega_d = 2\omega_1 + 2j_0$ . In principle, the coupling is determined by the iris size and there is no reason why we could not have a coupling of  $j_0 = 2\pi \times 100$  Hz. This would lead to a threshold amplitude of 2 nm.

The second way that we can excite the field in the cavity is to drive the cavity at the difference frequency of the cavities,  $\omega_d = \omega_2 - \omega_1$ . This case is a little different than your typical DCE, but it is the generation of two photons from one phonon. Figure 2.6 illustrates better what is going on. Two processes are occurring in the cavity. In the first process, the photons in cavity 2 turn into a membrane phonon and a cavity 1 photon. In the second process, a membrane phonon adds to the cavity 1 photon to produce a cavity 2 photon. Initially only the phonon state is occupied and the photons are in the vacuum state. For this case,  $\omega_2 \rightarrow \omega_d + \omega_1$ . In this case, the equations of motion are simplified to,

$$\frac{da_1}{dt} = -i \left( \omega_1 - \frac{\omega_d}{2} \right) a_1 + \frac{\epsilon_0}{2} g_0 a_1^\dagger - \kappa a_1 - i j_0 a_2, \quad (2.40)$$

$$\frac{da_1^\dagger}{dt} = i \left( \omega_1 - \frac{\omega_d}{2} \right) a_1^\dagger + \frac{\epsilon_0}{2} g_0 a_1 - \kappa a_1^\dagger + i j_0 a_2^\dagger, \quad (2.41)$$

$$\frac{da_2}{dt} = -i \left( \omega_d + \omega_1 - \frac{\omega_d}{2} \right) a_2 - \kappa a_2 - i j_0 a_1, \quad (2.42)$$

and

$$\frac{da_2^\dagger}{dt} = i \left( \omega_d + \omega_1 - \frac{\omega_d}{2} \right) a_2^\dagger - \kappa a_2^\dagger + i j_0 a_1^\dagger. \quad (2.43)$$

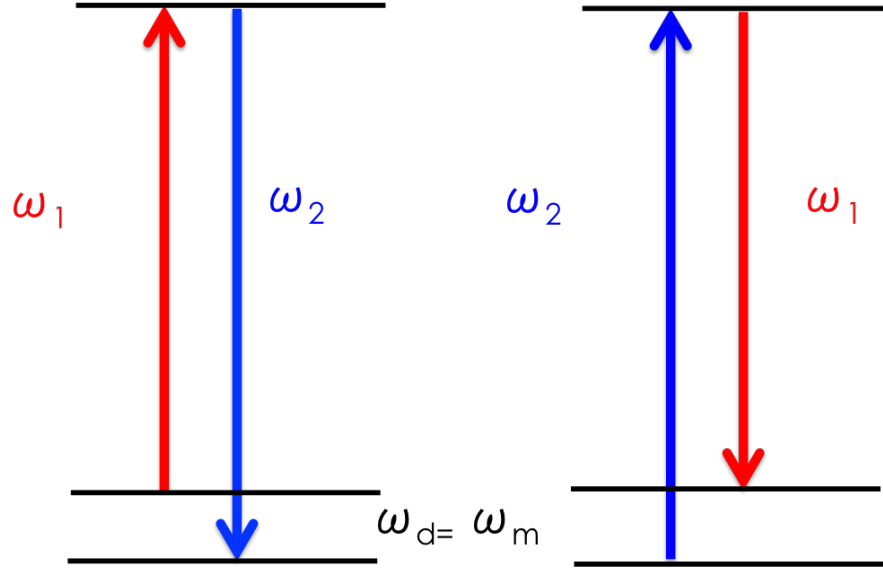


Figure 2.6: Energy level diagrams for the double cavity in the case  $\omega_d = \omega_2 - \omega_1$ .

Again, here the solution to this set of coupled equations takes up several lines and is not shown. But they lead to the following amplitude threshold for amplification of the fields  $a_1$  and  $a_2$ .

$$\epsilon^2 \geq \frac{16j_0^4 + 16\kappa^4 + 8j_0^2(4\kappa^2 - 4\omega_1^2 + 8\omega_1\omega_d - 3\omega_d^2) + (4\omega_1^2 - 8\omega_1\omega_d + 3\omega_d^2)^2}{g_0^2(4\kappa^2 + (\omega_d - 2\omega_1)^2)} + \frac{8\kappa^2(4\omega_1^2 - 8\omega_1\omega_d + 5\omega_d^2)}{g_0^2(4\kappa^2 + (\omega_d - 2\omega_1)^2)} \quad (2.44)$$

If we plug in our cavity values into this equation, with  $j_0 = 2\pi \times 3$  kHz, we get a threshold amplitude of 17.5 cm. This will never work for a cavity that is only 2.7 cm long.

We could excite the cavity modes while at the avoided crossing. The first case we will look at is the case in which we excite the cavity at the difference frequency of the cavities,  $\omega_d = \omega_+ - \omega_-$ . For this case,  $\omega_d = 2j_0$  and  $\omega_1 = \omega_2$ . In this case the

equations of motion are,

$$\frac{da_1}{dt} = -i(\omega_1 - j_0)a_1 + \frac{\epsilon_0}{2}g_0a_1^\dagger - \kappa a_1 - ij_0a_2, \quad (2.45)$$

$$\frac{da_1^\dagger}{dt} = i(\omega_1 - j_0)a_1^\dagger + \frac{\epsilon_0}{2}g_0a_1 - \kappa a_1^\dagger + ij_0a_2^\dagger, \quad (2.46)$$

$$\frac{da_2}{dt} = -i(\omega_1 - j_0)a_2 - \kappa a_2 - ij_0a_1, \quad (2.47)$$

and

$$\frac{da_2^\dagger}{dt} = i(\omega_1 - j_0)a_2^\dagger - \kappa a_2^\dagger + ij_0a_1^\dagger. \quad (2.48)$$

Again, here the solution to this set of coupled equations takes up several lines and is not shown. But they lead to the following amplitude threshold for amplification of the fields  $a_1$  and  $a_2$ .

$$\epsilon > \frac{2\sqrt{\kappa^2 + \omega_1^2}\sqrt{\kappa^2 + (\omega_1 - 2j_0)^2}}{g_0\sqrt{\kappa^2 + (\omega_1 - j_0)^2}} \quad (2.49)$$

If we use our cavity values with  $\omega_d = 2j_0 = 2\pi \times 6$  kHz, then the amplitude threshold is 17.5 cm. This is not an achievable amplitude.

Another way we could excite the modes of the cavity is to drive the system at the addition frequency,  $\omega_d = \omega_+ + \omega_-$ . We replace  $2\omega_1 = 2\omega_2 = \omega_d$ . The equations of motion are,

$$\frac{da_1}{dt} = \frac{\epsilon_0}{2}g_0a_1^\dagger - \kappa a_1 - ij_0a_2, \quad (2.50)$$

$$\frac{da_1^\dagger}{dt} = \frac{\epsilon_0}{2}g_0a_1 - \kappa a_1^\dagger + ij_0a_2^\dagger, \quad (2.51)$$

$$\frac{da_2}{dt} = -\kappa a_2 - ij_0a_1, \quad (2.52)$$

and

$$\frac{da_2^\dagger}{dt} = -\kappa a_2^\dagger + ij_0a_1^\dagger. \quad (2.53)$$

The amplitude threshold for these equations of motion is,

$$\epsilon > \frac{2j_0^2}{g_0\kappa} + \frac{2\kappa}{g_0}. \quad (2.54)$$

Notice here, if we let  $j_0 \rightarrow 0$ , we recover the single cavity threshold. This means that we need the cavities to be weakly coupled. If we plug in our cavity values with  $j_0 = 2\pi \times 3 \text{ kHz}$ , we get an amplitude threshold of  $3.1 \times 10^{-5} \text{ m}$ .

In general if you are at the avoided crossing,  $\omega_1 = \omega_2$ , then the threshold condition is,

$$\epsilon > \frac{\sqrt{16j_0^4 + 8j_0^2(4\kappa^2 - (\omega_d - 2\omega_1)^2) + (4\kappa^2 + (\omega_d - 2\omega_1)^2)^2}}{g_0\sqrt{(4\kappa^2 + (\omega_d - 2\omega_1)^2)}}. \quad (2.55)$$

In this Section, we showed that while the double cavity does give us more avenues to excite the modes, none of the small frequency driving cases had a small enough amplitude threshold to be feasible.

### A Raman-Like Process

The Raman effect is the inelastic scattering of photons due to an element or material that can vibrate. In the Raman effect, usually a higher energy photon inelastically turns into a phonon in the material and a lower energy photon [19]. See Figure 2.7 for the energy level diagram of this process. A similar type of process to the Raman

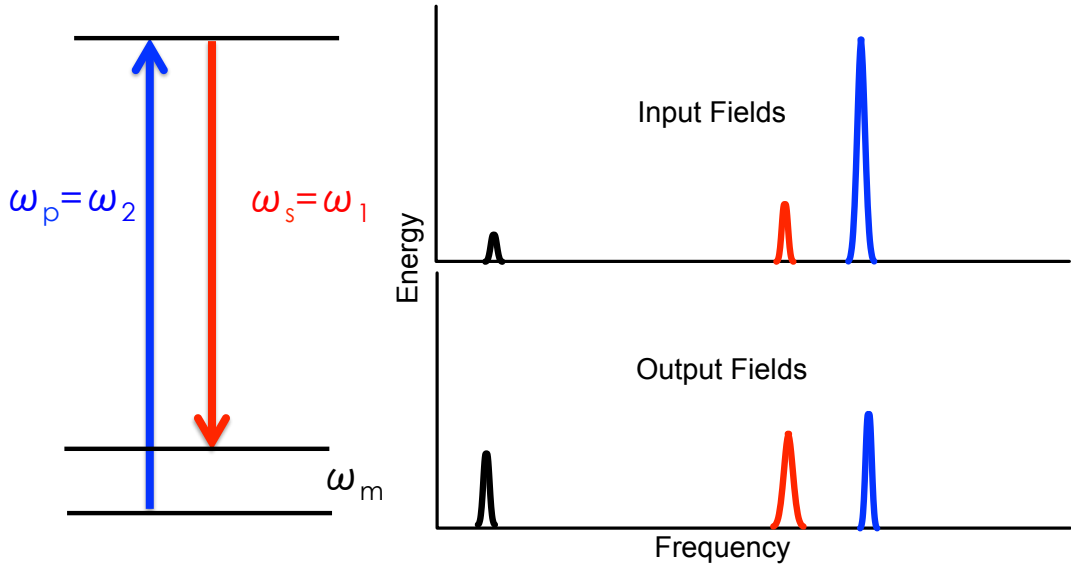


Figure 2.7: Energy level diagrams for Raman effect.

effect has already been seen in these types of cavities [20], [21]. The schematic of Reece's double cavity experiment is shown in Figure 2.8, and his main result is shown in Figure 2.9. In Reece's work, he was able to create gain in the lower resonance of this cavity setup by modulating the end wall at the splitting frequency of the cavity. The purpose of this cavity was to detect gravitational waves. In the absence of an external modulation of the end wall, gravitational waves can serve as the source of end wall modulation. The detection of a gravitational wave can be seen through the amplification of the lower resonance in this type of cavity. This result is important, because reciprocity demands that any device that can detect gravitational waves can also generate a coherent beam of gravitational radiation [22]. This is also true for LIGO, any interferometer that can extract power from a gravitational wave can also impart power into the gravitational wave, as shown in [23] and [24].

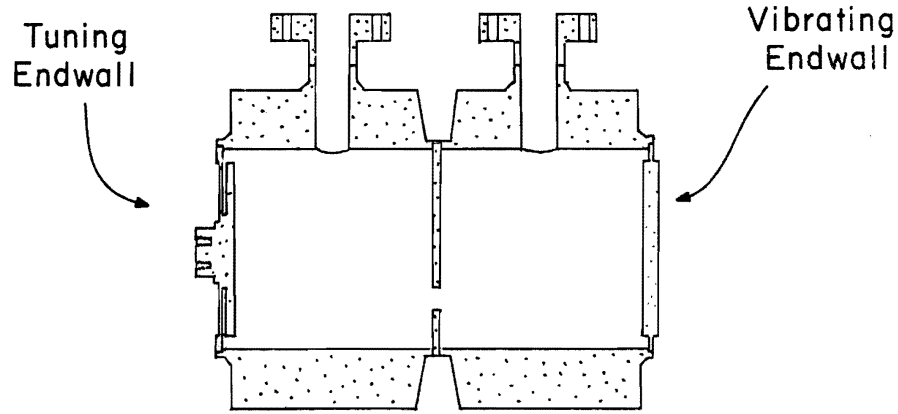


Figure 2.8: Schematic of Reece's double cavity experiment. [21]

Reece's work is a little different from what we want to do, but it is good to know that something similar can be observed in these types of cavities. What we would like to see is gain in the lower resonance by just inserting a pump at the upper frequency.

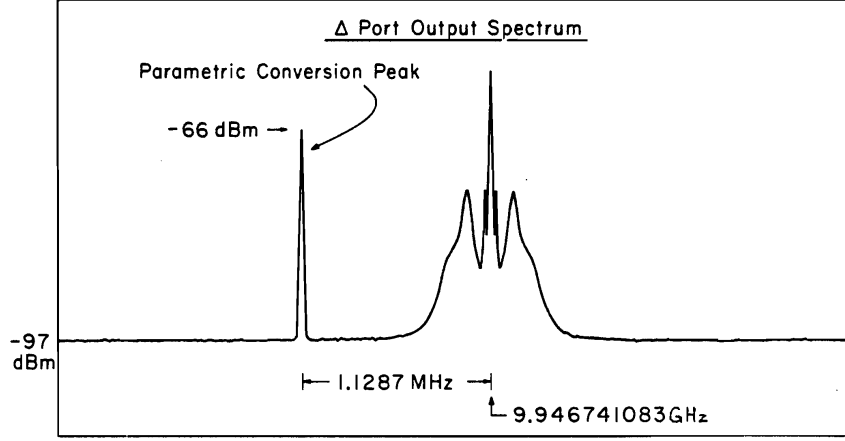


Figure 2.9: Results from Reece's double cavity experiment. Observation of Parametric Conversion. [21]

The Hamiltonian we will use to look at this process is,

$$\begin{aligned}
 H = & \hbar(\omega_1 - \omega_{in}) a_1^\dagger a_1 + \hbar(\omega_2 - \omega_{in}) a_2^\dagger a_2 + \hbar\omega_m b^\dagger b + \hbar g_0 a_1^\dagger a (b^\dagger + b) + \\
 & + \hbar j_0 (a_1^\dagger a_2 + a_1 a_2^\dagger) + \hbar \left( \Omega_1^* a_1 + \Omega_1 a_1^\dagger \right) + \hbar \left( \Omega_2^* a_2 + \Omega_2 a_2^\dagger \right).
 \end{aligned} \tag{2.56}$$

This is different from the previous Hamiltonians that we have written down. In this case, we do not prescribe the motion of the membrane. Instead, we allow the membrane motion to be a dynamic variable with  $b$  and  $b^\dagger$  the creation and annihilation operators for the membrane. We also introduce pump power terms  $\Omega_1$  and  $\Omega_2$ , which are related to the power being input into each cavity and are defined as,

$$\Omega_{1,2} = \sqrt{\frac{2P_{1,2}\kappa_{1,2}^{ex}}{\hbar\omega_{in}}}, \tag{2.57}$$

where  $P_1$  and  $P_2$  are the powers being pumped into cavity 1 and 2. Notice that we have already rotated to a frame rotating with input frequency  $\omega_{in}$ . The equations of motion are,

$$\frac{da_1}{dt} = (i(\omega_{in} - \omega_1) - \kappa_1) a_1 - ig_0 a_1 (b^\dagger + b) - ij_0 a_2 - i\Omega_1, \tag{2.58}$$

$$\frac{da_2}{dt} = (i(\omega_{in} - \omega_2) - \kappa_2) a_2 - ij_0 a_1 - i\Omega_2, \quad (2.59)$$

and

$$\frac{db}{dt} = \left(-i\omega_m - \frac{\gamma}{2}\right) b - ig_0 a_1^\dagger a. \quad (2.60)$$

where we have introduced the membrane decay rate,  $\gamma = \omega_m/Q_m$ . In the Raman effect we will set  $\Omega_2 = 0$  and  $\omega_{in} = \omega_2 = \omega_1 + \omega_m$ . This simplifies our equations of motion to,

$$\frac{da_1}{dt} = (i\omega_m - \kappa_1) a_1 - ig_0 a_1 (b^\dagger + b) - ij_0 a_2 - i\Omega_1, \quad (2.61)$$

$$\frac{da_2}{dt} = -\kappa_2 a_2 - ij_0 a_1, \quad (2.62)$$

and

$$\frac{db}{dt} = \left(-i\omega_m - \frac{\gamma}{2}\right) b - ig_0 a_1^\dagger a. \quad (2.63)$$

The steady state values for  $a_1$ ,  $a_2$ , and  $b$  are,

$$a_{1s} = \frac{i(j_0 a_{2s} + \Omega_1)}{i(\omega_m - g_0(b_s^\dagger + b_s)) - \kappa_1}, \quad (2.64)$$

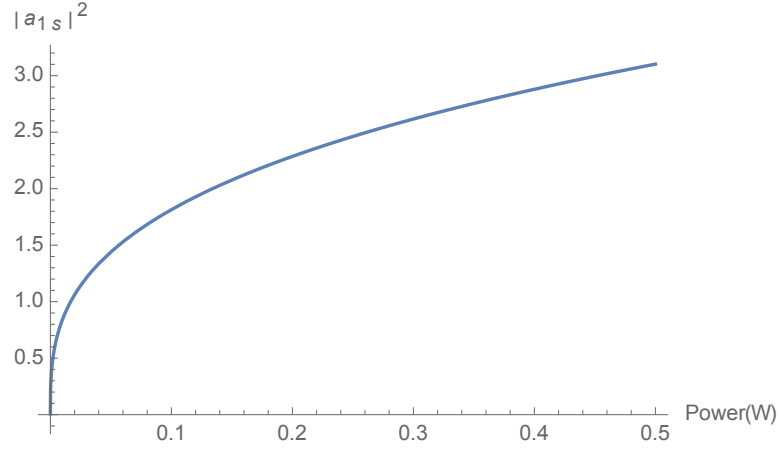
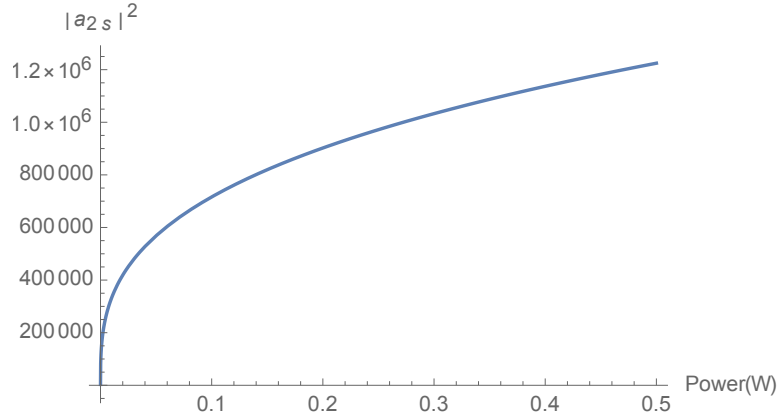
$$a_{2s} = \frac{-ij_0 a_{1s}}{\kappa_2}, \quad (2.65)$$

and

$$b_s = \frac{-ig_0 a_{1s}^\dagger a_{1s}}{i\omega_m + \frac{\gamma}{2}}. \quad (2.66)$$

These nonlinear coupled equations can be examined graphically. Figures 2.10, 2.11, and 2.12 are the total number of photons or phonons in the cavity modes and membrane, given our cavity values.

Figure 2.11 is not surprising because we are inserting photons at that cavity frequency,  $\omega_2$ . Figure 2.12 is interesting because even at  $250 \mu\text{W}$ , we have  $7 \times 10^{12}$  phonons in the membrane which is larger than the number of thermal phonons,  $n_{th} = \frac{1}{e^{\frac{\hbar\omega_m}{k_B T}} - 1}$ , at 50 mK, which is  $10^5$ . Figure 2.10 shows that we can excite the cavity resonance  $\omega_1$  at reasonable input power. As a simple estimation, the total number of

Figure 2.10: Number of photons with  $\omega_1$  in the cavity vs. input power.Figure 2.11: Number of photons with  $\omega_2$  in the cavity vs. input power.

photons leaving the cavity per second is  $N_{1_{out}} = 2\kappa_1 |a_1|^2$  which is shown in Figure 2.13. Figure 2.13 shows that at  $250 \mu\text{W}$ , we can expect 15 photons per second. Since the thermal noise associated with the cavity photons at 50 mK is very low,  $< 1$  photon every 100 s, we must look at the other noise and loss contributions to the output signal. The cables coming from the cavity and into the HEMPT amplifier will have 6 dB of loss. This corresponds to about a 75% loss in the number of photons per second. We have installed NbTi superconducting SMA cables in the line to the HEMPT amplifier. This installation was done in order to measure vacuum squeezing.



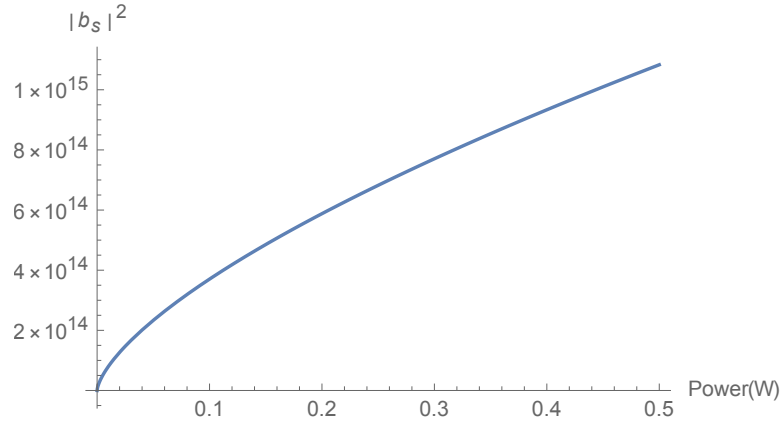


Figure 2.12: Number of phonons with  $\omega_m$  in the membrane vs. input power.

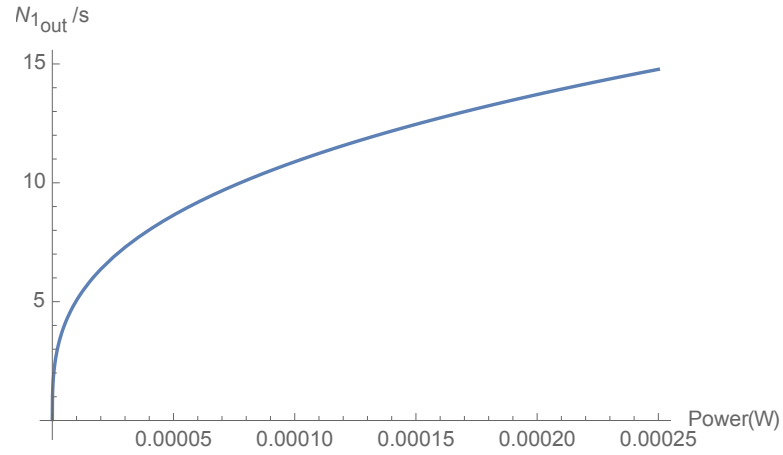


Figure 2.13: Number of photons with  $\omega_1$  leaving the cavity per second vs. input power.

This will reduce the losses to 0.5 dB. This will correspond to about a 10% loss in the number of photons per second. So in principle, we should be able to measure the photon flux coming out of the cavity.

### 2.3.3 Power Thresholds

According to the amplitude threshold calculations, our best case scenario, would be to look at the dynamical Casimir effect in the single cavity system. In this section, we calculate the amount of power we will need to get the membrane to move with the threshold amplitude.

#### The Preliminary Power Threshold from our Proposals

To solve for the full  $N(t)$  with losses and power input driving the membrane, we should allow  $\epsilon$  to be time dependent since the energy in the pump cavity which drives the motion of the membrane is not a constant. However for a calculation of the threshold power, we only need to assume that  $\epsilon$  has reached saturation. The value that we get for the power threshold, the minimum power input into the pump cavity that we need for the onset of DCE, will depend on what assumptions we make about the pump cavity and the membrane.

For example, if we assume (as was done in the cavity proposals),

i) that the cavity energy and membrane energy are equivalent, and that they decay with the cavity's quality factor  $Q_c$ ,

then we see that,

$$\frac{dE(t)}{dt} = P_{in} - \frac{\omega_c}{Q_c} E(t) \quad (2.67)$$

This assumption relies on the membrane being locked to the fields when being driven far off resonance, which is the case here ( $\omega_m \ll \omega_c$ ). Using Equation 2.67,  $P_{in} = \frac{\omega_c}{Q_c} E(t)$  at threshold. Now we plug in the minimum energy needed in the membrane found by using the threshold condition 2.24, to arrive at,

$$P_{thresh} = \frac{\omega}{Q} \frac{1}{2} m \left( \frac{2\pi c}{Q p^2} \left( \frac{L_z}{\mathcal{L}_{eff}} \right)^3 \right)^2. \quad (2.68)$$

Notice that the threshold scales as  $1/Q^3$ . This leads to a power threshold for our cavities of around  $100 \mu\text{W}$  which is great, but assumption i) is not valid and Equation

2.67 is not correct. The correct equation should read,

$$\frac{dE_c(t)}{dt} = P_{in} - \frac{\omega_c}{Q_c} E_c(t) - \frac{\omega_m}{Q_m} E_m(t) - \hbar \omega_c \frac{dN(t)}{dt}. \quad (2.69)$$

Near threshold, you can neglect the term  $\frac{dN(t)}{dt}$ , but  $Q_c \neq Q_m$  and  $\omega_c \neq \omega_m$ . We do not end up with Equation 2.67. We could allow the membrane motion to be a dynamical variable and use the Hamiltonian to calculate the equations of motion, but instead, we assume that the pump power is large enough that we can effectively view the pump cavity classically.

### Force Required for Membrane Motion

We can effectively model the equation of motion of the membrane as a damped driven harmonic oscillator.

$$\ddot{x} + \frac{\omega_m}{Q_m} \dot{x} + \omega_m^2 x = \frac{F_z}{m} \sin(2\omega_c t) \quad (2.70)$$

Here we have distinguished the membrane quality factor and resonant frequency as  $Q_m$  and  $\omega_m$ .  $Q_c$  and  $\omega_c$  represent the cavity. While Equation 2.70 is classical, we get the same result in the Heisenberg picture because the equation of motion is linear in  $x(t)$ . This means that we can carry the classical solutions over formally to quantum, except for the interpretation of  $x(t)$  as an operator and not a number. The solution to Equation 2.70 is,

$$x(t) = \frac{F_z}{m\omega_m (4\omega_c^2\omega_m^2 + Q_m^2 (\omega_m^2 - 4\omega_c^2)^2)} \times \quad (2.71)$$

$$\times [Q_m^2 \omega_m (\omega_m^2 - 4\omega_c^2) \sin(2\omega_c t) - 2Q_m \omega_c \omega_m^2 \cos(2\omega_c t)] + \propto e^{-t}$$

The first part is the steady state solution that we are concerned with, the additional piece that is proportional to  $e^{-t}$  we may neglect because we are looking for steady state amplitude. We can take three separate limits of this equation to simplify. First, for  $\omega_c \gg \omega_m$ , and only concerning ourselves with the steady state motion, we see that,

$$x(t) = \frac{F_z}{4m\omega_c^2} \sin(2\omega_c t). \quad (2.72)$$

This shows that the amplitude of oscillation of the membrane is given as,

$$\epsilon = \frac{F_z}{4m\omega_c^2}. \quad (2.73)$$

Notice that this amplitude does not depend on any other characteristics of the membrane except for the mass. This is because we are driving far above resonance.

If we instead drive at a frequency well below the mechanical resonance,  $\omega_m \gg \omega_c$ , we see that the steady state amplitude is given approximately by,

$$\epsilon = \frac{F_z}{m\omega_m^2}. \quad (2.74)$$

This amplitude does depend on the membrane resonance, but it does not depend on the quality factor of the membrane.

If we are on resonance  $\omega_m = 2\omega_c$ , the steady state solution becomes

$$x(t) = -\frac{F_z Q_m}{4m\omega_c^2} \cos(2\omega_c t), \quad (2.75)$$

with

$$\epsilon = \frac{F_z Q_m}{4m\omega_c^2}. \quad (2.76)$$

Notice that on resonance, the quality factor of the membrane matters and enhances the motion.

The force acting on the membrane is given by,

$$F_z = \int T_{zz} n_z dS, \quad (2.77)$$

where  $T_{zz}$  is the  $zz$  component of the Maxwell stress tensor,

$$T_{ij} =: \left[ \epsilon_0 E_i E_j + \frac{1}{\mu_0} B_i B_j - \frac{1}{2} \left( \epsilon_0 E^2 + \frac{1}{\mu_0} B^2 \right) \delta_{ij} \right] : . \quad (2.78)$$

The only non zero component of the  $TE_{011}$  mode at the end wall boundary is the magnetic field component  $B_\rho$  which is,

$$B_\rho = \frac{B_0 \pi R}{L \chi'_{01}} J'_0 \left( \frac{\chi'_{01} \rho}{R} \right) \cos \left( \frac{\pi z}{L} \right) e^{-i\omega_c t}. \quad (2.79)$$

$B_\rho$  will depend on the input power and  $Q_c$ . In equilibrium,  $P_{in} = P_{loss}$  so that the energy in the cavity is given by  $U = \frac{P_{in} Q_c}{\omega_c}$ .  $U$ , the total energy, can be calculated by integrating the energy density,  $u$ , or  $U = \int u dV$ . For electromagnetism,  $u = \frac{1}{2} \left( \epsilon_0 E^2 + \frac{B^2}{\mu_0} \right)$ . Within the volume of the cavity, the nonzero components of the  $TE_{011}$  mode are  $E_\phi$ ,  $B_z$ , and  $B_\rho$ . The energy density is then,

$$u = \frac{1}{2} \left[ \epsilon_0 \frac{B_0^2 \omega_c^2 R^2}{\chi_{01}'^2} J_0'^2 \left( \frac{\chi'_{01} \rho}{R} \right) \sin^2 \left( \frac{\pi z}{L} \right) \right] + \frac{1}{2} \left[ \frac{B_0^2}{\mu_0} \left( \frac{\pi^2 R^2}{L^2 \chi_{01}'^2} J_0'^2 \left( \frac{\chi'_{01} \rho}{R} \right) \cos^2 \left( \frac{\pi z}{L} \right) + J_0'^2 \left( \frac{\chi'_{01} \rho}{R} \right) \sin^2 \left( \frac{\pi z}{L} \right) \right) \right]. \quad (2.80)$$

Now we must integrate,

$$U = \int_0^L \int_0^{2\pi} \int_0^R u \rho d\rho d\phi dz. \quad (2.81)$$

After integration and some simplification we get,

$$U = \frac{1}{8} B_0^2 L R^2 J_0'^2 (\chi'_{01}) \left[ \frac{1}{\mu_0} \left( 1 + \frac{\pi^2 R^2}{L^2 \chi_{01}'^2} \right) + \frac{\epsilon_0 \omega_c^2 R^2}{\chi_{01}'^2} \right]. \quad (2.82)$$

Using  $U = \frac{P_{in} Q_c}{\omega_c}$  we can solve for  $B_0$ .

$$B_0^2 = \frac{P_{in} Q_c}{\omega_c} \frac{8}{L R^2 J_0'^2 (\chi'_{01}) \left[ \frac{1}{\mu_0} \left( 1 + \frac{\pi^2 R^2}{L^2 \chi_{01}'^2} \right) + \frac{\epsilon_0 \omega_c^2 R^2}{\chi_{01}'^2} \right]} \quad (2.83)$$

Now Equation 2.77 becomes,

$$F_z = \int \frac{\pi}{\mu_0} B_\rho^2 \rho d\rho. \quad (2.84)$$

We substitute 2.83 and 2.79 in 2.84 and after integration we have,

$$F_z = \frac{P_{in} Q_c}{\omega_c} \frac{4\pi^3 R^2}{L^3 \chi_{01}'^2 \mu_0 \left[ \frac{1}{\mu_0} \left( 1 + \frac{\pi^2 R^2}{L^2 \chi_{01}'^2} \right) + \frac{\epsilon_0 \omega_c^2 R^2}{\chi_{01}'^2} \right]}. \quad (2.85)$$

This can be simplified to,

$$F_z = \frac{2\pi^3 c^2 P_{in} Q_c}{\omega_c^3 L^3}, \quad (2.86)$$

which is the force acting on the membrane.

### The Corrected Power Threshold

We may rewrite the threshold condition for parametric amplification as,

$$\epsilon \geq \frac{L^3 \omega_c^2}{\pi^2 c^2 Q}. \quad (2.87)$$

Using Equations 2.87, 2.73, and 2.86 we can solve for the threshold power required for parametric amplification,

$$\frac{F_z}{4m\omega_c^2} \geq \frac{L^3 \omega_c^2}{\pi^2 c^2 Q_c}, \quad (2.88)$$

or

$$P_{in} \geq \frac{2mL^6 \omega_c^7}{Q_c^2 c^4 \pi^5}. \quad (2.89)$$

Plugging in the following values,  $\omega_c = 2\pi \times 10$  GHz,  $Q_c = 10^9$ ,  $L = 2.7$  cm, and  $m = 3 \times 10^{-6}$  kg we get a threshold power of,

$$P_{threshold} = 1.4 \times 10^6 \text{ W} \quad (2.90)$$

This is too much power for the dilution refrigerator. Now if we use the on resonance situation,  $\omega_m = \omega_d$ , then,

$$\frac{Q_m F_z}{4m\omega_c^2} \geq \frac{L^3 \omega_c^2}{\pi^2 c^2 Q_c}, \quad (2.91)$$

and we arrive at,

$$P_{in} \geq \frac{2mL^6 \omega_c^7}{Q_m Q_c^2 c^4 \pi^5} \quad (2.92)$$

Except for a factor of  $\pi$ , this is exactly Equation 2.68, but one of our  $Q$ 's here is the quality factor of the membrane. Notice though, that this is for the case when the membrane is resonant with the cavity. Because we are not resonant with the cavity, we lose a factor of  $Q_m$  in the threshold. Or, we end up with,

$$P_{in} \geq \frac{2mL^6\omega_c^7}{Q_c^2c^4\pi^5} \propto 1/Q^2. \quad (2.93)$$

We must work below  $250 \mu\text{W}$ ; if we plug this into Equations 2.86 and 2.73 we see that the force acting on the membrane will be  $4.6 \times 10^{-4} \text{ N}$  and the amplitude of oscillation will be  $\approx 10^{-20} \text{ m}$ . This is troublesome because according to Equation 2.87, we need  $10^{-11} \text{ m}$  of oscillation. Even more troublesome, zero point fluctuations  $\sqrt{\frac{\hbar}{2m\omega_m}}$  are on the order of  $10^{-17} \text{ m}$  for a 6 kHz oscillator. This means that we would need hundreds of milliwatts just to get above the zero point fluctuations.

Finally, while we did not begin with an assumption of slaved motion, we can show that the motion is in fact slaved, or locked to the field. By slavery here, we mean that the quality factor of the driving field determines the measured quality factor of the membrane. We will refer to this as  $Q$  Locking. We assume that the fields and therefore the force acting on the membrane decays with the quality factor of the cavity. As depicted in Figure 2.14, the input power is turned off after  $t = 500 \text{ s}$ . If we put this force profile into Equation 2.70 and plot the resulting motion, we get Figure 2.15. Notice, that the motion of the membrane decays with the  $Q$  of the cavity,  $Q_c$  and not  $Q_m$ . So it may be true that you can replace  $Q_m$  with  $Q_c$  in some cases, but this is not the case for us however. Here we are dealing with energy losses, and the measured quality factor here has no real meaning. Instead the measurement would just be a bad experimental technique. To accurately measure the quality factor of an oscillator, you must drive the oscillator with a force that has a lower quality factor than the membrane or  $Q_d \ll Q_m$ .

This consideration of  $Q$  locking has no effect on the steady state amplitude of the membrane because, as shown in Equation 2.73, the amplitude does not depend on  $Q_m$  in the limit  $\omega_m \ll \omega_c$ .

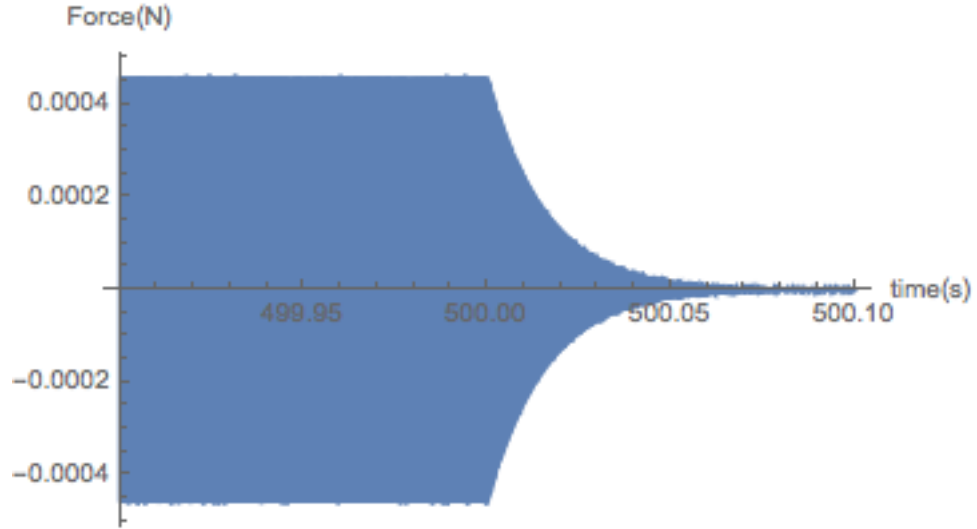


Figure 2.14: Force acting on the membrane vs. time

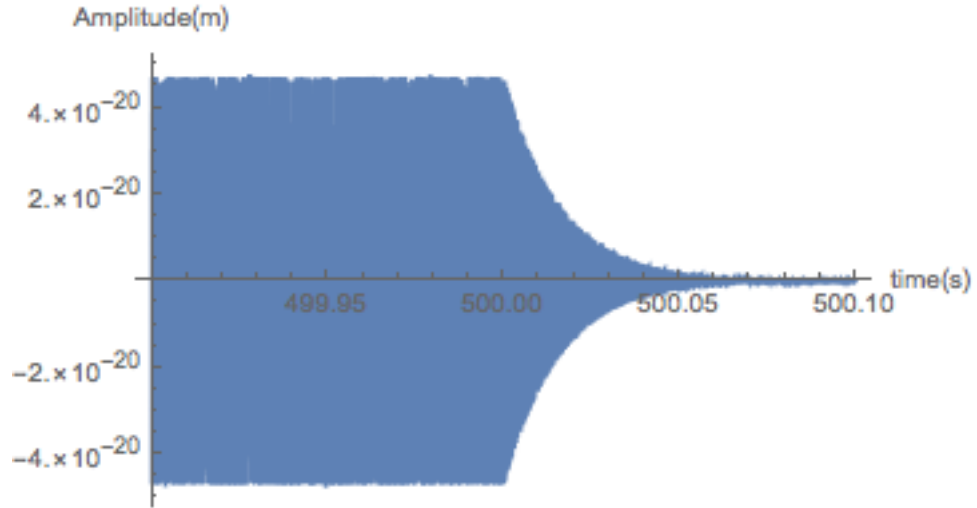


Figure 2.15: Oscillation of the membrane vs. time

### 2.3.4 DCE Conclusion

If we want to achieve the dynamical Casimir effect in our cavity we will need to replace our membrane with an element with a resonance that is much closer to  $2\omega_c$ . This result suggests that we must replace the mechanical motion of the membrane with



for instance, the electronic motion of cooper pairs in Josephson junctions. This is the essence of the work done by [11], where they observed the DCE in a superconducting circuit. Electronic motions can achieve a much higher frequency, so it is an easier way to meet the resonance conditions of the DCE.

## 2.4 Quadrature Squeezing

An interesting result of quantum mechanics is that it predicts that the level of uncertainty in the measurements of an observable are related to the uncertainty in the measurements of other non commuting observables. For example, in general if you have two observables  $A$  and  $B$ , then their uncertainties will be related by,

$$\langle(\Delta A)^2\rangle\langle(\Delta B)^2\rangle \geq \frac{1}{4}|\langle[A, B]\rangle|^2. \quad (2.94)$$

To give an example, we look at the uncertainties in position and momentum measurements. Plugging  $x$  and  $p_x$  into Equation 2.94, we get,

$$\langle(\Delta x)^2\rangle\langle(\Delta P_x)^2\rangle \geq \frac{1}{4}\hbar^2. \quad (2.95)$$

This shows that the more precise our measurement of  $x$ , the more imprecise our knowledge of  $p_x$  must be. If we replace the  $\geq$  with  $=$  then the observed state is said to be in a minimum uncertainty state.

Squeezing in general is achieved when you decrease the uncertainty in a specific measurement and increase the uncertainty in its conjugate variable. This allows, for example a measurement of  $x$  to a precision  $\Delta x < \frac{1}{\sqrt{2}}\hbar$ . These types of precision measurements are useful for example in interferometry experiments such as LIGO, where the uncertainty in position limits your ability to precisely measure the movement caused by a gravitational wave.

It is well known that the output of a parametric amplifier becomes squeezed when it is pumped just below threshold. Here, we show the theoretical maximum squeezing in such a device, and the theoretical maximum we should be able to achieve in our proposed setup. In this section, we follow the notation of Yurke [25] and Yuen [26].

We assume that the parametric amplifier transforms the modes according to the Bogoliubov transformation,

$$b = \mu a + \nu a^\dagger, \quad (2.96)$$

where  $a$  and  $a^\dagger$  are the annihilation and creation operators of the original state. With this transformation it is easy to see that the number of photons in the cavity is,

$$\langle N \rangle = \langle 0 | b^\dagger b | 0 \rangle = |\nu|^2. \quad (2.97)$$

Because the commutation relation,  $[b, b^\dagger] = 1$  implies that  $|\mu|^2 - |\nu|^2 = 1$ , knowing  $\langle N \rangle$  allows you to specify both  $\mu$  and  $\nu$ . The quadratures for which we will measure squeezing are defined as,

$$X_1 = b + b^\dagger, \quad (2.98)$$

and

$$X_2 = ib - ib^\dagger, \quad (2.99)$$

and obey the uncertainty relation,  $\Delta X_1 \Delta X_2 \geq 1$ . In the minimum uncertainty coherent state,  $\Delta X_1 = \Delta X_2 = 1$ . Using  $(\Delta X)^2 = \langle X^2 \rangle - \langle X \rangle^2$ , we can calculate the amount of squeezing we can obtain. Since the quadratures are linear in  $a$  and  $a^\dagger$ ,  $\langle X \rangle = 0$ , so we only need to determine  $\langle X^2 \rangle$ .

$$\langle X_1^2 \rangle = \langle 0 | X_1^2 | 0 \rangle = 1 + 2|\nu|^2 + 2|\nu|\sqrt{|\nu|^2 + 1} \quad (2.100)$$

$$\langle X_2^2 \rangle = \langle 0 | X_2^2 | 0 \rangle = 1 + 2|\nu|^2 - 2|\nu|\sqrt{|\nu|^2 + 1} \quad (2.101)$$

These equations show that squeezing is maximized when  $\nu$  is large. If we are below threshold then the maximum value of  $\nu$  is  $< 1$ . This determines our maximum amount of squeezing that can be obtained from any parametric amplifier system. For  $\nu = 1$ , Eq 2.101 gives,  $(\Delta X_2)^2 = 0.17$  or equivalently 7.7 dB of squeezing from the coherent value of 1.

If we can write an input output relationship for the fields of a device in the form 2.96, then we can immediately determine the squeezing. With no losses, the

transformation has the form shown in Eq 2.10.

$$b = \cosh(p^2 c^2 \pi^2 \epsilon t / 2\omega L_z^3) a + \sinh(p^2 c^2 \pi^2 \epsilon t / 2\omega L_z^3) a^\dagger \quad (2.102)$$

Since we are dealing with very small time scales,  $\tau = Q/\omega = 8$  ms, Eq 2.102 is a very good approximation. We include losses due to the quality factor  $Q$ , by limiting the amount of time that the input signal interacts with the cavity to  $\tau$ . Or equivalently,

$$\nu = \sinh(p^2 c^2 \pi^2 \epsilon \tau / 2\omega L_z^3). \quad (2.103)$$

Eq 2.103 can be simplified by using the threshold condition in Eq 2.24 to simplify Eq 2.103 to,

$$\nu = \sinh\left(\frac{\omega \tau}{2Q}\right) = \sinh(1/2). \quad (2.104)$$

Plugging this into Eq 2.101 we find that,

$$(\Delta X_2)^2 = 0.367. \quad (2.105)$$

This corresponds to a squeezing power of 4.3 dB from the unsqueezed value of 1. This predicted squeezing power is on par with other experiments of this type. For the best reported squeezing, see [27].

Because we were not able to achieve reasonable thresholds, we were not able to perform any squeezing experiments.

## 2.5 Conclusion

We were able to show that the dynamical Casimir effect is not feasible in either the single or double cavity at our maximum steady state power limit of  $250 \mu\text{W}$ . The result of the dynamical Casimir effect thresholds are shown in the Tables below. Because the dynamical Casimir effect was not feasible, the quadrature squeezing near threshold is also not feasible. We were able to show that Raman like effects are possible in the double cavity setup even at  $250 \mu\text{W}$ .

There are two ways that the dynamical Casimir effect in our cavities can become plausible. We can either find a mechanical element that has a mechanical resonance in the 10 GHz range, or we can look for a cavity structure that has a better optomechanical coupling  $g_0$ . The Tables below will serve as a good guide to select the right material and cavity structure in future experiments.

Single Cavity	
Case	Threshold Amplitude
General	$\epsilon > \frac{\omega_c}{Q_c g_0} \sqrt{1 + Q_c^2 \left( \frac{\omega_d}{\omega_c} - 2 \right)^2}$
$\omega_d = 2\omega_c$	$\epsilon > \frac{\omega_c}{Q_c g_0}$

Table 2.1: Dynamical Casimir Effect Single Cavity Thresholds

Single Cavity		
Case	Extra Conditions	Our Value $\epsilon(m)$
General	$\omega_d = \omega_m$	0.175
$\omega_d = 2\omega_c$	none	$8.75 \times 10^{-11}$

Table 2.2: Dynamical Casimir Effect Single Cavity, Our Lab Thresholds

Double Cavity	
Case	Threshold Amplitude
$\omega_d = \omega_1 + \omega_2$	$\epsilon \geq \frac{4j_0^2 + 4\kappa^2 + (\omega_d - 2\omega_1)^2}{g_0 \sqrt{4\kappa^2 + (\omega_d - 2\omega_1)^2}}$
$\omega_d = \omega_2 - \omega_1$	$\epsilon^2 \geq \frac{16j_0^4 + 16\kappa^4 + 8j_0^2(4\kappa^2 - 4\omega_1^2 + 8\omega_1\omega_d - 3\omega_d^2) + (4\omega_1^2 - 8\omega_1\omega_d + 3\omega_d^2)^2}{g_0^2(4\kappa^2 + (\omega_d - 2\omega_1)^2)} +$ $+ \frac{8\kappa^2(4\omega_1^2 - 8\omega_1\omega_d + 5\omega_d^2)}{g_0^2(4\kappa^2 + (\omega_d - 2\omega_1)^2)}$
$\omega_d = \omega_+ + \omega_-$ , $\omega_1 = \omega_2$ , $2\omega_1 = 2\omega_2 = \omega_d$	$\epsilon > \frac{2j_0^2}{g_0\kappa} + \frac{2\kappa}{g_0}$
$\omega_d = \omega_+ - \omega_-$ , $\omega_1 = \omega_2$ , $\omega_d = 2j_0$	$\epsilon > \frac{2\sqrt{\kappa^2 + \omega_1^2}\sqrt{\kappa^2 + (\omega_1 - 2j_0)^2}}{g_0\sqrt{\kappa^2 + (\omega_1 - j_0)^2}}$
$\omega_1 = \omega_2$ , General	$\epsilon > \frac{\sqrt{16j_0^4 + 8j_0^2(4\kappa^2 - (\omega_d - 2\omega_1)^2) + (4\kappa^2 + (\omega_d - 2\omega_1)^2)^2}}{g_0\sqrt{4\kappa^2 + (\omega_d - 2\omega_1)^2}}$

Table 2.3: Dynamical Casimir Effect Double Cavity Thresholds

Double Cavity		
Case	Extra Conditions	Our Value $\epsilon(m)$
$\omega_d = \omega_1 + \omega_2$	$\omega_d = 20 \text{ GHz}, j_0 = 20 \text{ } 0\pi \text{ Hz}$	$2 \times 10^{-9}$
$\omega_d = \omega_2 - \omega_1$	$\omega_d = \omega_m = 2j_0$	0.175
$\omega_d = \omega_+ + \omega_-$ , $\omega_1 = \omega_2$ , $2\omega_1 = 2\omega_2 = \omega_d$	$2j_0 = \omega_m$	$3 \times 10^{-5}$
$\omega_d = \omega_+ - \omega_-$ , $\omega_1 = \omega_2$ , $\omega_d = 2j_0$	$2j_0 = \omega_m$	0.175

Table 2.4: Dynamical Casimir Effect Double Cavity, Our Lab Thresholds

## 2.6 Recent Research

In this section, we will look at two recent papers that claim to show feasibility of detecting the dynamical Casimir effect.

### 2.6.1 DCE with Forcing

In May of this year (2019), Butera and Carusotto published a paper where they looked at the dynamical Casimir effect for a single cavity in the formalism of optomechanics [16]. In their paper, they treat the membrane motion as a dynamic degree of freedom.

This is different from our approach in which we prescribed the motion. They add a generic driving force,  $F(t) \sim F_0 e^{-i\omega_d t}$ , that drives the membranes' motion. If the driving is strong enough, it is equivalent to prescribing the motion. Their threshold force was found to be,

$$F_0^{th} = \frac{2\omega_c \omega_m}{8Q_m Q_c g_0 x_{zpf}}. \quad (2.106)$$

If the driving is on resonance with the membrane, then we can show that this threshold is equivalent to our  $\omega_d = \omega_m = 2\omega_c$  DCE case. In Section 2.3.3 we calculated the force required to move the membrane for different resonance conditions and we can use this to relate this paper's findings with ours. Using Equation 2.76 we see that the relationship between their threshold and ours can be found using,

$$F_0 = \epsilon \frac{4m x_{zpf} \omega_c^2}{2\hbar Q_m}. \quad (2.107)$$

Solving for  $\epsilon$  using Equation 2.106 and 2.107 will give  $\epsilon = \omega_c / g_0 Q_c$  which is exactly our threshold condition. This confirms equivalence between the prescribed motion method and the forcing method of analysis. They go on to analyze back reaction effects of the DCE field on the membrane and conclude that these effects will be very small and most likely not detectable. Their next course of action is very interesting, they intend to use a similar formalism to look at the back reaction of Hawking radiation on the horizon of a black hole, specifically during the late stages of evaporation. This will be very important work that should give us very valuable insights into quantum gravity.

### 2.6.2 2 Photon Raman-DCE

In a preprint paper (February 2019) Qin et. al. look at a novel way of approaching the dynamical Casimir effect [28]. Their approach is different from the typical approach of just driving a membrane. They drive the membrane with a forcing function, but they also implement a detuned 2 photon driving of the cavity. The energy level diagram that is provided in the paper is shown in Figure 2.16.

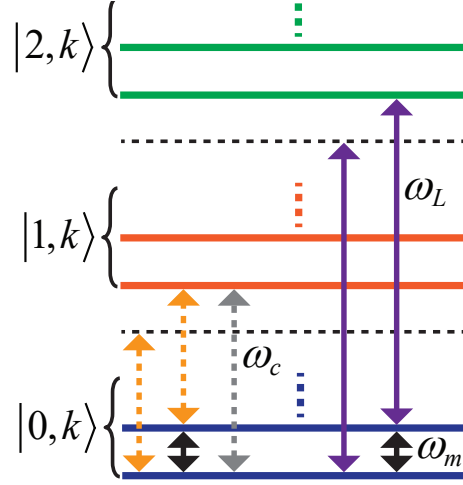


Figure 2.16: Energy level diagram for 2 photon driving DCE [28].

As can be seen from Figure 2.16, the process they are proposing is one where a photon and a phonon become two photons. The resonance condition is  $2\omega_c = \omega_l + \omega_m$ , where  $\omega_l$  is the driving frequency. This has all of the characteristics of the dynamical Casimir effect without (in my opinion) actually being the dynamical Casimir effect. There is a moving membrane whose phonons get converted into photons. There is a production of correlated photon pairs. But this is still different from the actual DCE where 1 phonon become 2 photons. This is really just a 2 photon Raman effect, they even say this in the paper. They state, “The process can be interpreted, in the laboratory frame, as two-photon hyper-Raman scattering.” The real reason why this is not the real DCE is because in the real DCE there is the possibility of creating other particles from vacuum and not just photons, i.e. gravitons, neutrinos, and other massless as well as massive particles. That was the premise of our graviton laser proposal. This two photon Raman DCE has no possibility of creating gravitons.



## 2.7 Our Lab Values

Symbol	Meaning	Definition	Value
$m$	Membrane mass		$3 \times 10^{-6} \text{ kg}$
$L$	Cavity length		$27 \times 10^{-3} \text{ m}$
$\omega_m/2\pi$	Mechanical resonance frequency		$6 \times 10^3 \text{ Hz}$
$\omega_L$	Microwave/laser input frequency		
$\omega_c/2\pi$	Cavity resonance frequency		$10 \times 10^9 \text{ Hz}$
$x_{\text{zpf}}$	Zero-point fluctuations	$x_{\text{zpf}} = \sqrt{\frac{\hbar}{2m_{\text{eff}}\Omega_m}}$	$2.1 \times 10^{-17} \text{ m}$
$\gamma_m/2\pi$	Mechanical decay rate	$\gamma_m = \frac{\omega_M}{Q_M}$	$1 \text{ Hz}$
$\kappa/2\pi$	Cavity decay rate	$\kappa = \frac{\omega_c}{2Q_c}$	$5 \text{ Hz}$
$Q$	Quality Factor		$Q_c = 10^9$
$g_0/2\pi$	Frequency-pull parameter	$g_0 = \frac{d\omega_c}{dL} = \frac{p^2 c^2 \pi^2}{\omega_0 L^3}$	$2 \times 10^{10} \frac{\text{Hz}}{\text{m}}$
$g/2\pi$	Optomechanical coupling	$g = g_0 x_{\text{zpf}}$	$3.8 \times 10^{-7} \text{ Hz}$

## Chapter 3

# Gravitational Waves

Gravitational waves (GR) are time dependent solutions to the Einstein equations. Einstein's equations predict that a gravitational wave will be emitted from a mass density undergoing quadrupolar motion. Until recently, only indirect evidence for GR waves, such as the energy loss in the Hulse-Taylor binary star system has been known [29]. The recent measurement by LIGO of GR waves from a double black hole collision has provided the first direct evidence of their existence [30]. Our lab worked on a project that aimed to generate and detect GR waves using a different method.

The project relied on a superconducting triple cavity parametric amplifier, see Figure 2.2. In order to detect the presence of GR waves, a pump depletion method is employed. A moving membrane creates gravitons and photons from the vacuum. Pump depletion while on resonance with the GR wave cavity modes is a direct result of the production of GR waves.

If superconductors are mirrors for gravitational waves, then we may use our high Q SRF cavities to produce DCE gravitons in the same manner that we seek to produce DCE photons. In this section, we show the formalism that can be used to show whether it is possible for superconductors to reflect gravitational waves.

In particular, we will describe a mechanism which quantifies how gravitational waves interact with superconductors. In addition, we investigate a “charge separation effect,” also dubbed the “Heisenberg-Coulomb effect,” which was first proposed in [31], and later referenced in [32]. This effect is a result of the Cooper pairs being

condensed into a quantum mechanical zero-momentum eigenstate and therefore, by the Heisenberg uncertainty principle, being *non-local*. Hence they cannot follow any classical trajectories in the presence of a gravitational wave.

In contrast to this, each ion in its lattice site can respond *locally* to the gravitational wave, and thereby the ionic lattice can oscillate in its deformation accordingly. It is found that the zero-point energy of the phonon modes of the lattice dominates the response of the lattice to the wave. The *difference* in motion of the Cooper pairs (negatively charged), and the lattice ions (positively charged) results in the charge separation effect. According to [31], this creates an electric field which opposes the supercurrents induced by the gravitational wave. The resulting Coulomb force acts as a very strong restoring force that makes the superconductor extremely “stiff” to gravitational waves. The mass supercurrents produced by this effect will radiate gravitationally. Therefore, the incoming gravitational wave will be re-radiated back out, and the superconductor will act as a mirror to gravitational waves.

Quantum mechanically, the “charge separation effect,” provides a mechanism for energy transfer from the gravitational wave to the superconductor. This may allow us to interpret quantum mechanically an absorption and emittance of gravitons by the superconductor. Of course, this type of description would require quantized gravity, which currently has not been formulated. Quantizing gravity is a daunting undertaking which we do not seek to explore here.

In a paper published last year [33], we showed that using a description of gravity using the free energy densities of the Cooper pairs and the ionic lattice, one finds that the ionic lattice and Cooper pairs indeed follow slightly different trajectories in the presence of a gravitational wave. The following is a short outline of the important results.

It is well established in General Relativity, that gravitational waves can be described by the metric perturbation,  $h_{ij}^{TT}$ , in the transverse-traceless (TT) gauge. This gauge eliminates unphysical degrees of freedom from the metric leaving only the “plus” and “cross” polarization wave fields,  $h_{\oplus}$  and  $h_{\otimes}$ , respectively [34]. However, the TT gauge can only describe plane-waves *in vacuum*. It does not provide a description of gravitational waves *in matter*.

Therefore, we begin with a metric which is constructed in accordance with the Helmholtz decomposition theorem [35]. This formulation is gauge invariant (to linear order in the metric) and isolates the radiative degrees of freedom which are characterized by the transverse-traceless part of the metric perturbation,  $h_{ij}^{\tau\tau}$ . Such a formulation is well suited for describing the interaction of gravitational waves with quantum matter such as a superconductor.

We use two constituent equations, one for the material strain  $T_{ij}^{\tau\tau} = -su_{ij}^{\tau\tau}$ , which describes how a material responds to a stress, where  $s$  is the *material* shear modulus, and  $u_{ij}^{\tau\tau}$  is the dimensionless strain tensor of the material. The other is for the gravitational strain  $T_{ij}^{\tau\tau} = -\mu_G h_{ij}^{\tau\tau}$ ; it describes the stress produced in a material due to a gravitational wave and is referred to as the gravitational constituent equation [36]. Combining these two equations allows us to determine how the material responds to a gravitational wave given a specific gravitational shear modulus  $\mu_G$ .

$$u_{ij}^{\tau\tau} = \frac{\mu_G}{s} h_{ij}^{\tau\tau} \quad (3.1)$$

$\mu_G$  is determined by the gravitational constituent equation where  $T^{ij}$  can be found using the free energy density  $\mathcal{F}$ , and the following relation,

$$T^{ij} = \left( \frac{\partial \mathcal{F}}{\partial h_{ij}} \right)_T. \quad (3.2)$$

This equation comes from the Helmholtz free energy density with stresses and strains present  $d\mathcal{F} = -\mathbb{S}dT + T^{ij}dh_{ij}$ , where  $\mathbb{S}$  is the entropy density.

We may use the Debye Model for the ionic lattice and the Ginsburg-Landau theory for the Cooper pair density. Using these theories, we find that the gravitational shear modulus of each is,

$$\mu_{G(CP)} = \frac{e^2 n_s}{m_e} (A^i)^2 + \alpha n_s + \frac{\beta}{2} n_s^2 \quad (3.3)$$

and

$$\mu_{G(LI)} \approx \frac{3\hbar\omega n}{2} - \frac{\pi}{3\hbar\beta^2 v L_x L_z}. \quad (3.4)$$

These Equations and Equation (3.1) allows us to find the relative strain induced by the gravitational wave ( $U_{ij}^{\tau\tau} \equiv u_{ij(LI)}^{\tau\tau} - u_{ij(CP)}^{\tau\tau}$ ). The numeric result was found to be,

$$U_{ij}^{\tau\tau} \approx (10^{-2}) h_{ij}^{\tau\tau}, \quad (3.5)$$

or the relative strain is approximately 1% of the gravitational wave strain. This result illustrates that the gravitational wave can impart energy into the superconductor. Equivalently, we can say that the gravitational wave interacts with the quantum system in a real way. This analysis does not however, indicate that the GR wave is reflected from the superconductor.

# Chapter 4

## Black Holes

This chapter covers black holes, one of the most exciting predictions from general relativity. The feature that makes a black hole a “black” hole is the spacetime feature called an event horizon. This horizon is the surface for which nothing can pass from the interior region and into the outside universe. Not even light can escape from the region interior to this horizon. Just this year, the first ever picture of the event horizon of a black hole was published [37]. This is an incredible result considering that no light can escape from a black hole. The results of this paper are in complete agreement with classical general relativity. While this is reassuring for anyone who studies general relativity, it offers no insight into quantized or modified theories of gravity.

Mathematically, the black hole is characterized by a very simple metric. In the case of spherical symmetry and time independence the black hole spacetime is characterized by the line element of the form,  $ds^2 = -f(r)dt^2 + \frac{dr^2}{f(r)} + r^2d\Omega^2$ , where  $f(r)$  is a generic function that depends on the radial coordinate  $r$  and  $d\Omega^2$  is the line element on the unit two-sphere. From this equation you can see that if  $f(r) = -\infty, 0, \infty$  then you will have coordinate singularities. Some of these coordinate singularities are also physical singularities, but calculations of the curvature scalars shows that the event horizon is not a physical singularity. The solution  $f(r) = 0$  gives you the horizons of the black hole. As an example, the simplest case, known as the Schwarzschild black hole, which has mass but no rotation and no charge, has a metric defined by

$f(r) = 1 - \frac{2M}{r}$  in geometrized units. This tells us that the horizon of the black hole is located at  $r_H = 2M$ .

In this chapter, we will look at various open black hole problems and how to solve them using concepts from quantum mechanics such as the idea of intrinsic mass and quantum electrodynamics.

## 4.1 Black Holes and Their Problems

It is well known that many solutions in classical general relativity possess unphysical spacetime signatures. For example, black hole solutions contain Cauchy horizons leading to mass inflation instabilities, singularities leading to the famous information paradox, naked singularities and closed time-like curves [38], [39], [40], [41]. These issues led to the weak and strong cosmic censorship conjectures [42], [43]. That the singularity should be hidden behind a horizon and that the fate of an observer be predictable, is widely accepted. Hawking conjectured in [44] and [45], that closed timelike curves (CTCs) were unphysical and that the application of quantum mechanics would remove the existence of CTCs. The three major problems facing black hole physics represent a breakdown in the interpretation of the mathematical results of GR. Allowing the problems to exist means allowing for predictions that don't obey accepted theories, which are valid in all other areas of physics.

The following are the three problems with some explanation:

- 1) The Information Paradox

The matter falling into a black hole possesses information. This matter gets compressed into the singularity of the black hole as it infalls. As the black hole evaporates via Hawking radiation the mass decreases. This process predominantly emits thermal particles (the dominant emission is photons) in the process which do not carry any of the information about the matter that fell into the black hole [46], [47], [48]. Assuming that the black hole completely evaporates, the black hole vanishes and all of the information that fell into the black hole is lost to the universe forever. In clearer language, you go from a pure state to a

mixed state. This clearly violates the laws of entropy. There have been several attempts to solve this problem, some of which are very promising.

– A) Singularity Removal (Regular Blackholes)

The first real attempt to solve this problem was done by Bardeen [49]. He developed a metric which had no singularity, these are called regular black holes. If there is no singularity then there is no problem because the information does not get compressed to a point and there will likely result a remnant when the blackhole finishes evaporation. This result was promising, but it had no realistic physical interpretation. The Lagrangian that you get out from the metric which he postulated is unfamiliar [50].

– B) Blackhole Remnants

Adler in [51] postulated, based on the argument that the heat capacity reaches zero, that blackholes could not evaporate into nothingness, and that a remnant containing all of the information of the blackhole would be left. This work, like that of Bardeen had little physical interpretation. Basically, they just required that the black hole must possess some property. Additionally, in the late stages of evolution of the black hole, quantum gravity must dominate and could change the description of entropy and heat capacity. For these reasons, this attempt is speculative.

– C) Loop Quantum Gravity

The recent work from Ashtekar, [52], [53] on black hole singularities, in my opinion, has been the most promising. In their recent work, they extended Loop Quantum Gravity (LQG) further into the black hole than has ever been done before, to show that the singularity gets removed by applying LQG.

• 2) Cauchy Problem-Mass Inflation Instability

Some black hole metrics such as the metric for a charged black hole possess more than one horizon. In the Reissner Nordström (RN) metric, you get two horizons [54], [55]. The outer horizon is the event horizon, and the inner horizon



is known as the Cauchy horizon. Physically at the event horizon, the photons being emitted from the horizon out to infinity get infinitely redshifted. This is fine, but at the inner Cauchy horizon, photons being emitted get infinitely blue shifted. This leads to an instability in the calculated energy and mass.

- 3) Naked Singularities and CTCs

Another Interesting problem is that of the naked singularity. The horizons for RN have the following form [54], [55],

$$r_{\pm} = M \pm \sqrt{M^2 - Q^2}. \quad (4.1)$$

If  $Q > M$ , no horizons exist and you get a naked singularity. Naked singularities are a problem because the spacetime around them allows for Closed Time-Like Curves (CTCs). What this means is that there are solutions for which a future event can influence an event in the past. This is not physical. In the early years of black hole physics, many people tried to model the electron as a black hole, but after much effort this was abandoned because of these issues [56], [57]. Clearly an electron will have  $e \gg m_e$ .

#### 4.1.1 The Cause of the Problems

The reason most of these problems arise is due to the way we define mass in our equations. To illustrate this, we will work with the spherically symmetric time independent metric of Reissner Nordström. Any spherically symmetric time independent metric has the form [38],

$$ds^2 = -f(r)dt^2 + \frac{dr^2}{f(r)} + r^2 d\Omega^2, \quad (4.2)$$

where  $f(r)$  is a generic function that depends on the radial coordinate  $r$ , and  $d\Omega^2$  is the line element on unit two-sphere. When we solve for  $f(r)$  using Einstein's equations,  $G^{\mu\nu} = \kappa T^{\mu\nu}$  coupled to linear or nonlinear electromagnetic fields, we end

up with the following equation for  $G^{00} = \kappa T^{00}$  [58],

$$\frac{d}{dr} (r(1 - f(r))) = -\kappa r^2 (e(r)^2 \mathcal{L}_{\mathcal{F}} + \mathcal{L}), \quad (4.3)$$

where  $e(r)$  is the electric field,  $\mathcal{F}$  is the field invariant  $\frac{1}{4}F^{\mu\nu}F_{\mu\nu}$ , and  $\mathcal{L}_{\mathcal{F}}$  is the partial derivative of the electromagnetic Lagrangian  $\mathcal{L}$  with respect to the invariant  $\mathcal{F}$ . Solving Equation 4.3 for  $f(r)$ , assuming linear electromagnetic fields (Maxwell), we arrive at,

$$f(r) = 1 - \frac{C_1}{r} + \frac{Q^2}{r^2}, \quad (4.4)$$

where  $Q$  is the charge of the black hole. The integration constant,  $C_1$ , is determined by assuming that we must retrieve newtonian gravity at infinity and must appear in all effective quantum theories as well. This limit requires us to replace  $C_1 \rightarrow 2M$ . This mass  $M$  is the gravitating mass as seen from infinity  $M_g$ . While this may appear reasonable, and is the standard approach, upon closer inspection we see that there is a problem. We rewrite  $f(r)$  as,

$$f(r) = 1 - \frac{2M(r)}{r}, \quad (4.5)$$

where  $M(r) = M_g - \frac{Q^2}{2r}$ . This second piece can be viewed as the modification of the mass due to subtracting away the electric field mass energy from  $r \rightarrow \infty$ . We show this by writing  $f(r)$  as,

$$f(r) = 1 - \frac{2(M_g - M_E(r))}{r}, \quad (4.6)$$

where  $M_E(r)$  is a generic function of  $r$  that modifies the mass. Equation 4.3 can now be rewritten as,

$$M_E'(r) = -4\pi r^2 \rho(r), \quad (4.7)$$

where  $-\rho(r) = T^0_0 = \mathcal{L} + 2|\mathcal{F}|\mathcal{L}_{\mathcal{F}} = \mathcal{L} + e(r)^2 \mathcal{L}_{\mathcal{F}}$  or equivalently,

$$M_E(r) = - \int 4\pi r^2 \rho(r) dr = + \int_r^\infty 4\pi r^2 \rho(r) dr = + \int \rho(r) dV. \quad (4.8)$$

Here  $V$  is the volume outside the sphere of radius  $r$ . Written this way, we see that Equation 4.8 is an integration to find the total mass energy that exists outside of the sphere of radius  $r$  (Notice the absence of  $\sqrt{g_{rr}}$ ). This makes sense physically because at  $r$ , the force due to the mass that exists in the region from  $r \rightarrow \infty$  vanishes inside the mass shell due to Gauss' theorem, so you have to subtract it away from the gravitating mass. Since  $M_g$  is calculated at infinity, one must modify the effective mass as seen at  $r$ . We will label the mass in the shell from  $r \rightarrow \infty$  as  $M_E(r)$  because in this case, it comes from the  $E$  field <sup>1</sup>.

This method breaks down when  $M_E(r)$  becomes greater than  $M_g$ . This is what leads to the CTC problem. It does not make sense for the “modified mass” to become negative before reaching the event horizon. Think of it in the following way, the gravitating mass  $M_g$  is a combination of all of the mass energies as seen from infinity which includes some “intrinsic mass”  $M_0$  that does not depend on anything, and the total field energy as seen from infinity,  $M_E(r_H)$ , where  $r_H$  is the outermost event horizon of the black hole <sup>2</sup>. We neglect rotation for now.  $M_g = M_0 + M_E(r_H)$ , thus  $M_g - M_E(r)$  can never be negative before reaching the event horizon. It does not make sense that we should allow the energy of the fields to exceed the actual energy of the black hole as seen from infinity. Allowing  $M_g - M_E(r)$  to be negative, leads directly to unphysical spacetimes. In general, since linear electromagnetic fields diverge as  $r \rightarrow 0$ , you will always encounter a region where this becomes negative. Since quantum mechanics puts a limit on the energy at small scale through shielding, it is reasonable that one might hope that quantum mechanics will come in and save the day. We will show in the following sections, that application of quantum mechanics does save us from Cauchy horizons. It may be true that quantum mechanics could save us from naked singularities as well, but we will show that effective quantum theories are not sufficient for this task. Instead, we will show that you can solve the naked singularity issue without applying quantum mechanics.

---

<sup>1</sup>Later, we will identify  $M_E(r_H)$  with the extractable energy of the black hole. We keep the same subscript as they are equivalent.

<sup>2</sup>This is an argument that is meant to be intuitive. Interpreted this way, the energy of the fields in the region  $r_H \rightarrow \infty$  should include the Jacobian,  $\sqrt{g_{rr}}$ . However as we show later through entropic arguments, this  $\sqrt{g_{rr}}$  is not there when we do the calculation formally and not by intuition.

## 4.2 QED Blackholes

It is well known that the presence of quantum fields alters many of the classical properties of black holes. In this section we consider the lowest-order QED corrections to the location and temperature of the event horizons of charged black holes. We conjecture that QED effects protect realistic charged black holes from the phenomenon of mass inflation.

### 4.2.1 Introduction

The discovery that black holes possess thermodynamic properties linking relativity, gravitation, quantum mechanics, and statistical physics has stimulated an enormous body of work over the last four decades. Remarkably, its central relevance to some of the most difficult problems in theoretical physics continues unabated to this day. This paper focuses on an aspect of the relationship between gravitation and quantum fields that is the flip side of the more commonly studied quantum particle creation effects due to classical black hole backgrounds, to wit, the question of how the presence of quantum fields alters the black hole spacetime, a well-posed problem that has an unambiguous solution provided we accept some reasonable physical restrictions.

Our discussion will be based on the formalism of nonlinear electrodynamics coupled to gravity. Only the necessary portions of this formalism are summarized here; for more detailed presentations suited to our purposes the reader is referred to [59] (for general properties of nonlinear electrodynamics, see Boillat [60] and Plebanski [61]). We assume that the fields giving rise to the black hole geometry may be described by a Lagrangian density of the form  $\mathcal{L}(\mathcal{F}, \mathcal{G})$ , with <sup>3</sup>  $\mathcal{F} = \frac{1}{4}F^{\mu\nu}F_{\mu\nu}$  and  $\mathcal{G} = \frac{1}{4}F^{\mu\nu}\tilde{F}_{\mu\nu}$  the quadratic invariants of the electromagnetic field,  $F_{\mu\nu} = \partial_\mu A_\nu - \partial_\nu A_\mu$  the field tensor, and  $\tilde{F}_{\mu\nu} = \frac{1}{2}\epsilon_{\mu\nu\rho\sigma}F^{\rho\sigma}$  its dual. The demands of relativistic invariance,  $U(1)$  gauge invariance, and slowly varying fields are sufficient to justify this assumption. If in addition we limit ourselves to weak fields and neglect higher order corrections,

---

<sup>3</sup>Greek indices run from 0 to 3 and our metric has signature  $(-, +, +, +)$ . The solution of the spherically symmetric problem uses the conventional  $(t, r, \theta, \phi)$  coordinate system.

the effective Lagrangian must be of the form [62]<sup>4</sup>

$$\mathcal{L} = -\mathcal{F} + a\mathcal{F}^2 + b\mathcal{G}^2 \quad (4.9)$$

The normalization of the first term is chosen so as to reproduce Maxwell's theory for  $a = b = 0$ , and the coefficients  $a$  and  $b$  are determined by the specific theory giving rise to these corrections. For instance, for QED,  $a = 8\alpha^2/45m^4$ ,  $b = 14\alpha^2/45m^4$  with  $\alpha$  the fine structure constant and  $m$  the mass of the electron, whereas for Born-Infeld  $a = b = 1/2E_0^2$ , with  $E_0$  a constant with dimension of electric field.

The energy-momentum tensor associated with  $\mathcal{L}(\mathcal{F}, \mathcal{G})$  is

$$T^{\mu\nu} = -\mathcal{L}_{\mathcal{F}} F^{\mu\lambda} F^{\nu}_{\lambda} + (\mathcal{L} - \mathcal{G}\mathcal{L}_{\mathcal{G}})g^{\mu\nu} \quad (4.10)$$

where  $\mathcal{L}_{\mathcal{F}} = \partial\mathcal{L}/\partial\mathcal{F}$  and  $\mathcal{L}_{\mathcal{G}} = \partial\mathcal{L}/\partial\mathcal{G}$ . Setting up the Einstein equations

$$G^{\mu\nu} = 8\pi G T^{\mu\nu} \quad (4.11)$$

is fairly straightforward for a spherically symmetric system with metric

$$ds^2 = -f(r)dt^2 + \frac{dr^2}{f(r)} + r^2 d\Omega^2 \quad (4.12)$$

The result is

$$(r^2 f')' = -16\pi G r^2 (\lambda_+^2 \mathcal{L}_{\mathcal{F}} + \mathcal{G}\mathcal{L}_{\mathcal{G}} - \mathcal{L}) \quad (4.13)$$

$$[r(1-f)]' = -8\pi G r^2 (\lambda_-^2 \mathcal{L}_{\mathcal{F}} - \mathcal{G}\mathcal{L}_{\mathcal{G}} + \mathcal{L}) \quad (4.14)$$

Here primes indicate derivatives with respect to  $r$  and the quantities

$$\lambda_{\pm} = \sqrt{\sqrt{\mathcal{F}^2 + \mathcal{G}^2} \pm \mathcal{F}} \quad (4.15)$$

---

<sup>4</sup>For an analysis of when this form of the Lagrangian is valid, see Appendix A

are proportional to the eigenvalues of the field tensor  $F_{\mu\nu}$ . The equations of motion for the fields may be obtained from the conservation law  $\nabla_\nu T^{\mu\nu} = 0$  or from the Euler-Lagrange equations for  $\mathcal{L}(\mathcal{F}, \mathcal{G})$ . In the region outside the sources we find

$$\nabla_\nu D^{\mu\nu} = 0 \quad (4.16)$$

$$\nabla_\nu \tilde{F}^{\mu\nu} = 0 \quad (4.17)$$

with  $D^{\mu\nu} = \mathcal{L}_{\mathcal{F}} F^{\mu\nu} + \mathcal{L}_{\mathcal{G}} \tilde{F}^{\mu\nu}$ . In the next section we shall apply Eqs. (4.13, 4.14) and (4.16, 4.17) to the Lagrangian (4.9).

### 4.2.2 QED-corrected Schwarzschild metric

As we have already mentioned, the form of the Lagrangian (4.9) is required by symmetry considerations and the assumption of weak, slowly varying fields. As such, it does not depend on a specific theory, although the assignment of numerical values to  $a$  and  $b$  must be done within the context of a particular theory or model. The point here is that if needed, we may borrow the QED values, say, from the results in Refs. [63–66] (see also the excellent review by Dunne [67]), which are strictly valid for constant uniform fields, because we know from our arguments above that the generic form of the Lagrangian must be as in Eq. (4.9) even when the fields are not uniform (provided, of course, that their variation is not too rapid). This is important for several reasons. First, it tells us that we may use the weak field limit of the Euler–Heisenberg Lagrangian without running into a contradiction despite the obvious fact that in our case the fields are not uniform. Second, it implies that our approximation can be trusted near the event horizon for large black holes but not over the whole space-time. Third, it makes it plain that this approximation may be improved by adding derivative terms and/or higher loop corrections to (4.9).

Consider now the spherically symmetric ansatz for the fields

$$F_{01} = E(r) \quad (4.18)$$

$$F_{23} = H(r) \sin \theta \quad (4.19)$$

Then  $D^{01} = -E\mathcal{L}_{\mathcal{F}} - (H/r^2)\mathcal{L}_{\mathcal{G}}$ ,  $D^{0\nu} = 0$  for  $\nu \neq 1$ , and Eq. (4.16) implies

$$\partial_1(\sqrt{-g}D^{01}) = 0 \quad (4.20)$$

For the metric (B.1),  $\sqrt{-g} = r^2 \sin \theta$ , so that

$$D^{01} = \frac{A}{r^2} \quad (4.21)$$

with  $A$  constant. A similar calculation using Eq. (4.17) shows that  $H$  is a constant. Therefore our  $F_{23}$  is identical to the Reissner–Nordström  $F_{23}$ , and we are allowed to identify  $H = P/4\pi$ , with  $P$  the magnetic charge.

Applying the result (4.21) to the effective Lagrangian (4.9) we get

$$E(1 - 2a\mathcal{F}) - 2b \frac{H}{r^2} \mathcal{G} = \frac{A}{r^2} \quad (4.22)$$

The invariants  $\mathcal{F}$  and  $\mathcal{G}$  are easily computed with the ansatz (4.18, 4.19); one finds  $\mathcal{F} = \frac{1}{2}(-E^2 + H^2/r^4)$  and  $\mathcal{G} = -EH/r^2$ . However, since terms in  $a, b$  are small corrections, we may use the zero-order field  $E \approx A/r^2$  for these invariants in (4.22). This yields  $\mathcal{F} \approx (H^2 - A^2)/2r^4$ ,  $\mathcal{G} \approx -AH/r^4$ , and

$$E \approx \frac{A}{r^2} + \frac{A[a(H^2 - A^2) - 2bH^2]}{r^6} \quad (4.23)$$

From the asymptotic form of the field we see that  $A = Q/4\pi$ , with  $Q$  the electric charge.

Having determined the fields we may now find the solution for the metric function  $f(r)$ . We proceed from Eq. (4.14) and the observation that the exact form of the invariants for our spherically symmetric system entails  $\lambda_-^2 = E^2$ . To first order in  $a, b$ , Eq. (4.14) becomes

$$[r(1 - f)]' \approx \frac{4\pi G(A^2 + H^2)}{r^2} - \frac{8\pi G}{r^6} \left[ \frac{a}{4}(A^2 - H^2)^2 + bA^2H^2 \right] \quad (4.24)$$

Integrating once and solving for  $f$  gives

$$f(r) \approx 1 - \frac{2GM}{r} + \frac{\beta}{r^2} - \frac{\gamma}{r^6} \quad (4.25)$$

with

$$\beta = 4\pi G (A^2 + H^2) = \frac{G}{4\pi} (Q^2 + P^2) \quad (4.26)$$

$$\gamma = \frac{2\pi G a}{5} (A^2 - H^2)^2 + \frac{8\pi G b}{5} A^2 H^2 = \frac{G}{640\pi^3} [a(Q^2 - P^2)^2 + 4bQ^2 P^2] \quad (4.27)$$

where  $Q, P$  are the charges in Heaviside units, or

$$\beta = G(q^2 + p^2) \quad (4.28)$$

$$\gamma = \frac{G}{40\pi} [a(q^2 - p^2)^2 + 4bq^2 p^2] \quad (4.29)$$

for  $q, p$  in Gaussian units.

### 4.2.3 Horizons

We now examine the horizon structure of the spacetime behind the solution (4.25). Setting  $p = 0$  for simplicity, we see from (4.29) that in the absence of QED effects ( $a = b = 0$ ),  $\gamma = 0$  and we recover from (4.25) the classical Reissner–Nordström solution and the associated horizons at  $r_{0\pm} = GM \pm \sqrt{(GM)^2 - Gq^2}$ .

Although we are interested mainly in realistic astrophysical scenarios, we shall first discuss the case of a *classically* extreme Reissner–Nordström black holes ( $GM^2 = q^2$ ) for completeness. The condition  $f(r) = 0$  with

$$f(r) \approx \left(1 - \frac{GM}{r}\right)^2 - \frac{\gamma}{r^6} \quad (4.30)$$

may be recast in the form

$$x^4(x-1)^2 - \left(\frac{4\xi}{27}\right)^2 = 0 \quad (4.31)$$



where  $x = r/r_0 \equiv r/GM$  and

$$\xi = \frac{27}{4} \frac{\sqrt{\gamma}}{(GM)^3} = \frac{27}{4GM} \sqrt{\frac{a}{40\pi G}} \quad (4.32)$$

For  $\xi > 1$  ( $M \lesssim 1.16 \times 10^4 M_\odot$ ) there is a single horizon at

$$r_+ = \frac{1}{3}GM \left[ 1 + \left( 2\xi + 1 + 2\sqrt{\xi(\xi + 1)} \right)^{1/3} + \left( 2\xi + 1 - 2\sqrt{\xi(\xi + 1)} \right)^{1/3} \right] \quad (4.33)$$

Since  $r_+ > GM \equiv r_0$ , this result implies that the horizon of a QED-corrected extreme Reissner–Nordström black hole of mass  $M \lesssim 1.16 \times 10^4 M_\odot$  is larger than the horizon of its classical counterpart.

For  $\xi < 1$  ( $M \gtrsim 1.16 \times 10^4 M_\odot$ ) there are three horizons. The outermost horizon is again given by (4.33). The intermediate horizon  $r_-$  and the innermost horizon  $r_{\text{in}}$  are most conveniently stated in terms of the angle  $\phi = \cos^{-1}(1 - 2\xi)$ ,  $0 < \phi < \pi$ , as

$$r_- = \frac{1}{3}GM \left( 1 + 2 \cos \frac{\phi}{3} \right) \quad (4.34)$$

and

$$r_{\text{in}} = \frac{1}{3}GM \left( 1 - 2 \cos \frac{\phi + \pi}{3} \right) \quad (4.35)$$

It is easy to check that  $0 < r_{\text{in}} < 2GM/3 < r_- < GM < r_+ \lesssim 3.36 GM$ .

For  $a = 0$ , QED effects are absent,  $r_{\text{in}} = 0$ , and we recover the single classical horizon at  $r_0 = GM$ . On the other hand, for black holes of mass  $M \gg 1.16 \times 10^4 M_\odot$ ,  $\xi \ll 1$ , and

$$r_\pm = GM \pm \sqrt{\frac{a}{40\pi G}} \quad (4.36)$$

$$r_{\text{in}} = \sqrt{GM} \left( \frac{a}{40\pi G} \right)^{1/4} \quad (4.37)$$

Note that the existence of the innermost horizon is due entirely to QED effects. Even though one would normally expect quantum mechanics to play a negligible role since we are far away from the Planck scale, Eq. (4.35) shows that general relativity and quantum mechanics can conspire to produce strong gravitational effects such as

event horizons before we reach the regime of quantum gravity ( $r_{\text{in}}$  is approximately 80% of  $r_-$  for a black hole of mass  $1.2 \times 10^4 M_\odot$ ). Quantum effects also split the single classical horizon, giving rise to a narrow region between  $r_+$  and  $r_-$  where the metric function  $f(r)$  changes sign and  $r$  becomes timelike. Between  $r_-$  and  $r_{\text{in}}$   $f(r)$  becomes positive again, but the third horizon at  $r_{\text{in}}$  gives rise to a new inner region where only infall is possible. We shall come back to these expressions in the following section on the Hawking temperature of QED-corrected black holes.

Astrophysical black holes are not expected to form near (classical or quantum) extremality. Indeed, an upper limit of  $10^{-18}$  for the ratio  $\sigma \equiv q/\sqrt{GM}$  appears reasonable [68]. It will prove convenient to establish at the outset the limits this demand places on our conclusions regarding realistic charged black holes. From (4.9) we see that the weak-field limit breaks down for  $a|\mathcal{F}| \sim 4\pi$  in Gaussian units. Since  $|\mathcal{F}| = E^2/2$  for  $p = 0$ , we find that our analysis will be valid in regions with radii greater than

$$r_* \sim \left( \frac{aq^2}{8\pi} \right)^{1/4} \quad (4.38)$$

An immediate consequence of (4.38) is that for classically extreme black holes the prediction (4.35) of a quantum horizon at  $r_{\text{in}}$  is on solid ground for masses in the range  $1.16 \times 10^4 M_\odot \lesssim M \lesssim 1.26 \times 10^4 M_\odot$ . If the upper limit is exceeded, the prediction is marginal in the sense that  $r_{\text{in}}$  becomes slightly smaller than  $r_*$ , and higher-order corrections would be needed to decide with the same level of confidence whether this horizon exists for larger masses.

For realistic black holes we may replace  $q$  by  $\sigma\sqrt{GM}$  to obtain (numerical values for radii are in meters)

$$r_* \sim 9.1 \times 10^4 \sqrt{\sigma \frac{M}{M_\odot}} \quad (4.39)$$

which has an upper limit of  $9.1 \times 10^{-5} (M/M_\odot)^{1/2}$  for  $\sigma = 10^{-18}$ .

Consider now the last two terms in (4.25). Their ratio,

$$\frac{\gamma}{\beta r^4} = \frac{aq^2}{40\pi r^4} = \frac{1}{5} \left( \frac{r_*}{r} \right)^4 \quad (4.40)$$

shows that the QED correction is always smaller than the classical  $\beta/r^2$  term in  $f(r)$  wherever the weak-field limit holds. But that does not mean that a computation of the horizons by perturbative methods around  $r_{0\pm}$  is warranted. Indeed, for small charge-to-mass ratios,  $r_{0+} \approx 2GM$ , and  $r_{0-} \approx \sigma^2 GM/2$ . Hence

$$\frac{r_*}{r_{0+}} \approx 31.0 \sqrt{\frac{\sigma}{M/M_\odot}} < \frac{3.1 \times 10^{-8}}{\sqrt{M/M_\odot}} \quad (4.41)$$

$$\frac{r_*}{r_{0-}} \approx \frac{123.8}{\sigma^{3/2} \sqrt{M/M_\odot}} > \frac{1.24 \times 10^{29}}{\sqrt{M/M_\odot}} \quad (4.42)$$

In other words, for realistic black holes the effect of QED processes on the outer horizon may safely be examined using a straightforward approximation. To first order, we may replace  $r^6$  in (4.25) by  $r^2 r_{0+}^4$  and then solve a quadratic equation to obtain [69]

$$r_+ \approx GM + \sqrt{(GM)^2 - Gq^2 + \frac{\gamma}{r_{0+}^4}} \quad (4.43)$$

The inner horizon, however, will not yield to the same treatment as it is buried deep inside the region of radius  $r_*$  where higher-order QED corrections become important. This forces us to reconsider the very existence of the inner (Cauchy) horizon. It is obviously present in a purely classical context as a solution to the quadratic equation  $f(r) = 0$  for the RN metric function. But incorporating quantum effects brings the new scale  $r_*$  into the problem, and this scale clearly establishes  $r_{0-}$  as a mathematical artifact, since it lies outside the region where the classical and the lowest-order quantum analyses are valid. Although a more sophisticated approach is necessary to give a definitive answer to this question, the conjecture that the inner horizon may not exist in the full theory deserves serious consideration. We may reach the same conclusion as follows. According to (4.42), for large-mass black holes  $r_{0-}$  is many orders of magnitude smaller than  $r_*$ , and this is, in turn, much smaller than  $r_{0+}$ , so we are naturally led to ask about the exact solutions of  $f(r) = 0$  in (4.25). Unfortunately, the sextic equation cannot be solved in closed form, but it is possible to show that for realistic black holes there are four complex roots, one real negative root near  $-\gamma^{1/5}/(2GM)^{6/5} \approx -3.1[\sigma^2/(M/M_\odot)]^{2/5}$ , and one positive real root near

$r_{0+}$ . Additional positive real roots do not appear unless  $M \gtrsim 2 \times 10^{57} M_\odot$  (in the general case, there is either a single horizon, or three horizons, although nothing seems to forbid the merging of two of the three horizons into one to form a quantum analog of the classically extreme black hole). It therefore appears that QED effects have done away with the Cauchy horizon for realistic black holes - only the outer horizon remains. We reiterate that, because the approximations leading to the metric function  $f(r)$  in (4.25) are valid only for  $r > r_*$ , this should not be construed as proof that a Cauchy horizon will be absent in the exact theory. But (4.42) does unequivocally show that the horizon at  $r_{0-}$  is a prediction arising from a classical RN solution that has been pushed far beyond its limit of validity and must consequently be considered suspect. Obviously, the absence of an inner horizon is crucial to the stability of charged black holes: without a Cauchy horizon the phenomenon of mass inflation [70] cannot arise, and the interior solution becomes stable as a result of quantum field theory (as opposed to quantum gravity) effects.

#### 4.2.4 Surface gravity and Hawking temperature

The surface gravity for static spacetimes can be calculated by a well-known procedure [68, 71]. With  $V = \sqrt{f}$  the redshift factor, the surface gravity is given by  $\kappa = \sqrt{\nabla_\mu V \nabla^\mu V}$ , so that

$$\kappa = \frac{GM}{r_+^2} - \frac{\beta}{r_+^3} + \frac{3\gamma}{r_+^7} \quad (4.44)$$

and the black hole temperature follows from  $T = \kappa/2\pi$ . Replacing (4.43) in (4.44) and expanding to first order in  $a$  we get

$$T \approx T_{RN} + \frac{\gamma}{4\pi} \frac{(3r_{0+} - 2GM)}{r_{0+}^7 (r_{0+} - GM)} \quad (4.45)$$

where

$$T_{RN} = \frac{r_{0+} - GM}{2\pi r_{0+}^2} \quad (4.46)$$

is the temperature of the classical Reissner–Nordström black hole.

Astrophysical black holes are expected to have  $p = 0$  and large mass-to-charge ratios,  $GM^2 \gg q^2$ . In that case (4.45) simplifies to

$$T \approx T_{RN} + \frac{aq^4}{5120\pi^2 G^6 M^7} = T_{RN} + \frac{a\sigma^4}{5120\pi^2 G^4 M^3} \quad (4.47)$$

Since

$$T_{RN} \approx \frac{1}{8\pi GM} \left(1 - \frac{q^4}{16G^2 M^4}\right) = \frac{1}{8\pi GM} \left(1 - \frac{\sigma^4}{16}\right) \quad (4.48)$$

we see that the presence of charge drives the temperature below the Schwarzschild value  $(8\pi GM)^{-1}$ , whereas QED (as well as Born-Infeld) effects will increase the temperature. Furthermore, the ratio of these corrections is

$$\frac{aq^4}{5120\pi^2 G^6 M^7} \cdot \frac{128\pi G^3 M^5}{q^4} = \frac{a}{40\pi G^3 M^2} = \frac{2.94 \times 10^6}{(M/M_\odot)^2} \quad (4.49)$$

It is interesting to note that the charge and QED contributions to the temperature may achieve comparable magnitudes without violating our assumptions of weak fields ( $a|\mathcal{F}| \ll 4\pi$ ) or large mass-to-charge ratio ( $q^2 \ll GM^2$ ). Because these effects become comparable for masses such that  $G^3 M^2 \sim a/40\pi$ , or  $M \sim 1.7 \times 10^3 M_\odot$ , neglecting QED corrections to the temperature is not justified unless  $M \gg 1.7 \times 10^3 M_\odot$ . As we shall see in the next section, this observation is particularly relevant to the evaporation of charged black holes.

Extreme Reissner–Nordström black holes have zero temperature in a purely classical context. When QED corrections are taken into account, however, their temperature is given by

$$T = \frac{1}{\pi r_+} \left(1 - \frac{GM}{r_+}\right) \left(\frac{3}{2} - \frac{GM}{r_+}\right) \quad (4.50)$$

where we have used (4.44) and (4.30)–(4.33). For large-mass black holes this becomes

$$T \approx \frac{1}{4\pi(GM)^2} \sqrt{\frac{a}{10\pi G}} \quad (4.51)$$

Although certainly small in absolute terms, this temperature is surprisingly large in relative terms: for a black hole of mass  $10^6 M_\odot$ , the temperature (4.51) is only a factor of  $\sim 10^{-2}$  below the temperature of a Schwarzschild black hole of similar mass.

### 4.2.5 Black hole Evolution

Charged black holes lose mass and charge due to particle pair creation. Classically, black holes lose mass via Hawking radiation, but when a black hole is charged, it will also lose mass and charge due to the Schwinger effect, the production of particles due to strong electromagnetic fields. Here, we will show that the QED-corrected black hole's lifetimes and evolutions differ from their classical counterpart. Hiscock and Weems [72] thoroughly examined the role that charge and the Schwinger effect play in the evolution of a classically charged black hole (i.e., a black hole described by the standard RN metric without quantum corrections). The mass evolution of a charged black hole is given by

$$\frac{dM}{dt} = -\frac{\pi^2}{15\hbar^3} T^4 \alpha \sigma_0 + \frac{Q}{r_+} \frac{dQ}{dt} \quad (4.52)$$

The first term in (4.52) is the typical Hawking radiation term coming from the creation of massless thermal particles, and the second term is the mass loss due to electromagnetic pair creation.  $\alpha$  is the ratio of cross section to geometrical optics cross section and will not change from what was obtained in [72], which is  $\alpha = 2.0228$ , accounting for 3 massless neutrinos.  $\sigma_0$ , the geometrical optics cross section, and  $r_+$  will be solved using numerical methods.  $dQ/dt$  can be found using the Schwinger formula [66], and the result is

$$\frac{dQ}{dt} = -\frac{Q^2 e^3}{\pi^2 \hbar^2} \left[ \frac{1}{r_+} \exp\left(\frac{-r_+^2}{QQ_0}\right) - \sqrt{\frac{\pi}{QQ_0}} \operatorname{erfc}\left(\frac{r_+}{\sqrt{QQ_0}}\right) \right] \quad (4.53)$$

with  $Q_0 = \hbar e / \pi m^2 = 1.7 \times 10^5 M_\odot$ . Notice that the difference between classical and QED evolution arises from  $\sigma_0$ ,  $r_+$  and  $T$  in (4.52) and (4.53). In Figure 4.1,  $dQ/dt$  and  $dM/dt$  as well as their percent differences from the classical results are plotted for a  $Q = 10^{-18} M$  black hole. While there is a significant difference in the evolutions for small mass values, this difference only occurs for charge  $Q \ll e$ . So, for a real black

hole with  $Q = 10^{-18}M$ , the difference in both  $dM/dt$  and  $dQ/dt$  from the classical counterpart is negligible.

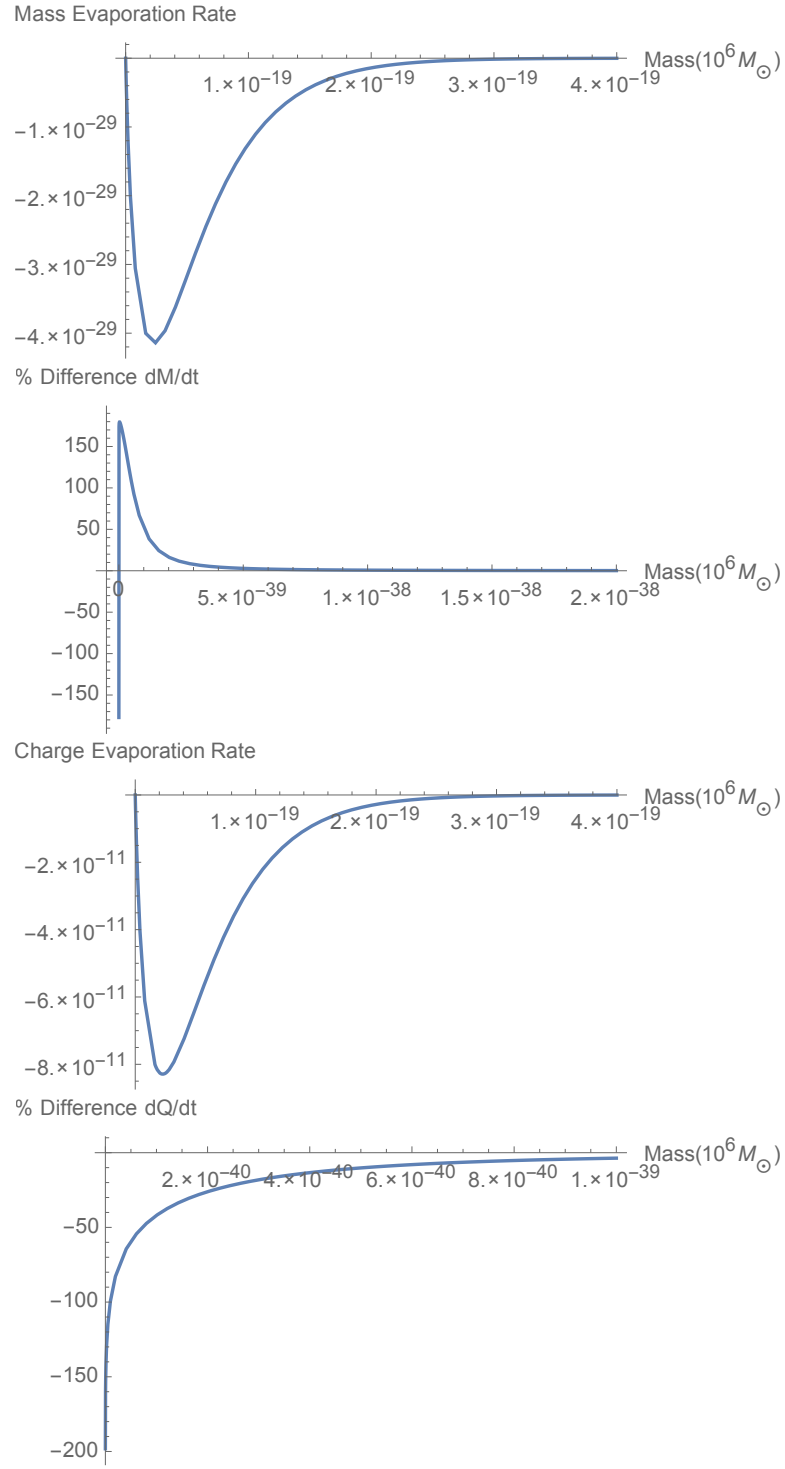


Figure 4.1: Evolution rates and % difference in evolution rates of a  $Q = 10^{-18}M$  black hole



Although there seems to be no difference in the evolution of a realistic black hole, we will show that this assumption is incorrect. We obtain  $M(t)$  and  $Q(t)$  by numerically integrating equations (4.52) and (4.53). Figure 4.2 shows the charge and mass evolution with respect to time of an initially  $150 \times 10^6 M_\odot$  black hole with a charge to mass ratio defined by  $Q^2/M^2 = 0.1$ .

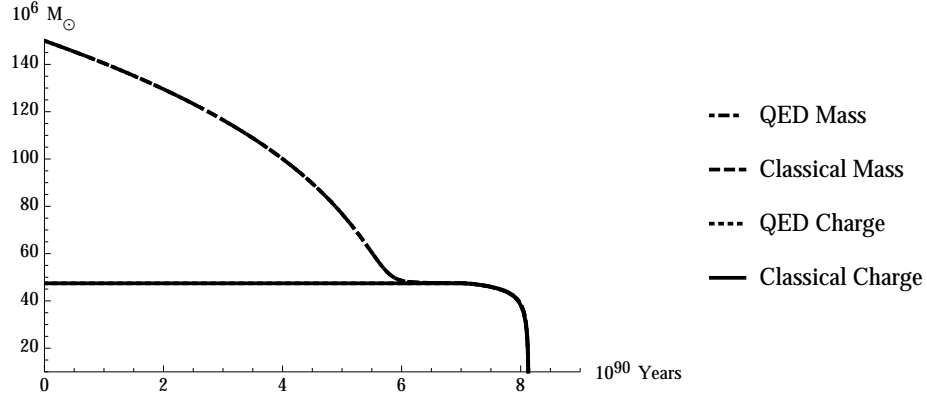


Figure 4.2: Evolution of a  $150 \times 10^6 M_\odot$  black hole with  $Q^2/M^2 = 0.1$ .

The difference in lifetime between the QED and classical black hole is a very small percentage of the overall lifetime and cannot be distinguished from the graph alone. A numerical calculation shows that it is approximately two millionths of a percent change, but the effect of the quantum correction decreases the lifetime by  $2 \times 10^{83}$  years. Notice that both the QED and classical black holes spend a significantly long time near the extremal limit. Indeed, any charged black hole will spend some part of its lifetime near the extremal limit [72]. Because of this, it is important to examine the evolution near extremality.

Figure 4.3 shows the percent differences between QED and classical evolution rates for a near-extremal black hole. Notice that below  $1 \times 10^6 M_\odot$  and above  $60 \times 10^6 M_\odot$  the difference in  $dM/dt$  is very large, and below  $10^5 M_\odot$ , the difference in  $dQ/dt$  is large. Below the lower limits, QED evolution rates are smaller than that of the classical case. This is because the slightly larger outer horizon lowers the Schwinger rate, and this difference becomes significant for small radii. Above  $60 \times 10^6 M_\odot$ ,  $dM/dt$  is larger because the classical black hole lacks a temperature. In Figure 4.4 we look at the

extremal case in more detail. We show the evolution of  $5 \times 10^3 M_\odot$ ,  $20 \times 10^6 M_\odot$ , and  $50 \times 10^6 M_\odot$  black holes. The difference in evolution for the  $20 \times 10^6 M_\odot$  and  $50 \times 10^6 M_\odot$  black hole is a small percentage of the total lifetime as expected from Figure 4.3. The difference in lifetime for the  $5 \times 10^3 M_\odot$  QED black hole however, is 50% of the classical lifetime. This shows that QED effects slows the evolution. Again, this is consistent with Figure 4.3.

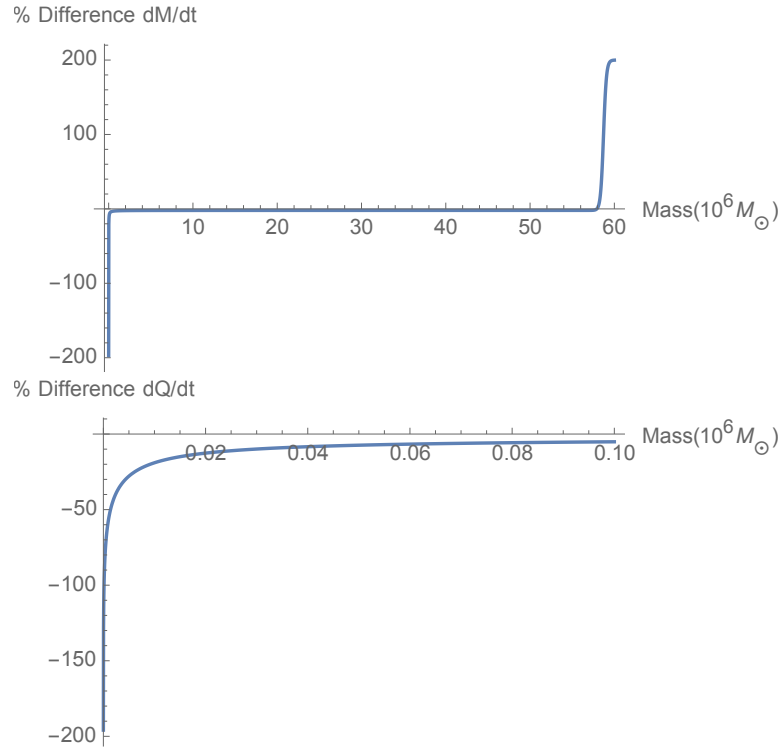


Figure 4.3: % difference in evolution rates of a  $Q = M$  black hole.

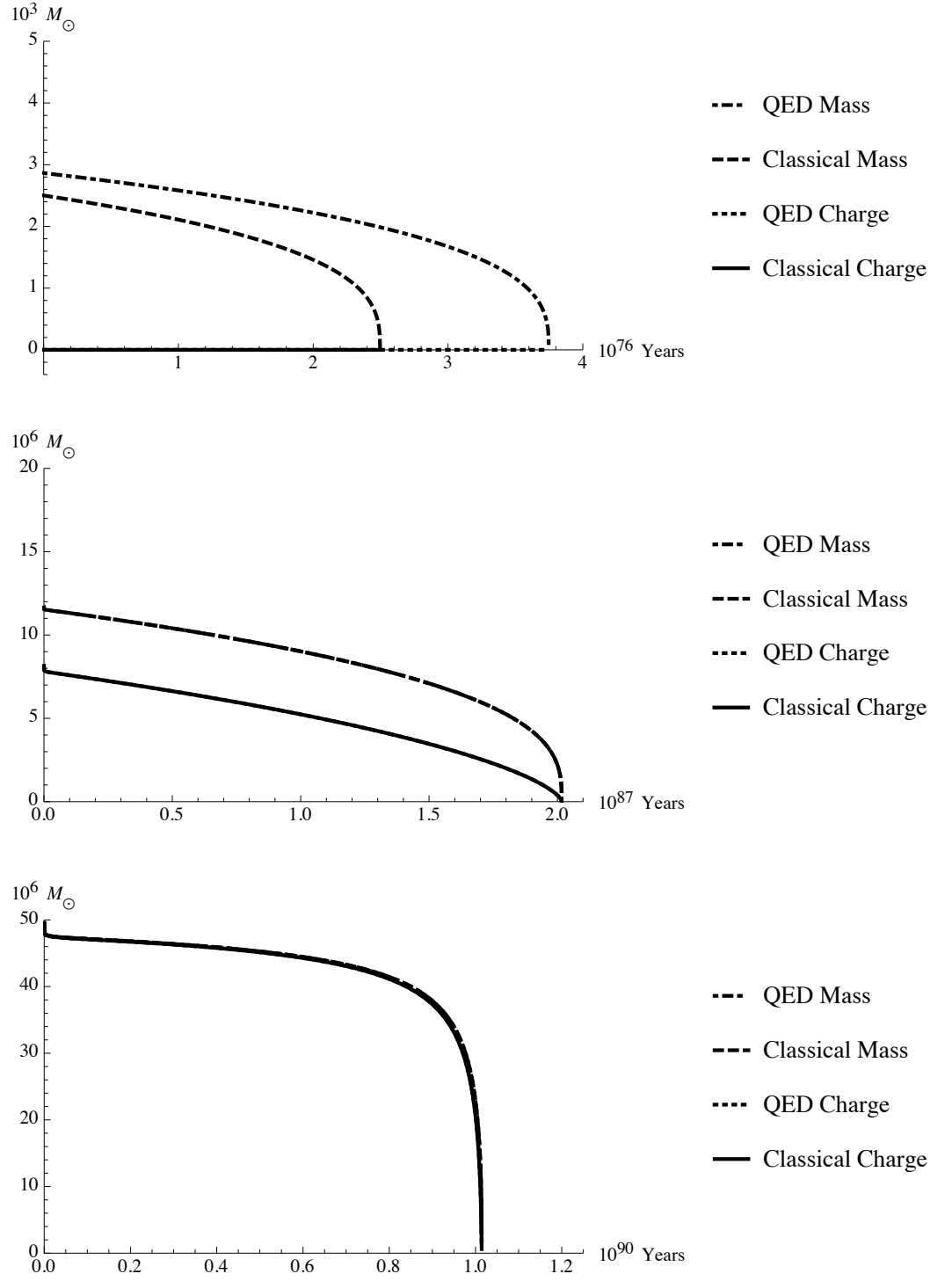


Figure 4.4: Evolution of near extremal black holes. Notice, the difference is indistinguishable for the  $20 \times 10^6 M_\odot$  and  $50 \times 10^6 M_\odot$  black holes.

### 4.2.6 Discussion

Our results show that QED effects alter the classical Reissner–Nordström metric. The main feature is the appearance of a new length scale  $r_*$  below which quantum effects become dominant. Since  $r_{0-} \ll r_*$ , the Cauchy horizon of classical Reissner–Nordström black holes lies in a region where the classical solution can no longer be trusted to give correct predictions, and the very existence of this horizon is cast into doubt. Although not conclusive, our work lends credence to the conjecture that QED effects may do away with the Cauchy horizon. Because of its obvious impact on the phenomenon of mass inflation and the stability of the black hole’s interior, this section revisits this conjecture from alternative points of view.

1. It may be tempting to argue that our conclusions are voided by the fact that we are using a weak-field approximation to explore a phenomenon characterized by an unbounded growth of energy perturbations. Although that argument is ultimately circular, a simple counterexample based on the analogy with the well-known radiative instability of classical atomic models may nevertheless help to see where this seemingly intuitive objection goes wrong.

In the classical atomic model, the natural distance scale is set by the classical electron radius  $r_e = e^2/mc^2$ . Since this is on the order of the proton’s size, there is nothing stopping the accelerated electron from radiating its energy away until it reaches the nucleus. A semiclassical treatment introduces a new length scale,  $a_0 = \hbar^2/me^2 = r_e/\alpha^2$ , with  $\alpha$  the fine structure constant. This new scale suggests that a classical treatment may give reasonable answers for  $r > a_0$ , as is indeed the case: radiative lifetimes calculated using the classical model are not far off from the experimental values even for  $n = 2 \rightarrow n = 1$  transitions. For  $r < a_0$ , however, the semiclassical argument is sufficient to uncover a dramatic change in behavior. Using the ground state wave function (or almost any reasonable approximation of it), we may find the charge and current distributions to be used as input to the calculation of the radiated power from Maxwell’s equations. As these distributions are stationary, no power is radiated, and the radiative instability is seen to arise from an unwarranted extension of classical results to the region  $r < a_0$ . The analogy to our problem becomes evident with the replacements  $r_e \rightarrow r_{0-}$ ,  $a_0 \rightarrow r_*$ , radiative

instability  $\rightarrow$  mass inflation, and Maxwell's equations with quantum-corrected sources  $\rightarrow$  Einstein's equations with QED-corrected sources.

2. The above analogy may ease the reader's worries about a contradiction between our assumptions and our conclusions, but it certainly does not prove conclusively that the inner horizon is an unwarranted extrapolation of a classical solution to a region where it cannot possibly be valid. To that end, let us assume that quantum effects are negligible, and that the inner horizon does in fact exist. The electric field at the inner horizon is given by:

$$E_- = \frac{q}{r_{0-}^2} = \frac{q}{(\sigma^2 GM/2)^2} = \frac{4}{\sigma^3 G^{3/2} M} \quad (4.54)$$

If this field is comparable to the critical field  $E_{crit} = \pi m_e^2/e \approx 4 \times 10^{18} \text{V/m}$ , pair creation becomes significant and QED effects cannot be neglected. The prediction of an inner horizon is therefore a reliable classical prediction provided  $E_- \ll E_{crit}$ , or

$$M \gg \frac{4}{\sigma^3 G^{3/2} E_{crit}} \quad (4.55)$$

For  $\sigma = 10^{-18}$ , this gives the constraint  $M \gg 6.7 \times 10^{59} M_\odot$ . Masses satisfying this condition would have electric fields below the critical field, and a Cauchy horizon would be present since equations (4.40)-(4.42) guarantee that the weak-field limit applies all the way to the inner horizon. As a matter of fact, our analysis of the solutions of  $f(r) = 0$  shows that there are three horizons, just as in the classically extreme case. As this black hole evaporates and its mass decreases, the eventual violation of the condition (4.55) will lead back to the realistic scenario we discuss next. We emphasize that the three-horizon black hole is completely unrealistic: the masses required exceed the mass of the visible universe by at least 30-35 orders of magnitude.

Masses below  $6.7 \times 10^{59} M_\odot$  would have electric fields exceeding the critical field, and the assumption of negligible quantum effects at the inner horizon would then lead to a contradiction. For example, a 1-billion solar mass black hole would have an electric field at the inner horizon that is more than 50 orders of magnitude greater

than the critical field. It is then clear that, for realistic charged black holes, the classical Reissner–Nordström solution cannot be used to infer the existence of an inner Cauchy horizon since this region would be utterly dominated by quantum effects. Note that this conclusion stands on its own, since it is completely independent of the assumptions made elsewhere in this work.

3. It is natural to expect that similar effects will lead to the removal of Cauchy horizons in Kerr–Newman black holes as well. More generally, quantum fields might conceivably lead to nontrivial alterations of classical geometries in many cases. In fact, in a paper published recently [73], the authors have demonstrated that a semi-classical approach to  $2+1$ -dimensional BTZ spacetimes leads to similarly striking conclusions: naked singularities acquire a covering horizon, and rotating BTZ black holes develop a curvature singularity at the Cauchy horizon. In a sense, the Cauchy horizon is still present, but the spacetime cannot be continued beyond it since the divergence of the Kretschmann scalar shows that the geometry has developed a singularity at the horizon. Although this differs from our current work (here quantum effects seem to eliminate the Cauchy horizon, and the geometry is singular only at  $r = 0$ ), the main lesson in both cases is that quantum effects can potentially have a profound effect on spacetime geometries without the need for quantum gravity. Just as in our analysis, the authors of Ref. [73] are careful to emphasize that the breakdown of the perturbative approach implies that these results, while highly suggestive, cannot be taken as definitive.

### 4.2.7 Conclusion

We have developed the metric for a first-order quantum-corrected QED black hole. It was argued that, for realistic black holes, the inner (Cauchy) horizon appears to be absent from the QED-corrected metric. Indeed, it was shown that the inner horizon of the classical solution is an unwarranted extension of the classical metric to radii where quantum effects are no longer negligible. The absence of the inner horizon in the QED case eliminates the problem of mass inflation and the consequent instability of RN black holes, since Cauchy horizons are crucial to this process. In addition, we

have shown that the temperature of the quantum-corrected extremal black hole is nonzero, which leads to differences between classical and QED evolution.

## 4.3 Chronology Protecting Black Holes

### 4.3.1 Introduction

In this section, we show using an irreducible mass approach that naked singularities are only mathematical and will not and cannot exist in nature. Contrary to previous studies of charged rotating black holes, we show that these black holes have a real event horizon for all values of charge and angular momentum. It is impossible to either over charge or over rotate a black hole. This is both consistent with Hawking's suggestion that some mechanism must lead to chronology protection and Penrose's weak and strong cosmic censorship conjectures. Hawking conjectured in [44] and [45], that closed time-like curves (CTCs) were unphysical and that the application of quantum mechanics would remove the existence of CTCs. Here we will take a different approach by defining an intrinsic mass for the black hole and show that in general, the problematic areas of the spacetime are fixed and chronology is protected even before application of quantum mechanics to the gravitational field.

### 4.3.2 The Gravitating Mass of Coulomb Fields

As we showed in Section 4.1, we encounter the naked singularity issue whenever the effective mass is allowed to become negative. One way to solve the negative mass problem is to break up the gravitating mass  $M_g$  into its components,  $M_0$  and  $M_E$ .

$$M_g = M_0 + M_E(r_H) = M_0 + \int_{r_H}^{\infty} \rho(r) dV = M_0 + \frac{Q^2}{2r_H} \quad (4.56)$$

Notice, that  $M_E(r_H)$  as seen from infinity will be due to the integral from the outer horizon to infinity, so it is important that  $r_H$  is always the outer horizon. There is nothing that forbids us from breaking up  $M_g$  in this way,  $M_g$  was just an integration

constant after all. The  $M(r)$  that appears in Equation 4.5 becomes

$$M(r) = M_0 + \frac{Q^2}{2r_H} - \frac{Q^2}{2r}. \quad (4.57)$$

Equation 4.57 can also be written as,

$$M(r) = M_0 + M_E(r_H) - M_E(r). \quad (4.58)$$

The solution of  $f(r) = 0$  gives horizons at

$$r_{\pm} = M_0 + \frac{Q^2}{2r_H} \pm \sqrt{M_0^2 - Q^2 + \frac{M_0 Q^2}{r_H} + \frac{Q^4}{4r_H^2}}. \quad (4.59)$$

If we assume that  $r_+$  is the outer horizon,  $r_H$ , for all values of  $Q$ , then we will encounter a problem if  $Q > 2M_0$ . In this region,  $r_- > r_+$ , which means that the replacement,  $r_+ \rightarrow r_H$ , is no longer valid. In order to ensure that  $r_H$  is always the outermost horizon, we must break up the analysis into three parts. For  $Q < 2M_0$ ,  $r_+ = r_H$  and the solution is  $r_H = 2M_0$ . For  $Q < 2M_0$ , there are 2 horizons. In our QED paper [58] we showed that the inner horizon of Reissner Nordström is an artifact of extending a classical result to a region where quantum effects dominate and is rendered unphysical by QED effects. Application of QED should do that here also. At  $Q = 2M_0$ ,  $r_+ = r_-$ . For  $Q > 2M_0$ , we must solve Equation 4.59 with  $r_- = r_H$ . The solution still gives  $r_H = 2M_0$ . For all values of  $Q > 2M_0$ , the horizons  $r_{\pm}$  have merged to one value,  $r_{\pm} = 2M_0 = r_H$ . This means that the outermost horizon being located at  $2M_0$  is independent of the charge to mass ratio ( $Q/M_0 = \sigma$ ).

This is an important result, all charge to mass ratios are valid and do not form naked singularities. You will always get an event horizon because we have defined an intrinsic mass,  $M_0$ , which is the minimum perceived mass that an observer will see. Most black holes in the universe will have negligible charge, so to fully appreciate this result, it is important that we incorporate angular momentum  $J$ .



### 4.3.3 Adding Angular Momentum

We utilize the irreducible mass of Christodoulou [74], and Christodoulou and Ruffini [75] to incorporate angular momentum. Christodoulou and Ruffini calculated the amount of energy that could be extracted from a black hole. Their irreducible mass is the mass that is left over after all extractable energy has been removed. This is our “intrinsic” mass  $M_0$ . The formula, with  $M_{irr}$  replaced by  $M_0$  is,

$$M^2 = M_g^2 = \left( M_0 + \frac{Q^2}{2 \times 2M_0} \right)^2 + \frac{J^2}{(2M_0)^2}, \quad (4.60)$$

where we have introduced  $J$ , the angular momentum of the black hole. Notice, if you set  $J = 0$  we get the modified mass from Equation 4.56. We want to borrow the results of the irreducible mass calculation and put it into the metric to see if any naked singularities exist. The metric which describes a charged rotating black hole is the Kerr-Newman metric [76]. In Boyer Lindquist coordinates the metric has the form [77],

$$ds^2 = -\frac{\rho^2 \Delta}{\Sigma} dt^2 + \frac{\Sigma}{\rho^2} \sin^2 \theta (d\phi - \omega dt)^2 + \frac{\rho^2}{\Delta} dr^2 + \rho^2 d\theta^2, \quad (4.61)$$

where

$$\rho^2 = r^2 + a^2 \cos^2 \theta, \quad (4.62)$$

$$\Delta = r^2 - 2M_g r + Q^2 + a^2, \quad (4.63)$$

$$\Sigma = (r^2 + a^2)^2 - a^2 \Delta \sin^2 \theta, \quad (4.64)$$

$$\omega = a (r^2 + a^2 - \Delta) / \Sigma, \quad (4.65)$$

and  $a = J/M_g$ . The metric horizons are defined by,

$$\Delta = 0 = r^2 - 2M_g r + Q^2 + a^2. \quad (4.66)$$

The solution is

$$r_{\pm} = M_g \pm \sqrt{M_g^2 - Q^2 - a^2}. \quad (4.67)$$

The mass can be found using the equation of black hole “thermodynamics”,

$$\frac{\kappa}{8\pi}\delta A = \delta M - \Omega_H \delta J - V \delta Q, \quad (4.68)$$

with  $\Omega_H = \frac{a}{r_H^2 + a^2}$  defined as the black hole angular speed,  $V = \frac{Qr_H}{r_H^2 + a^2}$  the potential,  $A = 4\pi(r_H^2 + a^2)$  the area of the black hole, and  $\kappa = \frac{r_H - M_g}{r_H^2 + a^2}$  the surface gravity. In the specific problem we are considering, the variation of the entropy should be zero which means  $\delta A = 0$ . Integration of Equation 4.68 leads to the relation,

$$M_0 = \frac{1}{2}\sqrt{r_H^2 + a^2}. \quad (4.69)$$

If we let  $r_H = r_+$  as Christodoulou and Ruffini did, and then invert Equation 4.69 to solve for  $M_g$ , we arrive at Equation 4.60.

We on the other hand are concerned with the value of  $r_H$ , so we begin with Equation 4.69 and plug the solution of this into Equation 4.66, and then solve for  $r_H$ . The equation we solve is,

$$r^2 - 2M_g r + Q^2 + a^2 = r^2 - 2\left(\frac{J}{\sqrt{4M_0^2 - r_H^2}}\right)r + \frac{J^2}{\left(\frac{J}{\sqrt{4M_0^2 - r_H^2}}\right)^2} + Q^2 = 0. \quad (4.70)$$

If we set  $r = r_H$  in Equation 4.70 and then solve for  $r_H$  we arrive at,

$$r_H = \pm \frac{2M_0(4M_0^2 + Q^2)}{\sqrt{4J^2 + (4M_0^2 + Q^2)^2}}. \quad (4.71)$$

We are only concerned with the positive value which will give us the event horizon. Equation 4.71 reduces to  $r_H = 2M_0$  if we set  $J = 0$ , which is identical to our result from Equation 4.59. If we set  $Q = 0$ , we arrive at

$$r_H = \frac{2M_0^2}{\sqrt{M_0^2 + \frac{J^2}{4M_0^2}}}. \quad (4.72)$$

Equation 4.71 is the analytic expression of the outer horizon incorporating both charge  $Q$  and angular momentum  $J$ , and is valid for all values of  $J$  and  $Q$ . Now we must check that  $r_H \geq r_-$ .  $r_-$  can be solved from Equation 4.70, but instead of taking  $r_H = r$ , we simply solve for  $r$  holding  $r_H$  constant. This leads to 2 solutions and we will take the  $r_-$  solution. The  $r_+$  solution has already been calculated, it leads to  $r_H$ .  $r_-$  on the other hand is

$$r_- = \frac{4J^2 + (4M_0^2 + Q^2)^2 - |4J^2 - 16M_0^4 + Q^4|}{4M_0\sqrt{4J^2 + (4M_0^2 + Q^2)^2}}. \quad (4.73)$$

If  $Q^4 + 4J^2 > 16M_0^4$ , then  $r_H = r_-$ . If  $Q^4 + 4J^2 < 16M_0^4$ , then the ratio  $\frac{r_H}{r_-}$  is

$$\frac{r_H}{r_-} = \frac{16M_0^4 + 4M_0^2Q^2}{4J^2 + Q^4 + 4M_0^2Q^2}, \quad (4.74)$$

which is always more than 1 if  $Q^4 + 4J^2 < 16M_0^4$  is satisfied. Figures 4.5-4.7 are plots of  $r_H$  and  $r_-$  for various  $Q$  and  $J$ .

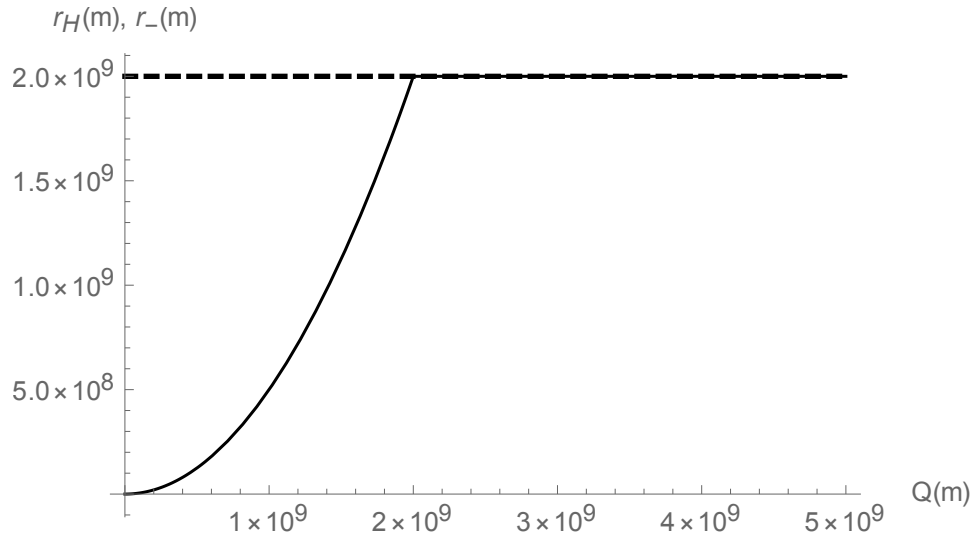


Figure 4.5: Plot of the horizons vs.  $Q$  for  $M_0 = 10^9 m$  and  $J = 0$ . The dashed line is  $r_H$  and the solid line is  $r_-$ .

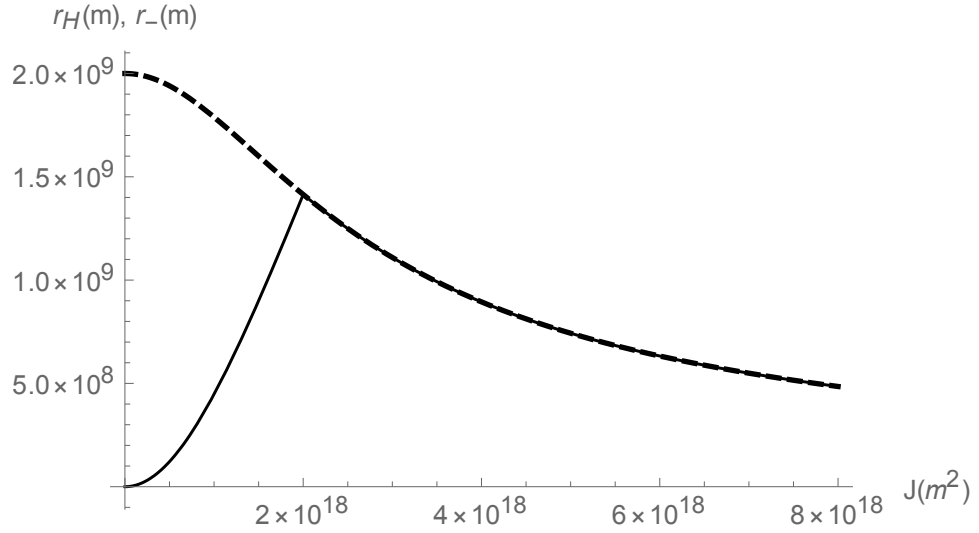


Figure 4.6: Plot of the horizons vs.  $J$  for  $M_0 = 10^9 m$  and  $Q = 0$ . The dashed line is  $r_H$  and the solid line is  $r_-$ .

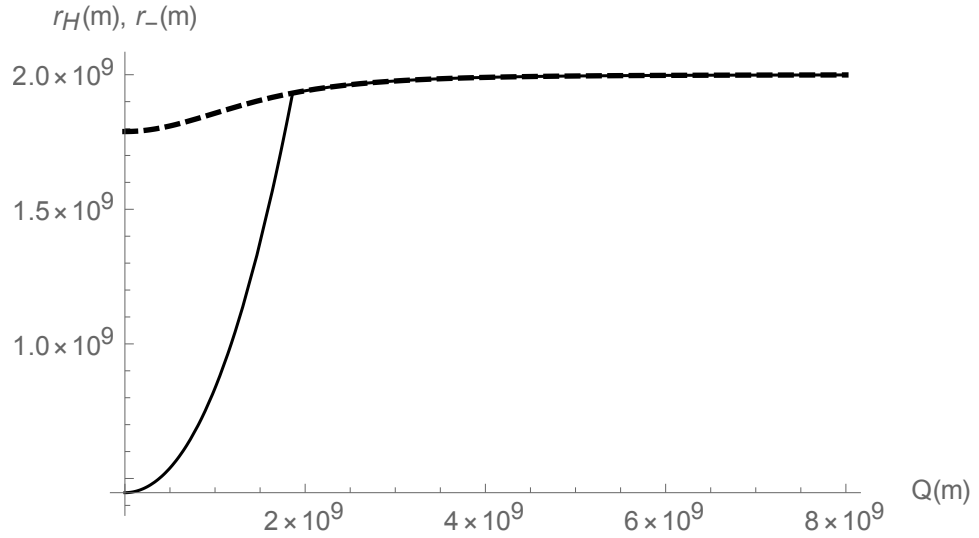


Figure 4.7: Plot of the horizons vs.  $Q$  for  $M_0 = 10^9 m$  and  $J = 10^{18} m^2$ . The dashed line is  $r_H$  and the solid line is  $r_-$ .

### 4.3.4 Naked Singularity Criteria

A black hole possessing an event horizon for all  $Q$  and  $J$  values is not surprising. The following relation must be true in order to have a “naked” singularity.

$$\left(\frac{a}{M_g}\right)^2 + \left(\frac{Q}{M_g}\right)^2 = a^{*2} + \sigma^2 > 1 \quad (4.75)$$

It turns out that Equation (4.75) is never greater than 1. It is only greater than 1 if you allow  $M_g$  to be independent of  $Q$  and  $J$ . However,  $M_g(Q, J)$  does depend on  $Q$  and  $J$  as shown in Equation 4.60. Figures 4.8-4.10 are plots of  $a^{*2} + \sigma^2$  for various  $Q$  and  $J$ .

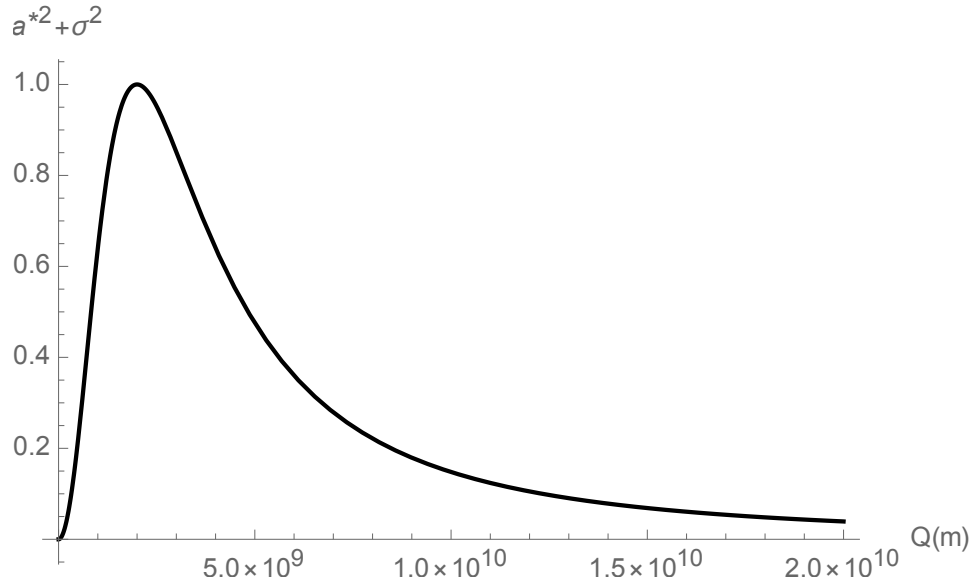


Figure 4.8: Plot of  $a^{*2} + \sigma^2$  vs.  $Q$  for  $M_0 = 10^9 m$  and  $J = 0$ .

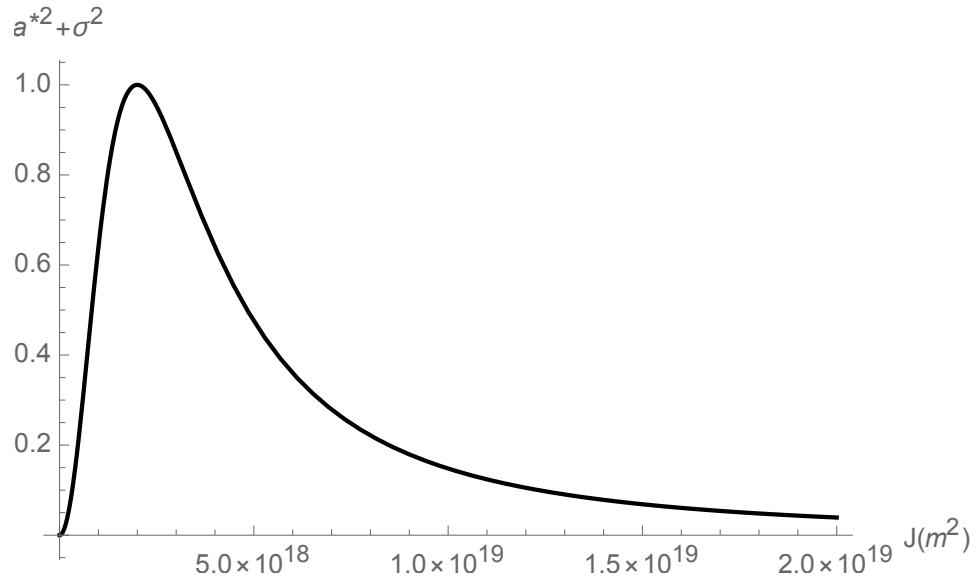


Figure 4.9: Plot of  $a^{*2} + \sigma^2$  vs.  $J$  for  $M_0 = 10^9 m$  and  $Q = 0$ .

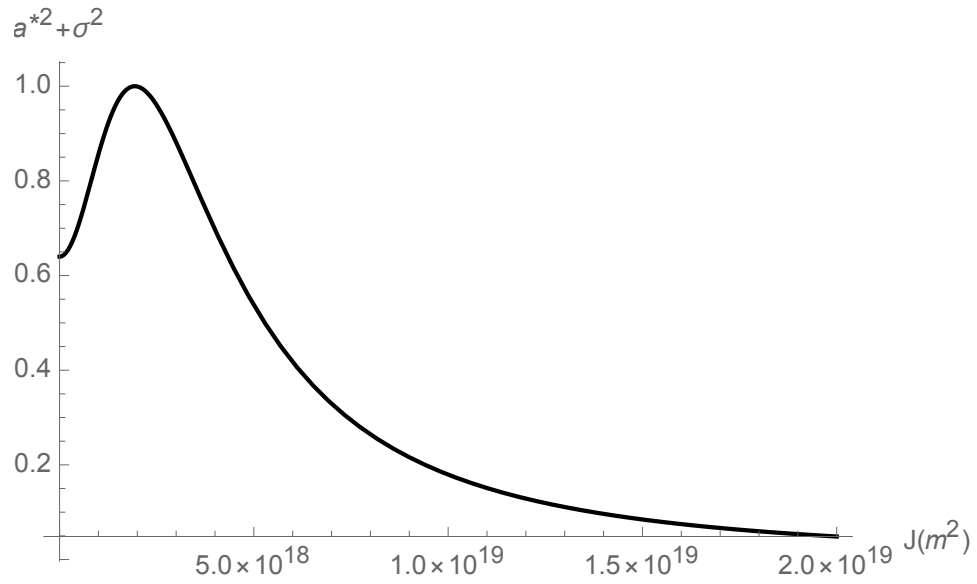


Figure 4.10: Plot of  $a^{*2} + \sigma^2$  vs.  $J$  for  $M_0 = 10^9 m$  and  $Q = 10^9 m$ .

### 4.3.5 Conclusion

In this section, we showed that naked singularities do not and cannot exist in nature.  $M_g$  depends on  $Q$  and  $J$  in such a way that the ratio  $a^{*2} + \sigma^2$ , will never be greater than 1. So, the criteria for having a naked singularity is never met. The reason why CTCs develop in other spacetimes such as the Gödel spacetime, is because they allow their mass as viewed from infinity to be independent of angular momentum  $J$  and charge  $Q$ . Allowing their masses to depend on  $J$  and  $Q$  as we did here, will remove the possibility of CTCs. There are no CTCs in the spacetime, and chronology is protected. For any given black hole with intrinsic mass  $M_0$ , you can add any  $J$  or  $Q$  that you want, and it will have a horizon. There is no such thing as over charging or over rotating a black hole. This does, however, neglect any internal forces such as Coulomb or centrifugal that may provide a limit, but the spacetime analysis does not provide a limit.

## 4.4 Application of QED To Modified Mass

The interesting thing about the result of having  $r_H = 2M_0$  with our approach of defining an intrinsic mass, is that it is valid for any  $M_E(r)$  that we plug into the system. That means it is valid for any  $\rho(r)$  and any Lagrangian  $\mathcal{L}$ , that we choose. This means that although we cannot at present go to full quantum mechanics, or go to any arbitrarily large  $n_{th}$  quantum correction, the result is still valid. Even though we may not know what  $\rho(r)$  might look like, we can still calculate the event horizon size as long as we know  $M_0$ . In this way, we can be sure that  $r_H = 2M_0$  is valid in every range without doing the explicit calculation.

Clearly, the result of  $2M_0$  always being the outer horizon, is going to be independent of the form of  $P(r)$ . This is because at  $r = r_H$ ,  $f(r)$  looks exactly like Schwarzschild. Thus, we are free to plug in any  $M_E(r)$  we want and we will get the same result. Quantum corrections are going to change the form of  $P(r)$ , but not the answer for the horizon, thus  $r_H = 2M_0$  is valid to all orders of quantum correction, which implies that it is valid for full quantum mechanics. (No insight is given here for

quantized gravity.) We will show that this is true for the  $M_E(r)$  that we calculated from QED. The difference for QED will be the absence of an inner horizon for small values of  $\sigma$ . Granted, it is harder to analyze because  $M_E(r)$  can only be calculated numerically. This is sufficient for what we need. We can also show that the development of a second horizon is always in a range where the equations, whether they be from Maxwell or QED, are not valid.

Here, we will show numerically for QED, that you get one real horizon for a black hole in the range of validity of the Lagrangian. We will use the following equations and solve for  $f(r) = 0$ . See Appendix B for details and the second order treatment of QED.

$$f(r) = 1 - \frac{2M(r)}{r}, \quad (4.76)$$

with

$$M(r) = M_0 + M_E(r_H) - M_E(r), \quad (4.77)$$

and

$$\frac{dM_E(r)}{dr} = -4\pi r^2 \left( \frac{e(r)^2}{8\pi} + \frac{3ae(r)^4}{4} + \frac{5Ae(r)^6}{8} \right), \quad (4.78)$$

with

$$e(r) + 4\pi ae(r)^3 + 3\pi Ae(r)^5 = \frac{Q}{r^2}. \quad (4.79)$$

We find the roots of  $f(r)$  using FindRoot[] in Mathematica, doing a search from the top and bottom. Here are plots of the roots of  $f(r)$  vs.  $(Q/M_0)$ .



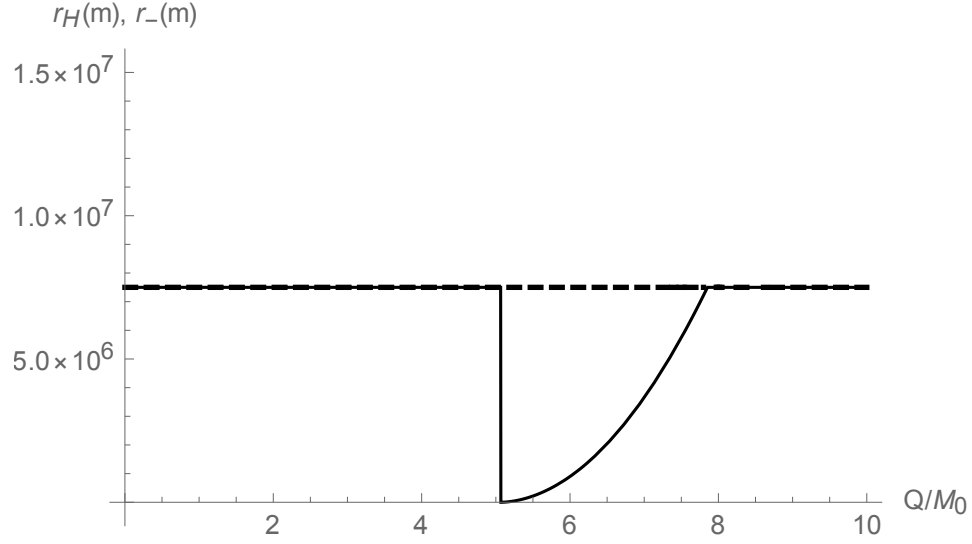


Figure 4.11: Plot of the roots of  $f(r)$  in meters vs.  $\frac{Q}{M_0}$  for  $M_0 = 2.5 \times 10^3 M_\odot$

To gain better insight, we plot these same roots as a  $\log(r)$  vs.  $\sigma$  along with the regions where the Lagrangian used is not valid. Here,  $\sigma = Q/M_0$ . We have included the regions  $\mathcal{L}_a > \mathcal{L}_{EM}$ ,  $\mathcal{L}_g > \mathcal{L}_a$ , and  $\mathcal{L}' > \mathcal{L}_a$ , where  $\mathcal{L}_a = a\mathcal{F}^2$ ,  $\mathcal{L}' = -b \left[ 18F^{\mu\nu}F_{\mu\nu,\alpha}^\alpha + 7F^{\mu\nu,\alpha}F_{\mu\nu,\alpha} - 2F^{\mu\nu}_{,\nu}F_{\mu\lambda}{}^{,\lambda} \right]$  and  $\mathcal{L}_g = -9bR_{\mu\nu\alpha\beta}F^{\mu\nu}F^{\alpha\beta}$ , where  $a = \frac{8\alpha^2\hbar^3}{45(4\pi)^2m_e^4cG} = 5.06 \times 10^{12}$  and  $b = \frac{\alpha\hbar^2}{180(4\pi)^2m_e^2c^2} = 3.8 \times 10^{-32}$  [78], [79], [80]. We do not include  $\mathcal{L}_g$  or  $\mathcal{L}'$  in our analysis and we show the invalid regions to show that we are justified in neglecting these terms.

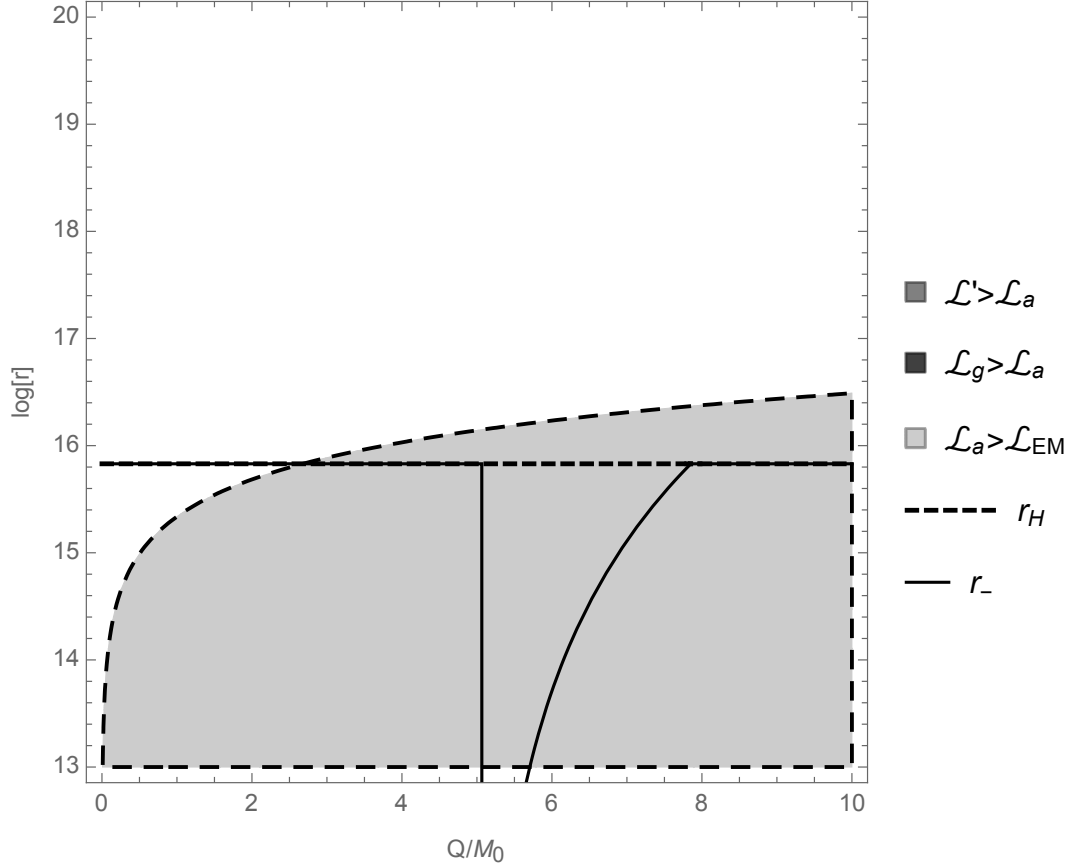


Figure 4.12: Plot of invalid regions as a  $\log(r)$  vs.  $\sigma$  plot for a  $M_0 = 2.5 \times 10^3 M_\odot$  blackhole. Here we chose  $2.5 \times 10^3 M_\odot$  because at only  $10^3 M_\odot$ ,  $r_H$  becomes invalid at  $\sigma > 1$ . The regions  $\mathcal{L}_g > \mathcal{L}_a$  and  $\mathcal{L}' > \mathcal{L}_a$  are outside of this plot window.

From Figures 4.11 and 4.12, we see that we get a similar result as the Maxwell only analysis. The key difference here is that for small enough charge to mass ratios, there is only one horizon. There is a region that has two horizons, much like the Maxwell analysis, however the specific Lagrangian being used is not valid in this region. We note here that Maxwell is also not valid in this region. For details on when specific Lagrangian corrections are valid see Appendix A. If we go to larger black holes in the  $10^6 M_\odot$  range, we see that there is a small range where the inner horizon seems to be valid. See Figures 4.13, 4.14, and 4.15.

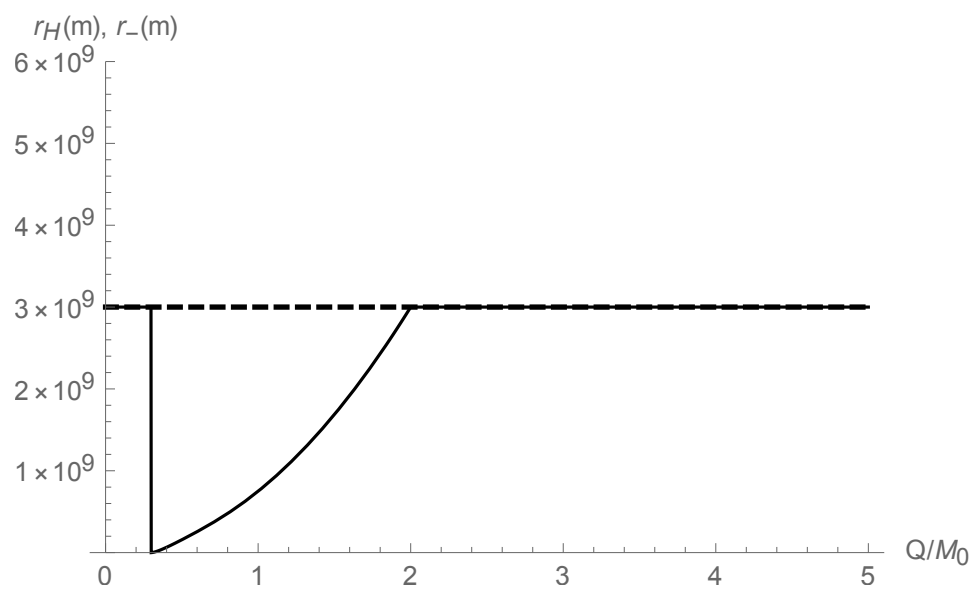


Figure 4.13: Plot of the roots of  $f(r)$  in meters vs.  $\frac{Q}{M_0}$  for  $M_0 = 10^6 M_\odot$

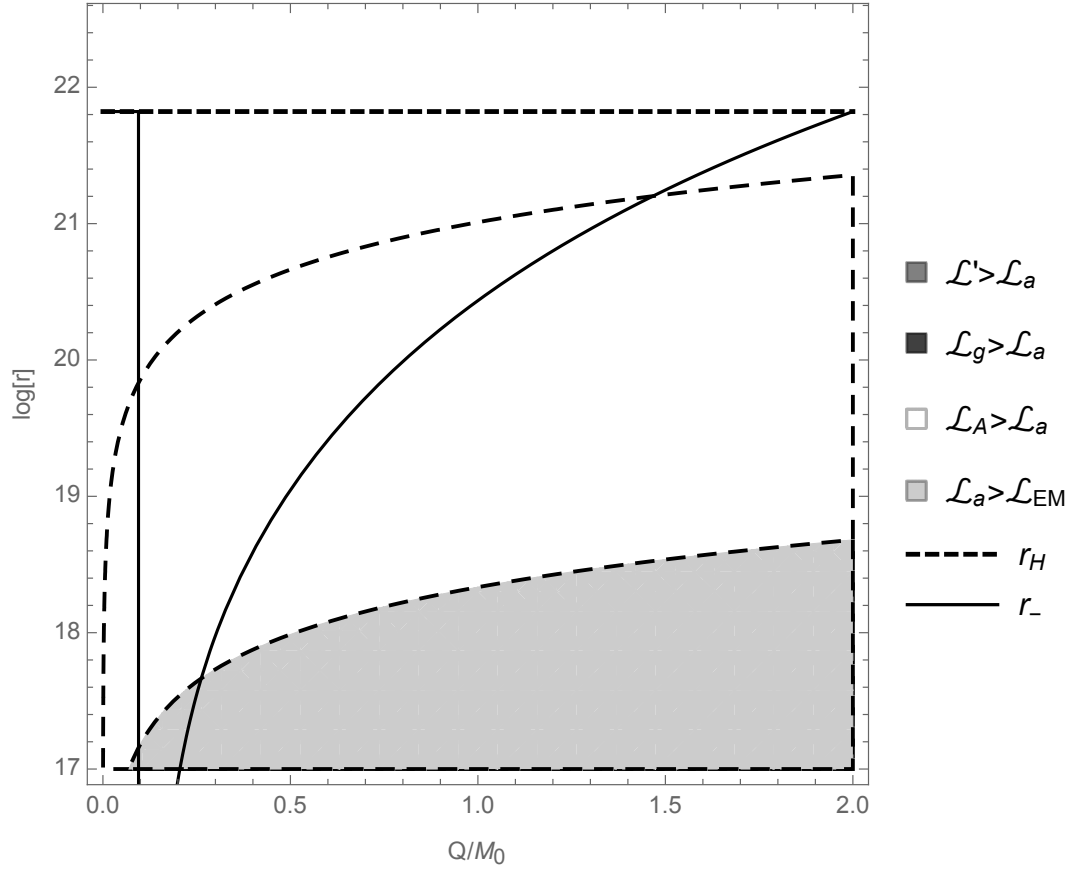


Figure 4.14: Zoomed in version of the Plot of invalid regions as a  $\log(r)$  vs.  $\sigma$  plot for a  $M_0 = 10^6 M_\odot$  black hole. Here  $A = 0$ . The regions  $\mathcal{L}_g > \mathcal{L}_a$  and  $\mathcal{L}' > \mathcal{L}_a$  are outside of this plot window.

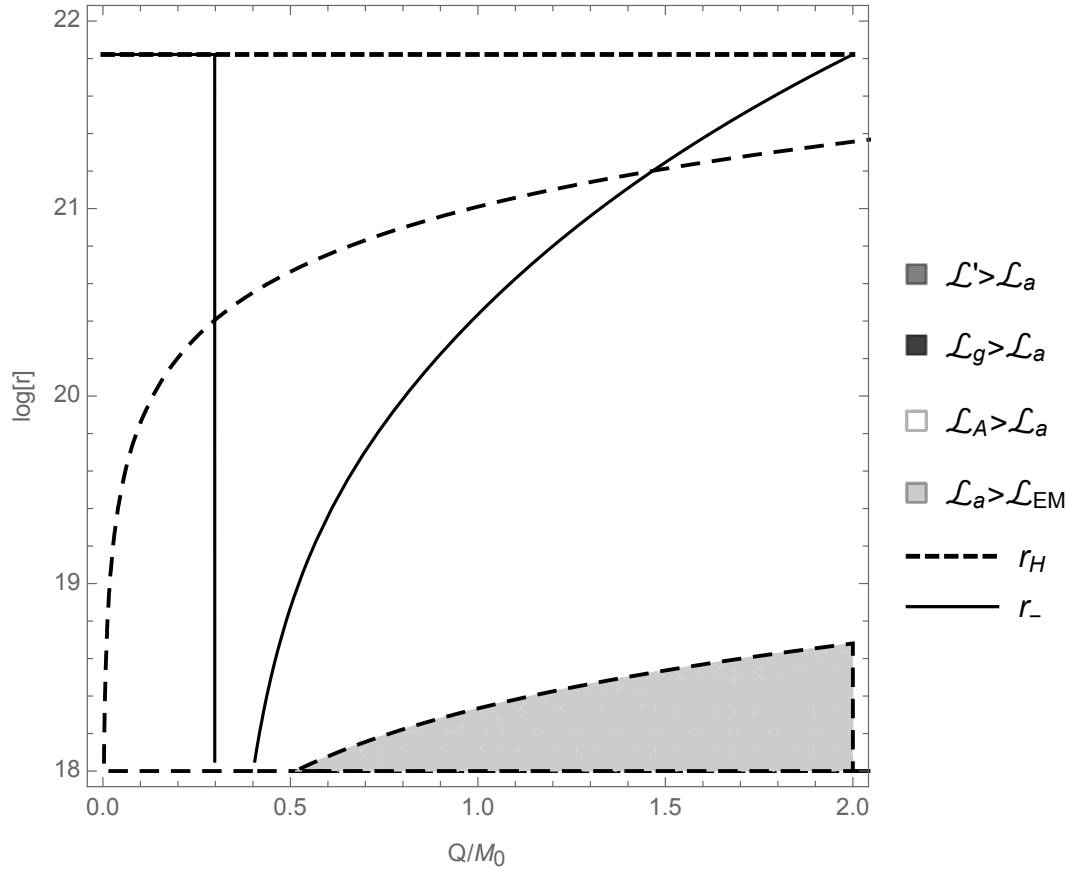


Figure 4.15: Zoomed in version of the Plot of invalid regions as a  $\log(r)$  vs.  $\sigma$  plot for a  $M_0 = 10^6 M_\odot$  black hole. The regions  $\mathcal{L}_g > \mathcal{L}_a$  and  $\mathcal{L}' > \mathcal{L}_a$  are outside of this plot window.

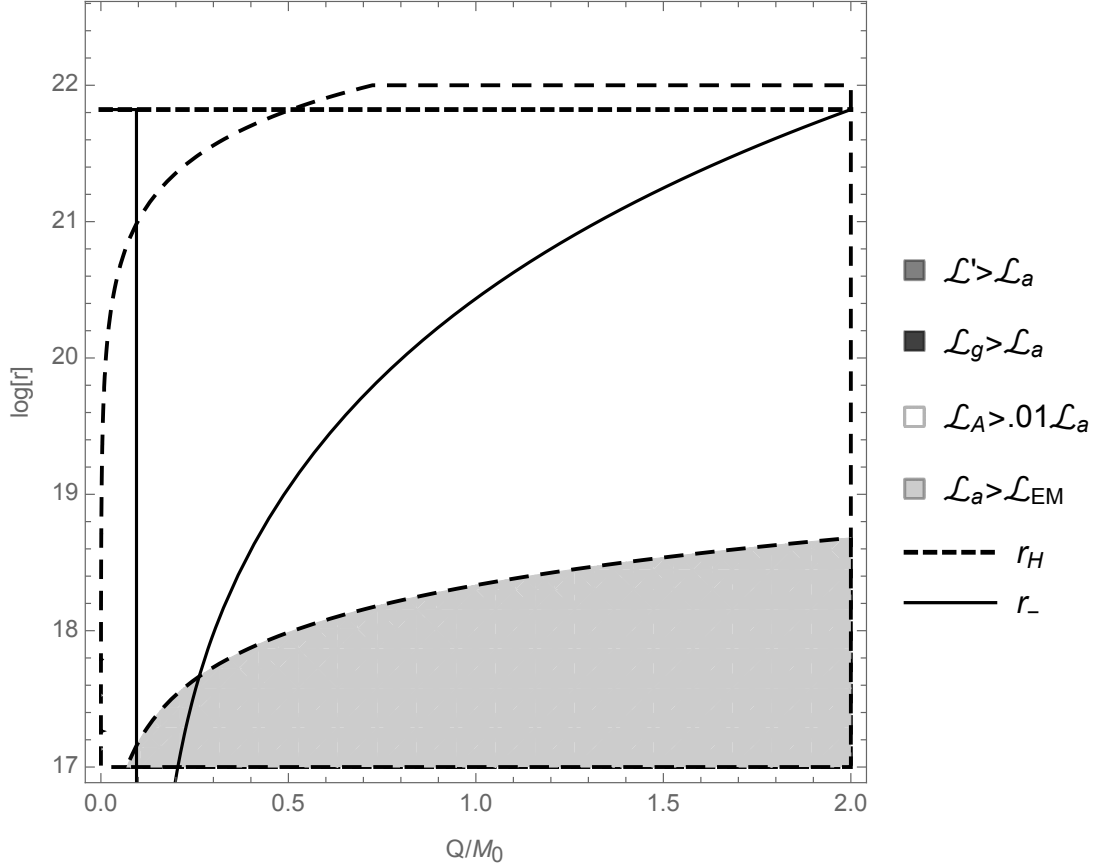


Figure 4.16: Zoomed in version of the Plot of invalid regions as a  $\log(r)$  vs.  $\sigma$  plot for a  $M_0 = 10^6 M_\odot$  black hole. The regions  $\mathcal{L}_g > \mathcal{L}_a$  and  $\mathcal{L}' > \mathcal{L}_a$  are outside of this plot window.

The valid region was defined using  $\mathcal{L}_A < \mathcal{L}_a$ , where  $\mathcal{L}_A = -A\mathcal{F}^3$ , with  $A = \frac{128\alpha\hbar^3}{28Gm_e^4c}a = 1.4 \times 10^{31}$ . This was a loose criterion. What we really need is  $\mathcal{L}_A < \mathcal{L}_a$ . Even if we use the criteria,  $\mathcal{L}_A < .01\mathcal{L}_a$ , then the entire region where the double root exists is now well within the invalid region, see Figure 4.16. We have shown here, that within the region in which our Lagrangian is valid, there are no naked singularities and there are no Cauchy horizons. Thus, we have shown that applying a modified mass approach combined with QED removes 2 of the 3 black hole problems.

The meaning might be deeper than this. We cannot show it directly here, but if we look at Figures 4.14 and 4.15, which are the same plot one with the second order correction applied and one without it, we see that the higher order correction makes the window in which you have an inner horizon smaller. The first order shrinks the window, and the second order correction shrinks it even further. It seems reasonable to assume that an  $n = \infty$  order correction, or a non-perturbative treatment, will remove that window entirely. We cannot show that this is true because that would require an application of full quantum mechanics and not just an effective theory approach. But this gives us an insight into how quantum mechanics removes problematic areas of the spacetime.

Next, we show that the charge to gravitating mass ratio  $Q/M_g$  can become larger than one when you model the system in QED. The figure of merit we are interested in is,

$$\sigma = \frac{Q}{M_g} = \frac{Q}{M_0 + M_E(r_H)}. \quad (4.80)$$

Figures 4.17 - 4.20 are plots of charge to mass ratio for QED. We plot  $\frac{Q}{M_g}$  vs.  $\frac{Q}{M_0}$  for various masses.

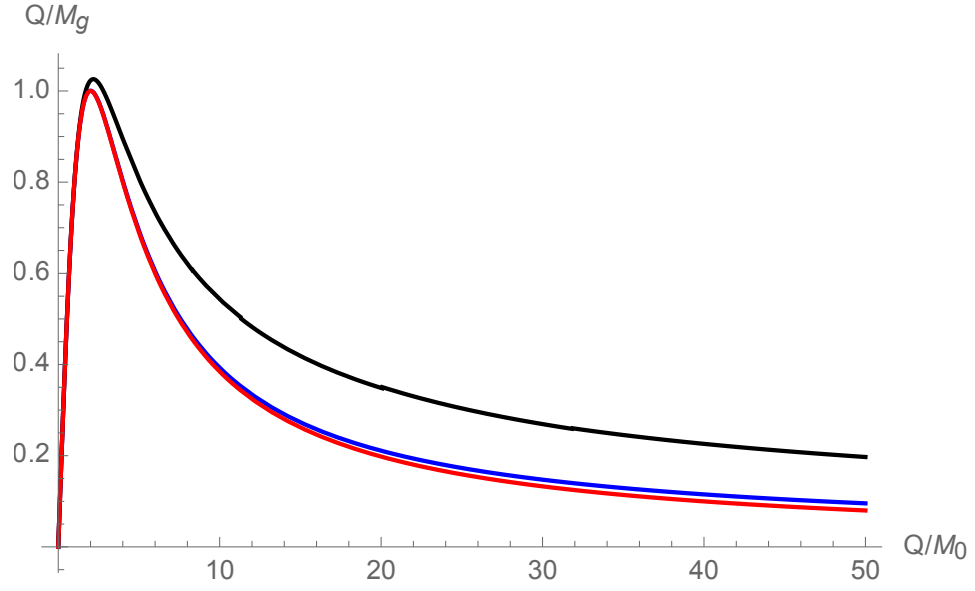


Figure 4.17: Plot of  $\frac{Q}{M_g}$  vs.  $\frac{Q}{M_0}$  for  $M_0 = 10^4 M_\odot$ .  $a = A = 0$  in Red,  $A = 0$  in Blue, and  $a, A \neq 0$  in Black.

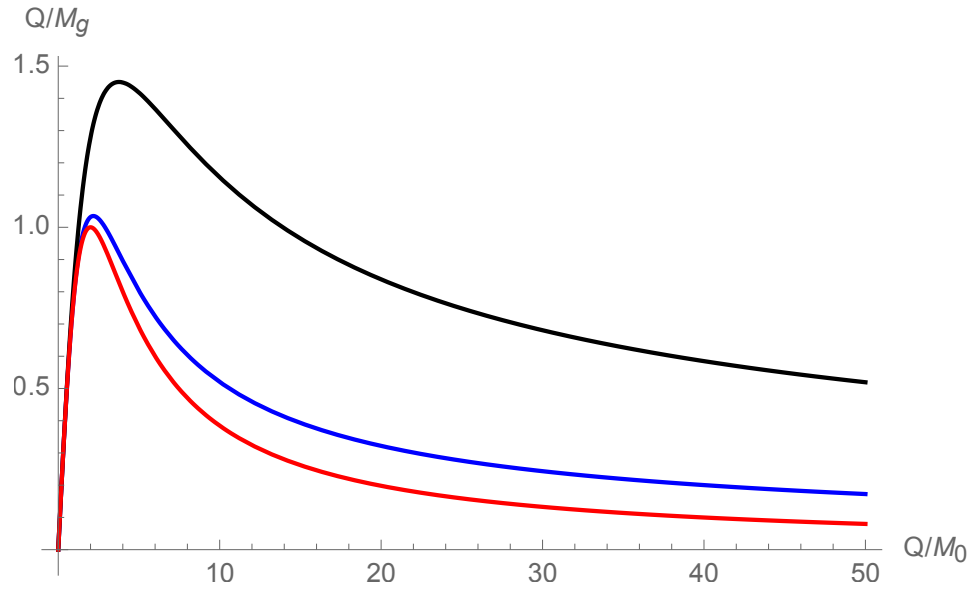


Figure 4.18: Plot of  $\frac{Q}{M_g}$  vs.  $\frac{Q}{M_0}$  for  $M_0 = 2.5 \times 10^3 M_\odot$ .  $a = A = 0$  in Red,  $A = 0$  in Blue, and  $a, A \neq 0$  in Black.



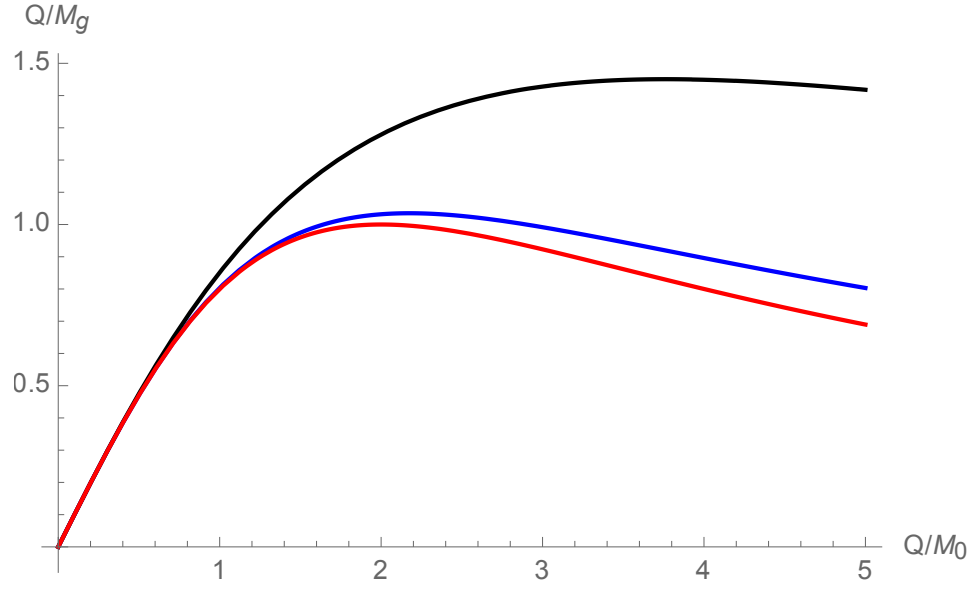


Figure 4.19: Plot of  $\frac{Q}{M_g}$  vs.  $\frac{Q}{M_0}$  for  $M_0 = 2.5 \times 10^3 M_\odot$ .  $a = A = 0$  in Red,  $A = 0$  in Blue, and  $a, A \neq 0$  in Black.

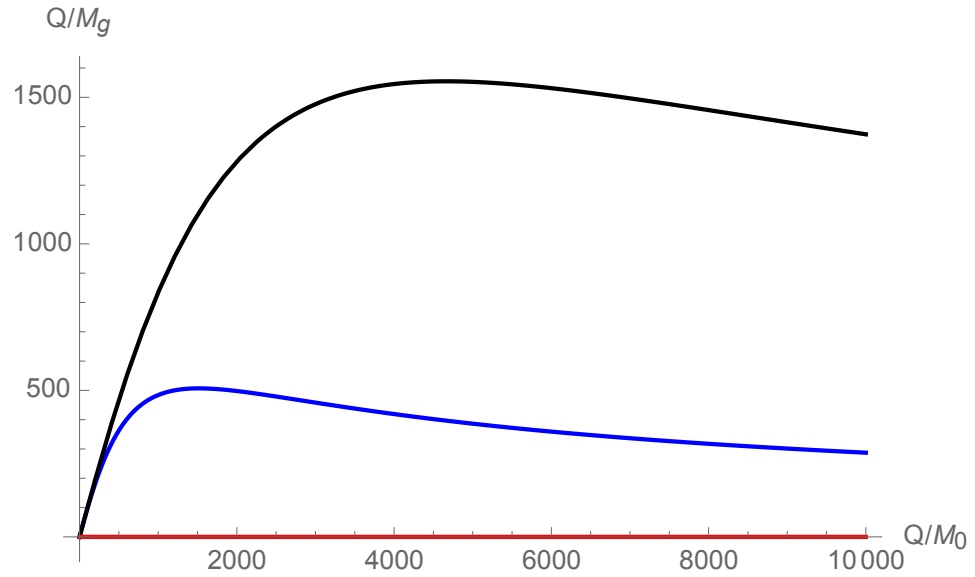


Figure 4.20: Plot of  $\frac{Q}{M_g}$  vs.  $\frac{Q}{M_0}$  for  $M_0 = 10^{-6} M_\odot$ .  $a = A = 0$  in Red,  $A = 0$  in Blue, and  $a, A \neq 0$  in Black.

From these graphs and the validity ranges in Figures 4.12 and 4.16, we see that no black hole will give us a  $\frac{Q}{M_g}$  value greater than 1 in the range in which our Lagrangian is valid.

In this section, we have shown that QED corrections tend to remove the Cauchy horizons of black holes. We see that higher order corrections do allow for  $Q/M_g > 1$  and even very large values of  $\sigma$  for small black holes. However, this does not mean that a naked singularity will develop, since the criteria for having a naked singularity will change when applying QED. Additionally, we also showed that our approach of defining an intrinsic mass for the black hole removes the possibility of having  $Q/M_g > 1$  in a range where the Lagrangian being used is valid. This says nothing about full quantum mechanics. Full quantum mechanics will be needed to allow us to do any valid analysis for the smaller black holes that allow for  $Q/M_g > 1$ .

# Chapter 5

## Conclusions and Future Direction

The main conclusions from my dissertation are summarized below:

- Threshold conditions for the single cavity dynamical Casimir effect were calculated, and it turns out that the threshold is too high for current experiments. A membrane or other moving boundary condition is needed with higher resonant frequency.
- Threshold conditions for the double cavity dynamical Casimir effect were calculated, and it turns out that the threshold is too high for the  $\omega_d = \omega_1 + \omega_2$  case for current experiments. In the  $\omega_d = \omega_2 - \omega_1$  case, the threshold was so large that it was physically impossible to achieve.
- The Raman effect was shown to be a reasonable experiment to study in our lab.
- Gravitational waves were shown to interact with superconductors by imparting energy to them.
- Black holes formulated using QED were shown to only have a single horizon. This solved the mass inflation instability problem.
- Black holes formulated using the irreducible mass approach, were shown to possess a horizon independent of their charge or mass. This solved the naked singularity problem and protected chronology.

- Black holes formulated using QED and the irreducible mass approach, within a valid limit, were shown to never become naked singularities and never possess an inner Cauchy horizon.

## 5.1 Future Direction

One of the main goals of the Chiao-Sharping collaboration has been to generate and detect gravitational waves. Most of the time, the road block to understanding how to achieve this goal was a lack of knowledge of quantum optomechanics, of general relativity, or of the interplay between quantum mechanics and general relativity. With this in mind, it is always important to gain insights into quantum mechanics and gravity whenever and however we can.

In this chapter, I will discuss future directions that can be taken to explore new physics.

### 5.1.1 Double Cavity 2 Photon Raman-DCE

In Section 2.6.2 we discussed the result of a recent paper where they look at a modified dynamical Casimir effect. I dismissed the idea as a glorified Raman effect. However, we could do this experiment in the lab. We have good single cavities that we can couple to membranes. Most of the equipment in the lab has a frequency limit of 12 GHz, so the input signal  $\omega_l$  would need to be at most 12 GHz. Since the equation for resonance is  $\omega_l + \omega_m = 2\omega_c$ , we would need our cavity frequencies to be  $\sim 6$  GHz. This means we would need to make larger cavities. To reach 6 GHz we would need  $L_z \sim R \sim 4$  cm. This cavity would still fit in the dilution refrigerator, the cylindrical chamber connected to the 50 mK plate has a radius of 8.5 cm and a length of 17 cm. Even with circulators and cabling there is plenty of space for not one but two, maybe even three 6 GHz cavities.

For the proposed experiment, you would need two cavities. One to drive the membrane at the membranes resonance, and one to perform the actual DCE. The system would be identical to Figure 2.1. You insert an amplitude modulated 6 GHz

signal into the pump cavity, the amplitude is modulated at the resonant frequency of the membrane,  $\omega_m$ . A 12 GHz signal is input into the signal/idler cavity. Under the resonant condition,  $\omega_l + \omega_m = 2\omega_c$ , you should see an output of correlated photons from the cavity with a frequency of 6 GHz.

Another experiment that can be performed in the lab is a double cavity 2 photon Raman-DCE. This experiment will be similar to the single cavity case, but we will instead implement the design of Figure 2.2. In this case we have two resonant conditions that we want to satisfy,  $\omega_l + \omega_m = \omega_1 + \omega_2$  and  $\omega_2 - \omega_1 = \omega_m$ . This allows for a method of easily separating the coupled photon output, which could lead to interesting insights into the photon correlation. Additionally, we could put another input at the frequency  $\omega_2$ . It is clear, from the work of Reece [20], that if you input a signal at the resonance  $\omega_2$ , you will get transduction from sideband generation, a 1 photon Raman like process. What is unclear is whether driving at both  $\omega_l$  and  $\omega_2$  will increase or decrease either the 1 photon or 2 photon Raman processes. In principle you should get both processes occurring.

### 5.1.2 Noise from Gravitational Wave Signals

One thing we can do that combines gravity and quantum optics is to look at LIGO data. One interesting thing that is unexplained so far about the LIGO data, is that in the first two events, as reported in [81], the noise between two different detectors were correlated. This seems to be a problem because noise in two different detectors should not be correlated at all, unless the signal that they are detecting is of a quantum mechanical nature. So what I am proposing is, if gravity is quantized it could explain the fact that the noise is correlated. If the signal is made up of gravitons then it will have shot noise which would lead to correlated noise in the motion of the detectors.

Additionally, the magnitude of the noise may be a way that we can place limits on the value of  $\hbar$  for gravity. We could make a model that incorporates some generic type of shot noise with some unspecified constant like  $\hbar_g$ , that would explain the correlations. We could then use the LIGO data to put limits on what  $\hbar_g$  could be.

Recently, Pang has worked on the question of whether you can use LIGO data to distinguish between the classical and quantum nature of a gravitational wave signal [82], [24]. Pang has done a very good job providing a framework here. While she does not address the question of  $\hbar$ , she does formulate the quantum back action of the gravitational wave on the mirrors of LIGO. In addition to the work by Pang, Bose and Grishchuk also showed that relic gravitational waves will have squeezing that can be observed in the laboratory [83]. So if we can develop a method for detecting relic gravitational waves, these waves will also have a squeezed signature if gravity is quantized.

### 5.1.3 A Comment on “Zero” Mass Black Holes

Suppose an object has no “bound, trapped, intrinsic mass” (This may be the case for elementary particles like the electron. Clearly weak and strong energies will be bound/trapped energies though.). If in the analysis that we did without rotation, if there is no intrinsic mass i.e.  $M_0 = 0$ , then the solution for  $f(r) = 0$  is valid only for  $r_H \rightarrow 0$ . Now,  $f(r) \rightarrow 0$  as  $(r \rightarrow 0 \text{ and } r_H \rightarrow 0)$ . This is a little different from the classical case in which  $f(r) \rightarrow -\infty$  as  $r \rightarrow 0$ . We do have a coordinate singularity, and a calculation of the Kretschmann scalar reveals that we have a true curvature singularity at  $r = 0$ . But are we naked? Yes and No,  $r_H \rightarrow 0$ , this is different from having a regular naked singularity where there is no horizon. In this case our horizon is at  $r = 0$ . This means that at the very least, we do not get CTCs like we would in regular naked singularities. But, there is an open ended question here, “can a point singularity be covered by a point shell?”

Right now we sit at an exciting era for general relativity and quantum mechanics. With the recent discoveries in the last few years, (the measurement of gravitational waves, and the imaging of a blackhole event horizon, [30], [37]), we have many new tools at our disposal for experimentally probing the interface between general relativity and quantum mechanics. Similar to when the laser was discovered, a lot of new and exciting research into fundamental physics is surely upon us.

# Appendix A

## Lagrangian Analysis

### A.1 Lagrangian Validity Analysis

In the beginning, I thought that the naked singularity problem was a result of using classical physics too close to the singularity. Indeed, this may be the case, however we show in Appendix B, that at present we do not have adequate quantum corrections to deal with this problem. We will discuss this problem in detail in Appendix B. Basically, no effective Lagrangian approach is valid for  $Q > M_g$ . In fact, in this Appendix I show that the classical result is not valid either. In fact, the classical result becomes invalid well before the QED effective Lagrangian becomes invalid. So while the QED result should be taken with some skepticism, we have shown that if we cannot accept the QED result, then we never should have trusted the classical result to begin with. Recall that the classical result would put  $r_+$  at  $r = 0$ . Clearly at this distance, full quantum effects matter and the classical result cannot be trusted. So, although the QED result is also not valid in the region of its predicted outer horizon, it is at least more valid than the classical result. Below we will show detailed calculations of the various Lagrangian terms that electromagnetism can have.

NOTE: Using the approach used in Section 4.3, both Maxwell and QED become valid for  $Q > M_0$ .

### A.1.1 Units

Units are always the hardest thing to deal with. In most of our published work we will use HSL units which is the standard practice of particle physics, but for calculations we use geometrized units. To be thorough we will also show SI units. The different types of Lagrangian terms that can be added to Maxwell can be found in the following very nice papers, [78], [79] and [80].

#### HSL

In Heaviside Lorentz units, the electromagnetic Lagrangian density has the simple form,

$$\mathcal{L}_{EM} = -\mathcal{F}, \quad (\text{A.1})$$

with

$$\mathcal{F} = \frac{1}{4}F^{\mu\nu}F_{\mu\nu} = -\frac{1}{2}e(r)^2, \quad (\text{A.2})$$

and

$$e(r)_{EM} = \frac{Q}{4\pi r^2}. \quad (\text{A.3})$$

Here, the subscript EM will always signify classical results. The first order QED correction is,

$$\mathcal{L}_a = a\mathcal{F}^2, \quad (\text{A.4})$$

with

$$a = \frac{8\alpha^2}{45m_e^4}. \quad (\text{A.5})$$

The dominant curvature term goes as [80],

$$\mathcal{L}_g = -9bR_{\mu\nu\alpha\beta}F^{\mu\nu}F^{\alpha\beta}, \quad (\text{A.6})$$

with

$$b = \frac{\alpha}{720\pi m_e^2}. \quad (\text{A.7})$$



The first order derivative term looks like [78],

$$\mathcal{L}' = -b \left[ 18F^{\mu\nu} F_{\mu\nu,\alpha}{}^\alpha + 7F^{\mu\nu,\alpha} F_{\mu\nu,\alpha} - 2F^{\mu\nu}{}_{,\nu} F_{\mu\lambda}{}^{,\lambda} \right]. \quad (\text{A.8})$$

For thoroughness, we will also write down the 2nd order QED correction which is [79],

$$\mathcal{L}_A = -A\mathcal{F}^3, \quad (\text{A.9})$$

with

$$A = \frac{128\pi\alpha}{7m_e^4}a. \quad (\text{A.10})$$

## SI

The equations in SI units are the following.

$$\mathcal{L}_{EM} = \frac{-\mathcal{F}}{\mu_0} \quad (\text{A.11})$$

$$\mathcal{F} = \frac{1}{4}F^{\mu\nu}F_{\mu\nu} = -\frac{1}{2}\frac{e(r)^2}{c^2} \quad (\text{A.12})$$

$$e(r)_{EM} = \frac{Q}{4\pi\epsilon_0 r^2} \quad (\text{A.13})$$

$$a = \frac{8\alpha^2\hbar^3\epsilon_0^2}{45m_e^4c} \quad (\text{A.14})$$

$$b = \frac{\alpha\hbar^2\epsilon_0}{720\pi m_e^2} \quad (\text{A.15})$$

$$A = \frac{128\pi\alpha\hbar^3\epsilon_0}{7m_e^4c^3}a \quad (\text{A.16})$$

## Geometrized

The equations in Geometrized units are the following.

$$\mathcal{L}_{EM} = \frac{-\mathcal{F}}{4\pi} \quad (\text{A.17})$$

$$\mathcal{F} = \frac{1}{4}F^{\mu\nu}F_{\mu\nu} = -\frac{1}{2}e(r)^2 \quad (\text{A.18})$$

$$e(r)_{EM} = \frac{Q}{r^2} \quad (\text{A.19})$$

$$a = \frac{8\alpha^2\hbar^3}{45(4\pi)^2m_e^4cG} = 5.06 \times 10^{12} \quad (\text{A.20})$$

$$b = \frac{\alpha\hbar^2}{180(4\pi)^2m_e^2c^2} = 3.8 \times 10^{-32} \quad (\text{A.21})$$

$$A = \frac{128\alpha\hbar^3}{28Gm_e^4c}a = 1.4 \times 10^{31} \quad (\text{A.22})$$

### A.1.2 The leading terms in each piece of the Lagrangian

In this section we will compare the Lagrangians. We will stick to Geometrized units.

We will assume that the leading term in  $e(r)$  is  $Q/r^2$ .

$$\mathcal{L}_{EM} = \frac{-\mathcal{F}}{4\pi} = \frac{1}{8\pi}e(r)^2 = \frac{Q^2}{8\pi r^4} \quad (\text{A.23})$$

$$\mathcal{L}_a = a\mathcal{F}^2 = a\frac{1}{4}e(r)^4 = \frac{aQ^4}{4r^8} \quad (\text{A.24})$$

$$\mathcal{L}_g = -b9R_{\mu\nu\alpha\beta}F^{\mu\nu}F^{\alpha\beta} = -b9(R_{0101}F^{01}F^{01} + R_{0110}F^{01}F^{10} + R_{1001}F^{10}F^{01} + R_{1010}F^{10}F^{10}) \quad (\text{A.25})$$

$$\mathcal{L}_g = \frac{72bM_gQ^2}{r^7} \quad (\text{A.26})$$

$$\mathcal{L}' = -b \left[ 18F^{\mu\nu}F_{\mu\nu,\alpha}{}^\alpha + 7F^{\mu\nu,\alpha}F_{\mu\nu,\alpha} - 2F^{\mu\nu}{}_{,\nu}F_{\mu\lambda}{}^{,\lambda} \right] \quad (\text{A.27})$$

The math here will not fit nicely so I will just put the result.

$$\mathcal{L}' = 256b\frac{Q^2}{r^6} \quad (\text{A.28})$$

$$\mathcal{L}_A = -A\mathcal{F}^3 = \frac{A}{8}e(r)^6 = \frac{AQ^6}{8r^{12}} \quad (\text{A.29})$$

### A.1.3 The inequalities

We want  $\mathcal{L}_{EM}$  to be the dominant term, then after that, we want  $\mathcal{L}_a$  to dominate. We will solve for the regions in which this is not satisfied.

#### A.1.4 $\mathcal{L}' \ll \mathcal{L}_{EM}$

$\mathcal{L}' \ll \mathcal{L}_{EM}$  is not valid when,

$$r < \sqrt{2048\pi b}. \quad (\text{A.30})$$

Notice that this is an absolute limit. If we go below this we are in trouble. It is independent of charge and mass. Its numeric value is  $1.56 \times 10^{-14}$  m.

#### A.1.5 $\mathcal{L}_a \ll \mathcal{L}_{EM}$

$\mathcal{L}_a \ll \mathcal{L}_{EM}$  is not valid when,

$$r < (2\pi a Q^2)^{1/4}. \quad (\text{A.31})$$

#### A.1.6 $\mathcal{L}_g \ll \mathcal{L}_a$

$\mathcal{L}_g \ll \mathcal{L}_a$  is not valid when,

$$r > \frac{aQ^2}{4 \times 72bM_g}. \quad (\text{A.32})$$

#### A.1.7 $\mathcal{L}' \ll \mathcal{L}_a$

$\mathcal{L}' \ll \mathcal{L}_a$  is not valid when,

$$r > \sqrt{\frac{aQ^2}{4 \times 256b}}. \quad (\text{A.33})$$

These inequalities can be displayed quite nicely as a log plot. The plot of  $r_+$  here is simply  $\log(2M_0)$ .

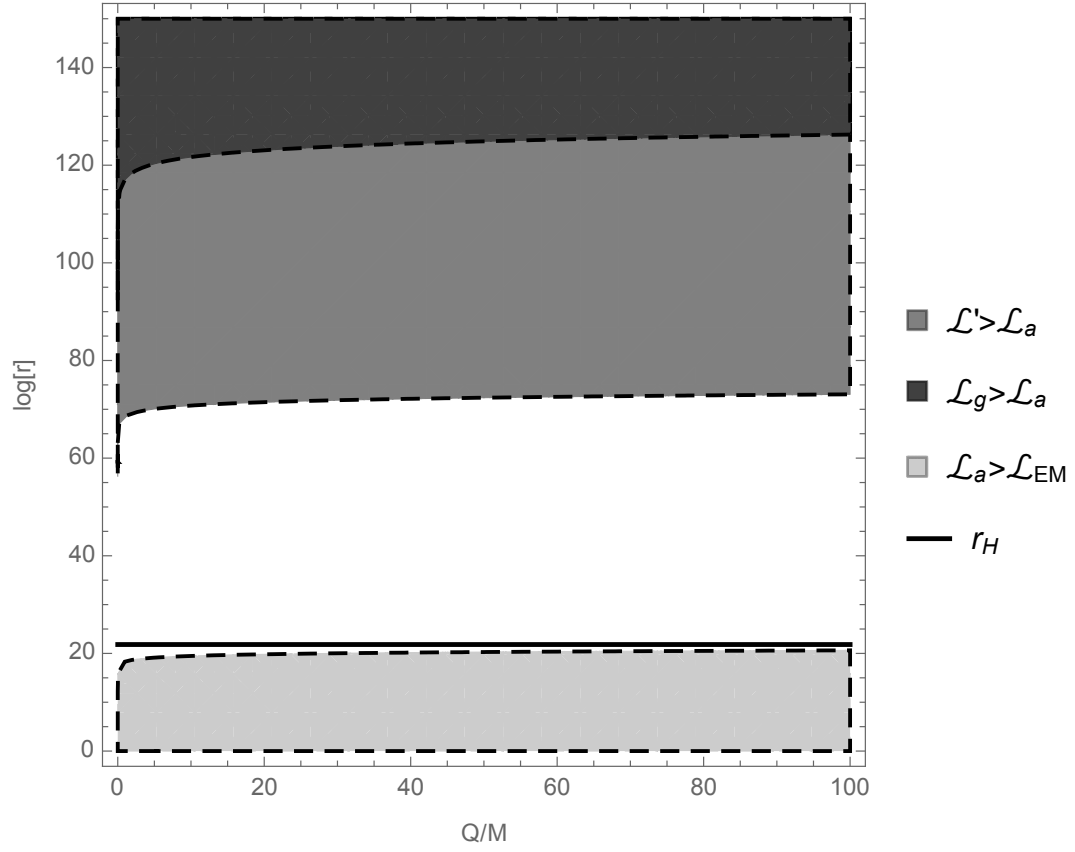


Figure A.1: Plot of invalid regions as a  $\log(r)$  vs.  $\sigma$  plot for a  $M_0 = 10^6 M_\odot$  blackhole. Here  $r_H = 2M_0$ . The region where our analysis is valid is the unshaded region.

We will come back to this plot when we analyze our solutions.

# Appendix B

## QED Analysis

### B.1 First and Second Order QED

In this Appendix, we analyze the first and second order QED corrections to show that effective theories are not capable of solving the naked singularity problem alone. We begin with a spherically symmetric time independent metric of the form,

$$ds^2 = -f(r)dt^2 + \frac{dr^2}{f(r)} + r^2d\Omega^2, \quad (\text{B.1})$$

with

$$f(r) = 1 - \frac{2M}{r} + \frac{2P(r)}{r}. \quad (\text{B.2})$$

Einstein's equations and the constraint equations allow us to write  $P(r)$  and  $e(r)$ , the modified electric field as,

$$\frac{dP(r)}{dr} = -4\pi r^2 \left( \frac{e(r)^2}{8\pi} + \frac{3ae(r)^4}{4} + \frac{5Ae(r)^6}{8} \right), \quad (\text{B.3})$$

with

$$e(r) + 4\pi ae(r)^3 + 3\pi Ae(r)^5 = \frac{q}{r^2}. \quad (\text{B.4})$$

Notice again, as before, the righthand side of Equation B.3 is  $-4\pi r^2 \rho(r)$ . Also notice, if we neglect  $a$  and  $A$  as they are small, we recover Maxwell. Using Equation B.4 we may plot  $e(r)$ . We do this for Maxwell, first order, and second order graphs.

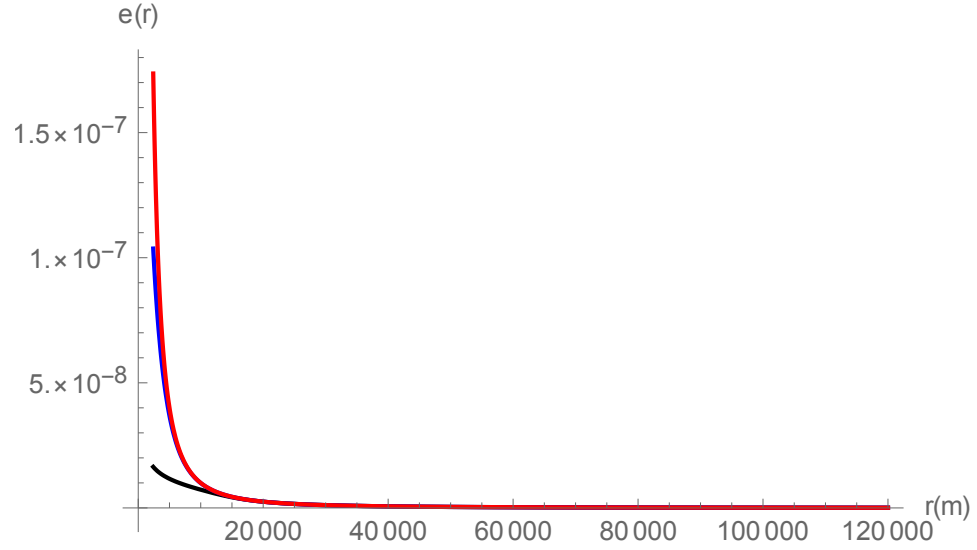


Figure B.1: Plot of  $e(r)$  vs.  $r$  for  $a = A = 0$  in red,  $A = 0$  in blue, and  $a, A \neq 0$  in black, for  $Q = 1\text{m}$ .

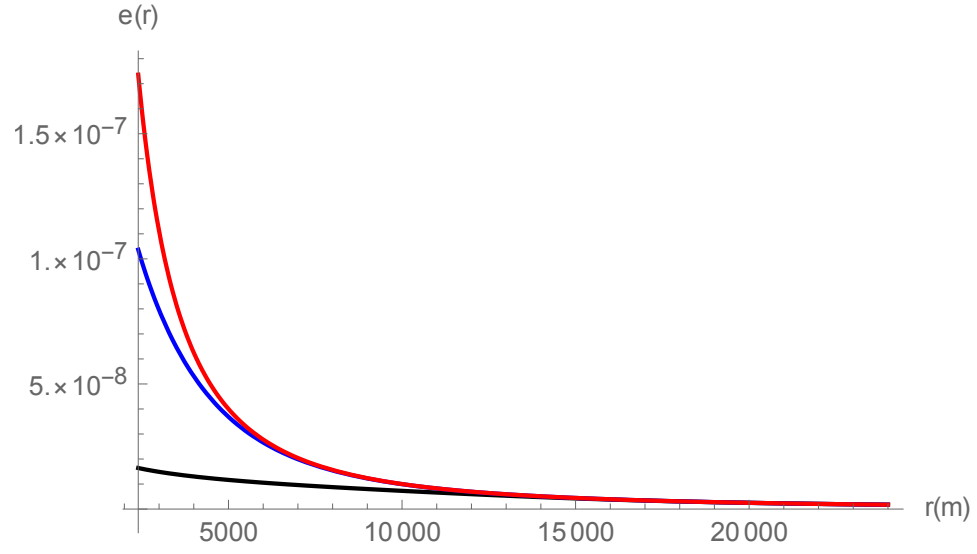


Figure B.2: Plot of  $e(r)$  vs.  $r$  for  $a = A = 0$  in red,  $A = 0$  in blue, and  $a, A \neq 0$  in black, for  $Q = 1m$ .

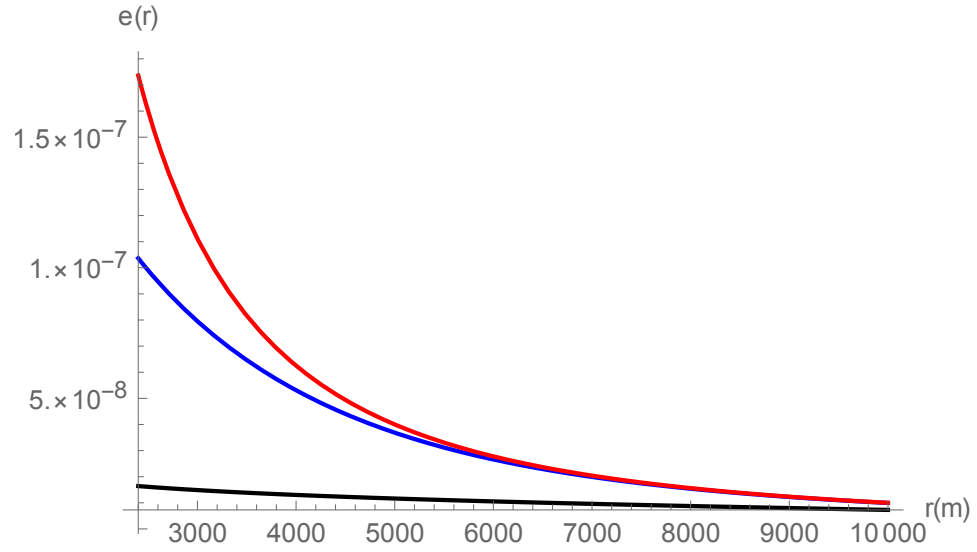


Figure B.3: Plot of  $e(r)$  vs.  $r$  for  $a = A = 0$  in red,  $A = 0$  in blue, and  $a, A \neq 0$  in black, for  $Q = 1m$ .

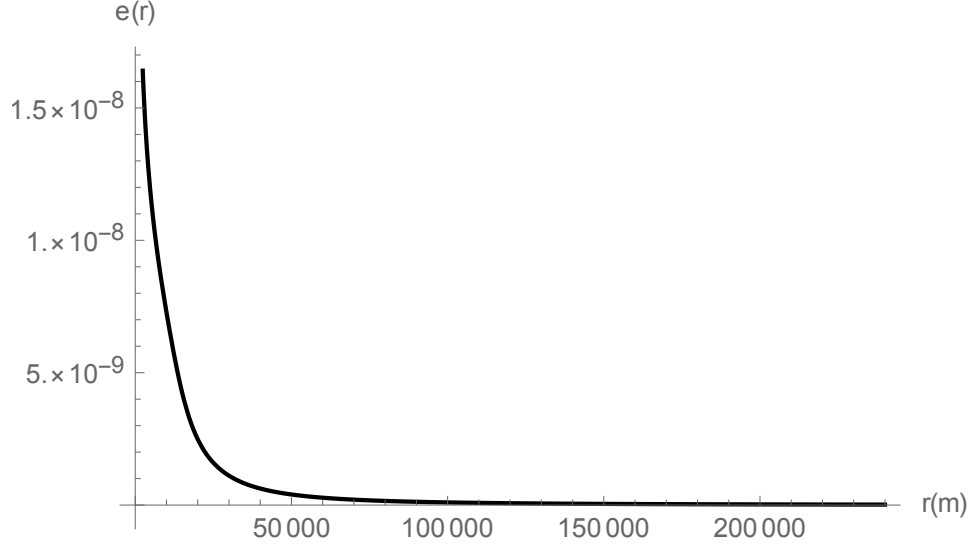


Figure B.4: Plot of  $e(r)$  vs.  $r$  for  $a, A \neq 0$  in black only. For  $Q = 1\text{m}$ .

Notice, that while the electric field still goes to infinity as  $r \rightarrow 0$ , it diverges slower and slower for higher quantum corrections. Notice, also, we have only shown the graphs of  $e(r)$  from  $r_*$  and higher,  $r_*$  is found from  $\mathcal{L}_{EM} > \mathcal{L}_a$ . In this case,  $r_* = 2.3675 \times 10^3 \text{ m}$  for  $Q = 1\text{m}$ .

$f(r)$  can only be evaluated numerically. This is fine for our analysis. The plots of  $r_+$  in the following graphs are found using  $f(r) = 0$  and Equations B.2, B.3 and B.4. To begin, we set  $A = 0$ .



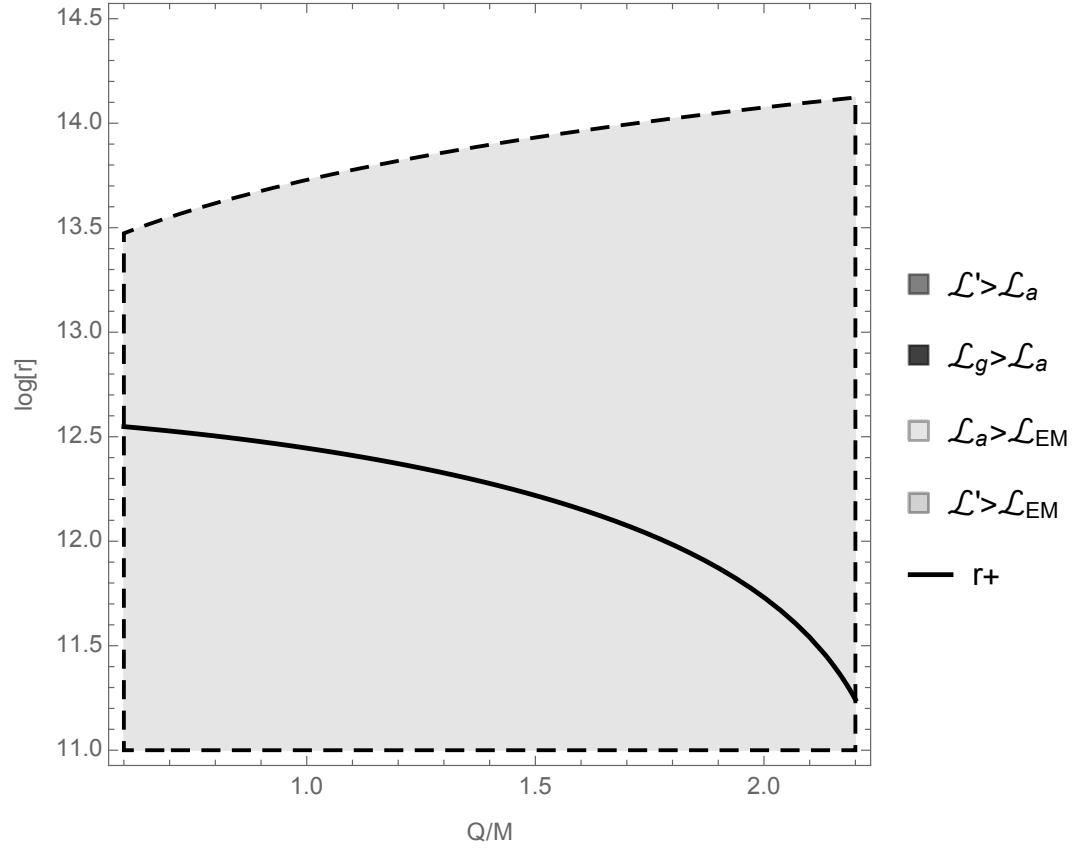


Figure B.5: Plot of invalid regions as a  $\log(r)$  vs.  $\sigma$  plot for a  $M = 10^2 M_\odot$  black hole. Roots of  $f(r)$  solved numerically using QED. The regions  $\mathcal{L}' > \mathcal{L}_{EM}$ ,  $\mathcal{L}_g > \mathcal{L}_a$  and  $\mathcal{L}' > \mathcal{L}_a$  are outside of this plot window.

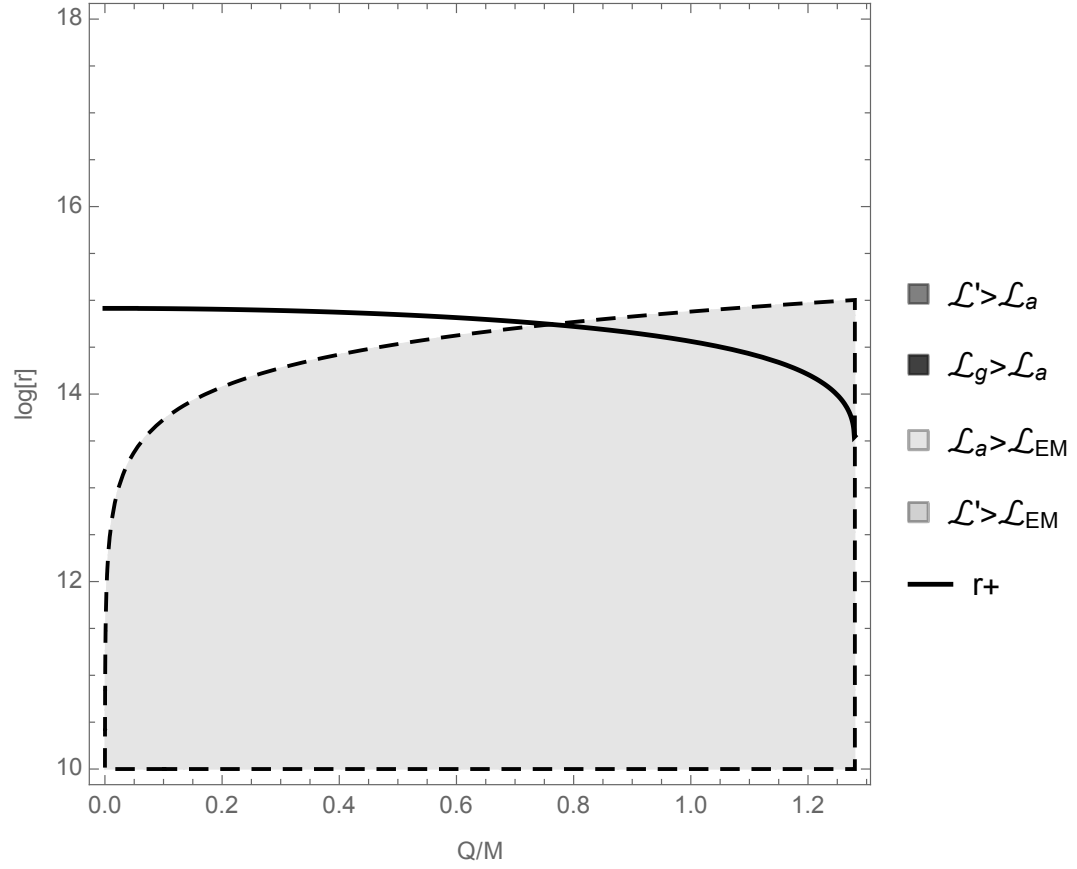


Figure B.6: Plot of invalid regions as a  $\log(r)$  vs.  $\sigma$  plot for a  $M = 10^3 M_\odot$  black hole. Roots of  $f(r)$  solved numerically using QED. The regions  $\mathcal{L}' > \mathcal{L}_{EM}$ ,  $\mathcal{L}_g > \mathcal{L}_a$  and  $\mathcal{L}' > \mathcal{L}_a$  are outside of this plot window.

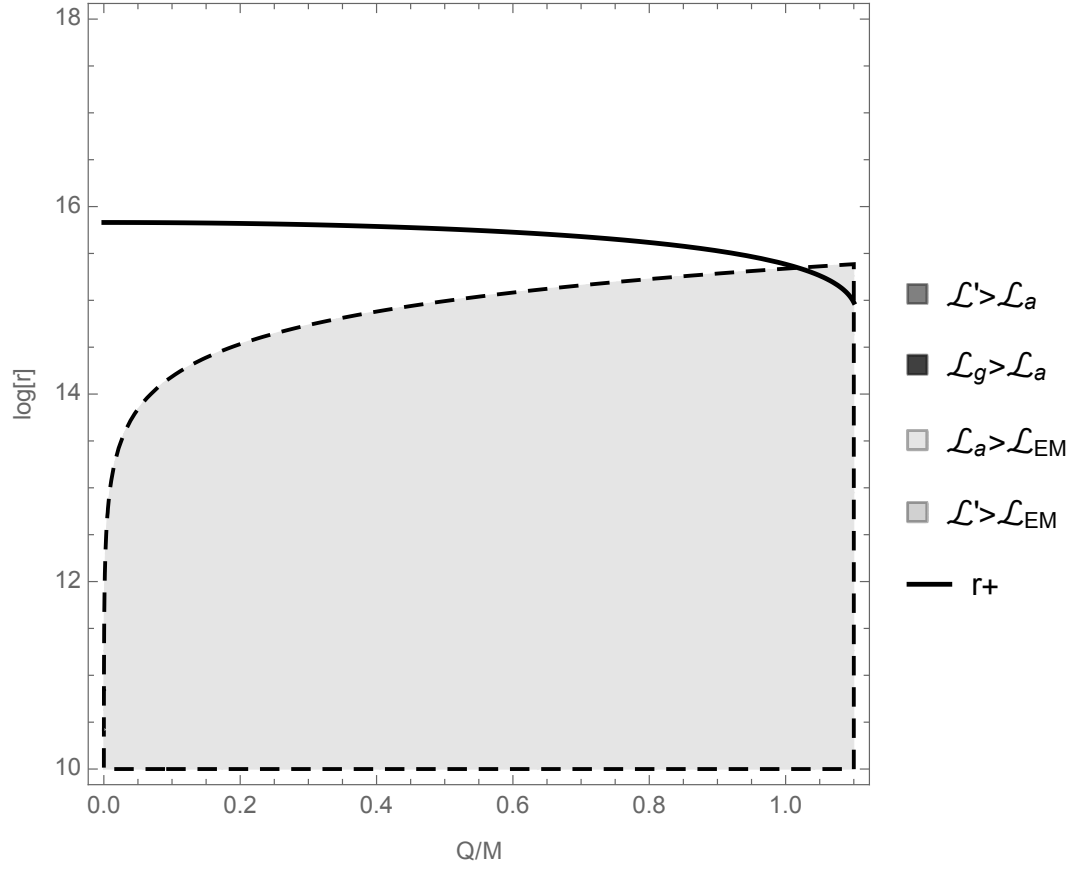


Figure B.7: Plot of invalid regions as a  $\log(r)$  vs.  $\sigma$  plot for a  $M = 2.5 \times 10^3 M_\odot$  black hole. Roots of  $f(r)$  solved numerically using QED. The regions  $\mathcal{L}' > \mathcal{L}_{EM}$ ,  $\mathcal{L}_g > \mathcal{L}_a$  and  $\mathcal{L}' > \mathcal{L}_a$  are outside of this plot window.

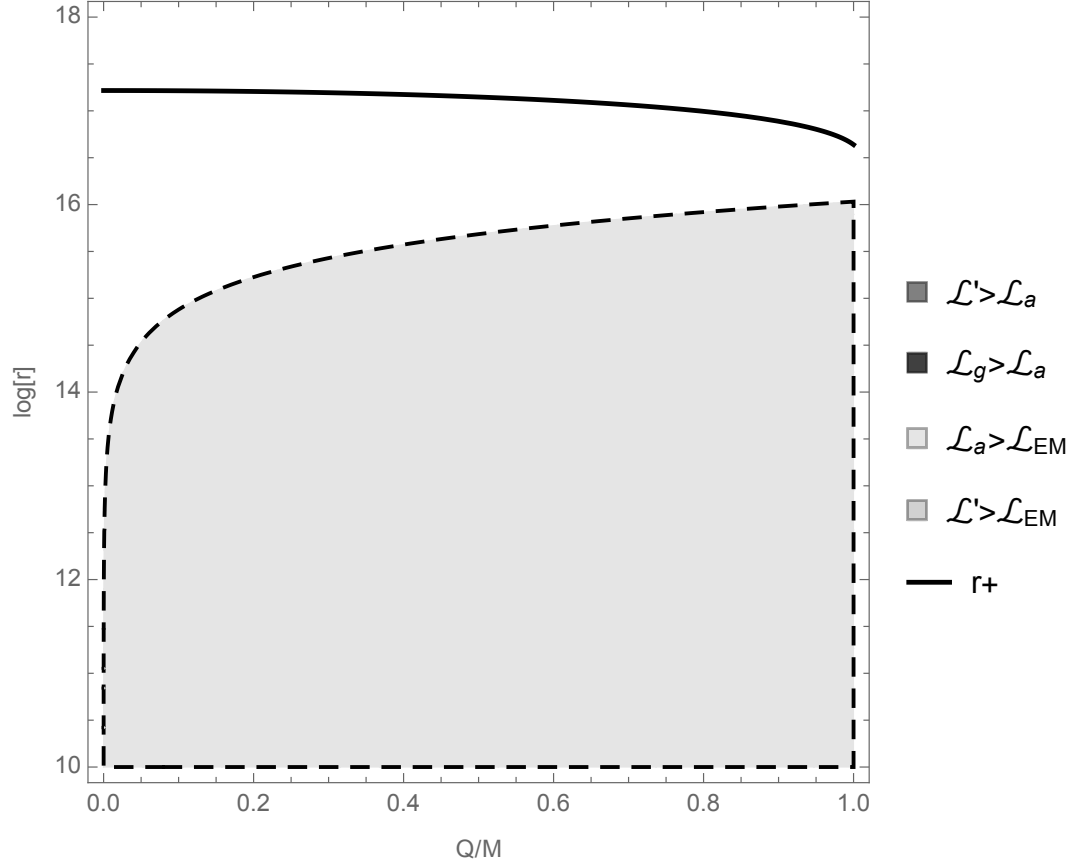
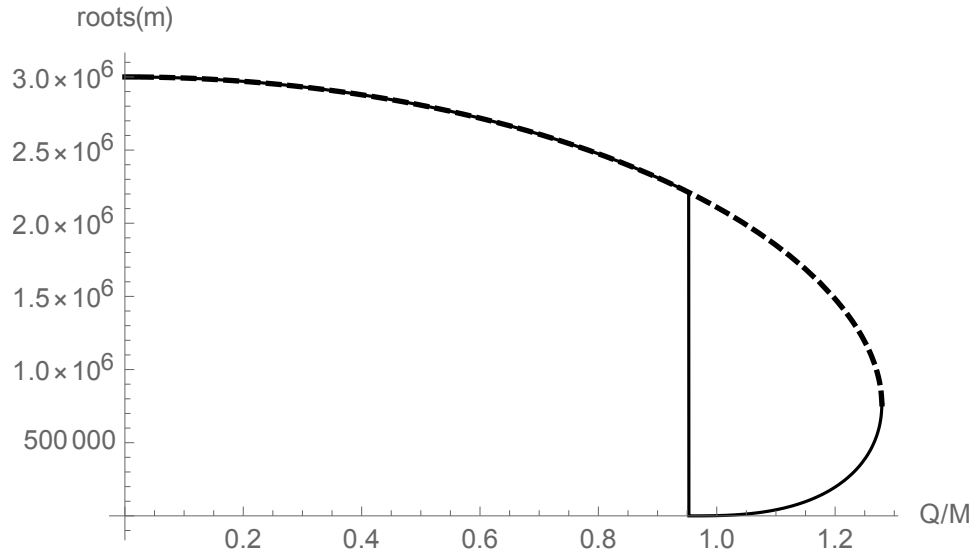
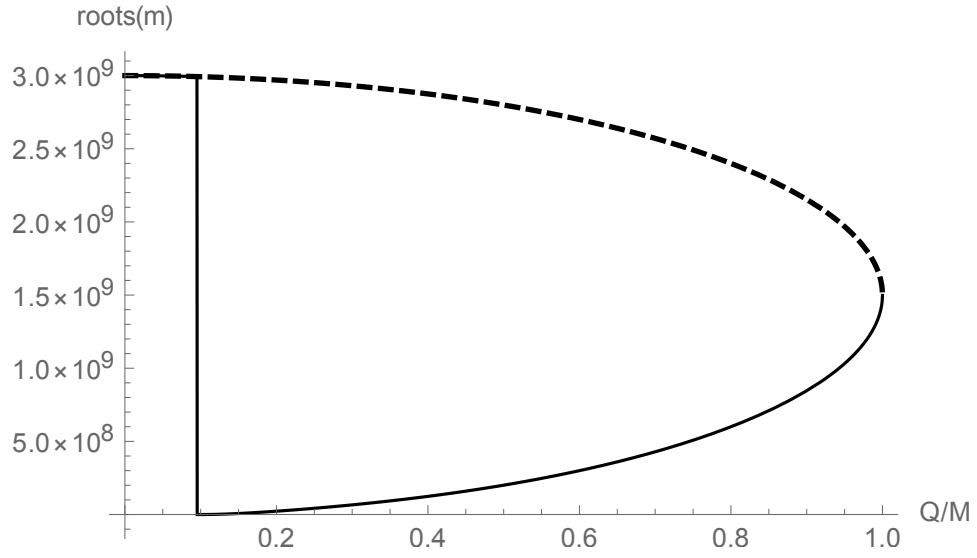


Figure B.8: Plot of invalid regions as a  $\log(r)$  vs.  $\sigma$  plot for a  $M = 10^4 M_\odot$  black hole. Roots of  $f(r)$  solved numerically using QED. The regions  $\mathcal{L}' > \mathcal{L}_{EM}$ ,  $\mathcal{L}_g > \mathcal{L}_a$  and  $\mathcal{L}' > \mathcal{L}_a$  are outside of this plot window.

Notice that while solutions for  $Q/M > 1$  exist, they are never in the valid range. In Figure B.8 we stop at  $\sigma = 1$  because the root becomes complex after that. Additionally, the extra root i.e. Cauchy horizon reappears as seen in the following plots. Notice however, that the extra horizon reappears only in the region where the calculation cannot be trusted. Below are the roots of  $f(r)$  for various masses.

Figure B.9: Roots of  $f(r)$  for a  $M = 10^3 M_\odot$  black hole.Figure B.10: Roots of  $f(r)$  for a  $M = 10^6 M_\odot$  black hole.

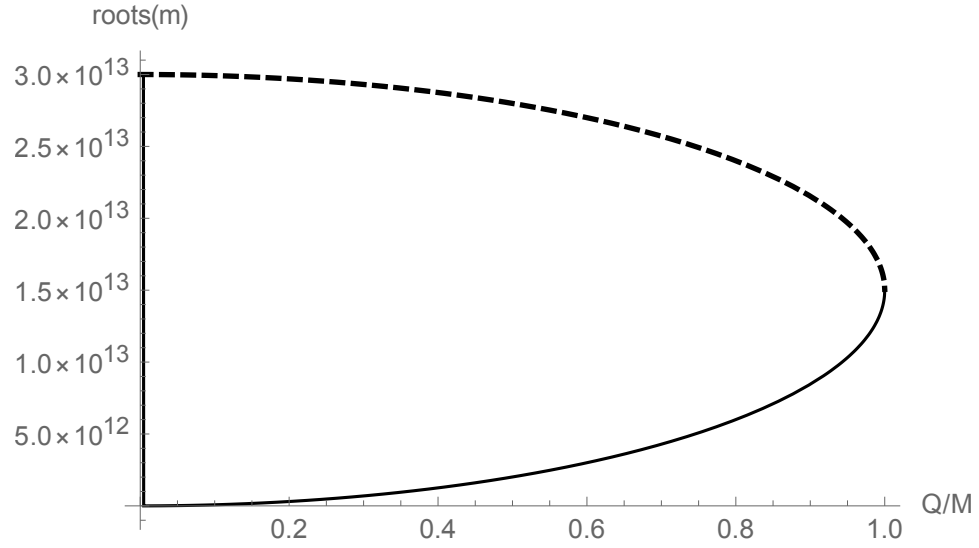


Figure B.11: Roots of  $f(r)$  for a  $M = 10^{10} M_{\odot}$  black hole.

So, to summarize, we were not able to find a valid solution for the event horizon of a black hole with  $Q/M > 1$ . The classical result, we may recall, is also not valid. So as it stands, no known (valid) solution exists zero, imaginary, or otherwise. This led us to reinterpret the mass as we did in Section 4.3.

# Bibliography

- [1] K. Eppley and E. Hannah, “The Necessity of Quantizing the Gravitational Field,” *Foundations of Physics.* **7** 51 (1977).
- [2] D. N. Page and C. D. Geilker, “Indirect Evidence for Quantum Gravity,” *Phys. Rev. Lett.* **47** 979 (1981).
- [3] R. C. Tolman, P. Ehrenfest, and B. Podolsky, “On the Gravitational Field Produced by Light,” *Phys. Rev.* **37** 602 (1931).
- [4] V. Faraoni and R. M. Dumse, “The Gravitational Interaction of Light: From Weak to Strong Fields,” *General Relativity and Gravitation* **31** 1 (1999).
- [5] N. Inan, “Formulations of General Relativity and their Applications to Quantum Mechanical Systems (with an emphasis on gravitational waves interacting with superconductors),” PhD Dissertation (2018).
- [6] S.A. Fulling and P.C.W. Davies, “Radiation from a Moving Mirror in Two Dimensional Space-Time: Conformal Anomaly,” *Proc. R. Soc. Lond. A.* **348** 1654 (1976).
- [7] R. Chiao, “Figure-8 SC antenna as a transducer that converts GR into EM radiation, coupled to a DC SQUID amplifier as a detector,” Internal memo, (2019).
- [8] R. Chiao, J. Sharping “Generation and Amplification of Gravitational Waves for Military Communication,” DARPA Grant Proposal (2014).

- [9] J. Sharping, R. Chiao, “Generation and Frequency Conversion of Quantum States in High ”Q” SRF Parametric Oscillators,” DSO Grant Proposal (2015).
- [10] G. Agarwal, “Quantum Optics,” Cambridge University Press (2013).
- [11] C. M. Wilson, G. Johansson, A. Pourkabirian, M. Simoen, J.R. Johansson, T. Duty, F. Nori, and P. Delsing, “Observation of the Dynamical Casimir Effect in a Superconducting Circuit,” *Nature*. **479** 7373 (2011).
- [12] M. Ruser, “Numerical Investigation of Photon Creation in a Three-Dimensional Resonantly Vibrating Cavity: Transverse Electric Modes,” *Phys. Rev. A* **73** (2006).
- [13] V.V. Dodonov, A.V. Dodonov, “Theory of the Dynamical Casimir Effect in Non Ideal Cavities with Time-Dependent Parameters,” *J. Phys.* **99** (2008).
- [14] M. Crocce, D. Dalvit, F. Mazzitelli, “Quantum Electromagnetic Field in a Three-Dimensional Oscillating Cavity,” *Phys. Rev. A* **66** (2002).
- [15] M. Crocce, D. Dalvit, F. Lombardo, F. Mazzitelli, “Hertz Potentials Approach to the Dynamical Casimir Effect in Cylindrical Cavities of Arbitrary Section,” *J. Opt. B* **7** (2005).
- [16] S. Butera and I. Carusotto, “Mechanical Backreaction Effect of the Dynamical Casimir Emission,” *Phys. Rev A* **99** 053815 (2019).
- [17] V. Macri, A. Ridolfo, O. Di Stefano, A. Frisk Kockum, F. Nori, and S Savasta, “Non-perturbative Dynamical Casimir Effect in Optomechanical Systems: Vacuum Casimir-Rabi Splittings,” *Phys. Rev. X* **8** 011031 (2017).
- [18] L. D. Landau and E. M. Lifshitz, “Quantum Mechanics,” Pergamon Press (1981).
- [19] C.V. Raman, “A New Radiation,” *Indian J. Phys.* **2** (1928).
- [20] C. E. Reece, P. J. Reiner, and A. C. Melissinos, “Parametric Converters for Detection of Small Harmonic Displacements,” *Nuclear Instruments & Methods in*



- Physics Research Section A-Accelerators, Spectrometers, Detectors, and Associated Equipment **245** (1986).
- [21] C. E. Reece, “A Superconducting Microwave Cavity Parametric Converter Transducer Sensitive to  $10^{-19}$  m Harmonic Motion,” PhD Dissertation (1983).
- [22] R. Chiao, R. Haun, N. Inan, B. S. Kang, L. Martinez, S. Minter, G. Muñoz, and D. Singleton, “A Gravitational Aharonov-Bohm Effect, and Its Connection to Parametric Oscillators and Gravitational Radiation,” in “Quantum Theory: a Two-Time Success Story,” edited by D. C. Struppa and J. M. Tollaksen, Springer 213 (2014).
- [23] P. R. Saulson, “How an Interferometer Extracts and Amplifies Power from a Gravitational Wave,” *Classical and Quantum Gravity*, **14** 9 2435-2454 (1997).
- [24] B. Pang and Y. Chen, “Fundamental Relations Between Measurement, Radiation, and Decoherence in Gravitational Wave Laser Interferometer Detectors,” *Phys. Rev. D* **99** 124016 (2019).
- [25] B. Yurke, “Use of Cavities in Squeezed-State Generation,” *Phys. Rev. A* **29** (1984).
- [26] H. Yuen “Two -Photon Coherent State of the Radiation Field\*,” *Phys. Rev. A* **13** (1976).
- [27] T. Eberle, S. Steinlechner, J. Bauchrowitz, V. Handchen, H. Vahlbruch, M. Mehmet, H. Muller-Ebhardt, and R. Schnabel, “Quantum Enhancement of the Zero-Area Sagnac Interferometer Topology for Gravitational Wave Detection,” *Phys. Rev. Lett.* **104** 251102 (2010).
- [28] W. Qin, V. Macri, A. Miranowicz, S. Savasta, and F. Nori, “Experimentally Feasible Dynamical Casimir Effect in Parametrically Amplified Cavity Optomechanics,” arXiv:1902.04216 [quant-ph] (2019).
- [29] J. H. Taylor and J. M. Weisberg, “Further Experimental Tests of Relativistic Gravity Using the Binary Pulsar PSR 1913 + 16,” *Astro. J.* **345** (1989).

- [30] B. P. Abbott et al. (LIGO Scientific Collaboration and the Virgo Collaboration), “Observation of Gravitational Waves from a Binary Black Hole Merger,” *Phys. Rev. Lett.* **116** 061102 (2016).
- [31] S. Minter, K. Wegter-McNelly, and R. Chiao, “Do Mirrors for Gravitational Waves Exist?,” *Physica E* **42** 234 (2010).
- [32] Q. Quach, “Gravitational Casimir Effect,” *Phys. Rev. Lett.* **114** 081104 (2015).
- [33] N.A. Inan, J.J. Thompson, R.Y. Chiao, “Interaction of Gravitational Waves with Superconductors,” *Fortschr. Phys.* (2016).
- [34] C. Misner, K. Thorne, and J. Wheeler, “Gravitation,” W. H. Freeman and Company (1973).
- [35] É. Flanagan and S. Hughes, “The Basics of Gravitational Wave Theory,” *New J. Phys.* **7** 204 (2005).
- [36] W. Press, “On Gravitational Conductors, Waveguides, and Circuits,” *General Relativity and Gravitation*, **11** 2 (1979).
- [37] The Event Horizon Telescope Collaboration, “First M87 Event Horizon Telescope Results. I. The Shadow of the Supermassive Black Hole,” *Astro. J. Lett.* **875** 1 (2019).
- [38] S. Chandrasekhar, “The Mathematical Theory of Black Holes,” Oxford University Press, (1983).
- [39] E. Poisson and W. Israel, “Internal Structure of Black Holes,” *Phys. Rev. D* **41** 1796 (1990).
- [40] S. W. Hawking, “Black Hole Explosions,” *Nature* **248** (1974). and “Particle Creation by Black Holes,” *Commun. Math. Phys.* **43** (1975).
- [41] K. Gödel, “An Example of a New Type of Cosmological Solutions of Einstein’s Field Equations of Gravitation,” *Rev. of Mod. Phys* **21** 447 (1949).

- [42] R. Penrose, “Gravitational Collapse: the Role of General Relativity,” *Riv. Nuovo Cimento* **1** **252** (1969). in “General Relativity, an Einstein Centenary Survey,” edited by S. W. Hawking and W. Israel, Cambridge University Press (1979).
- [43] S. W. Hawking and R. Penrose, “The Singularities of Gravitational Collapse and Cosmology,” *Proc. R. Soc. Lond. A* **314**, 529 (1970).
- [44] S. W. Hawking, “The Chronology Protection Conjecture,” in “Proceedings of the 6th Marcel Grossmann Meeting, Kyoto, Japan, June 23-29, 1991,” edited by H. Sato, World Scientific (1992).
- [45] S. W. Hawking, “Chronology Protection Conjecture,” *Phys. Rev. D* **46** 603 (1992).
- [46] S. Hawking, “Particle Creation by Black Holes,” *Commun. Math. Phys.* **43** 199-220 (1975).
- [47] S. Giddings, “Comments on Information Loss and Remnants,” *Phys. Rev. D* **49** 4078 (1994).
- [48] S. Mathur, “What the information Paradox is Not,” arXiv:1108.0302 [hep-th] (2011).
- [49] J. Bardeen, presented at GR5, Tiflis, U.S.S.R., and published in the conference proceedings in the U.S.S.R. (1968).
- [50] J. J. Thompson, “Black Holes in Nonlinear Electrodynamics,” MS Thesis (2014).
- [51] R.J. Adler, P. Chen, D.I. Santiago, “The Generalized Uncertainty Principle and Black Hole Remnants,” *Gen. Relativ. Gravit.* **33** 12 (2001).
- [52] A. Ashtekar, J. Olmedo, and P. Singh, “Quantum Transfiguration of Kruskal Black Holes,” *Phys. Rev. Lett.* **121** 241301 (2018).
- [53] A. Ashtekar, J. Olmedo, and P. Singh, “Quantum Extension of the Kruskal Spacetime,” *Phys. Rev. D* **98** 126003 (2018).

- [54] H. Reissner, “Über die Eigengravitation des elektrischen Feldes nach der Einsteinschen Theorie,” *Annalen der Physik* (in German) **50** 106-120 (1916).
- [55] G. Nordström, “On the Energy of the Gravitational Field in Einstein’s Theory,” *Verhandl. Koninkl. Ned. Akad. Wetenschap., Afdel. Natuurk., Amsterdam* **26** 1201-1208 (1918).
- [56] A. Einstein, L. Infeld, B. Hoffmann, “The Gravitational Equations and the Problem of Motion,” *Annals of Mathematics* **39** 1 (1938).
- [57] B. Carter, “Global Structure of the Kerr Family of Gravitational Fields,” *Phys. Rev.* **174** 5 1559-1571 (1968).
- [58] J.J. Thompson and G. Muñoz, “Charged Black Hole Horizons and QED Effects,” *Phys. Rec. D* **96** 064001 (2017).
- [59] J. Diaz-Alonso and D. Rubiera-Garcia, “Electrostatic Spherically Symmetric Configurations in Gravitating Nonlinear Electrodynamics,” *Phys. Rev. D.* **81** 064021 (2010).
- [60] G. Boillat, “Nonlinear Electrodynamics: Lagrangians and Equations of Motion,” *J. Math. Phys.* **11** (1970).
- [61] J. Plebanski, “Lectures on Nonlinear Electrodynamics,” *NORDITA*, (1968).
- [62] G. Muñoz, “Effective Lagrangians and Nonlinear Electromagnetism,” *Am. J. Phys.* **64** 1285 (1996).
- [63] Euler and B. Kockel, “The Scattering of Light by Light in the Dirac Theory,” *Naturwiss.* **23** 246 (1935).
- [64] W. Heisenberg and H. Euler, “Folgerungen aus der Diracschen Theorie des Positrons,” *Z. Physik* **98**, 714 (1936).
- [65] V. Weisskopf, “Über Die Elektrodynamik des Vakuums aus Grund der Quantentheorie des Elektrons,” *Det. Kgl. Danske Videnskab. Selskab. Mat.-Fys. Medd.* **14**, 1 (1936).

- [66] J. Schwinger, “On Gauge Invariance and Vacuum Polarization,” *Phys. Rev.* **82**, 664 (1951).
- [67] G. V. Dunne, “Heisenberg-Euler Effective Lagrangians: Basics and Extensions,” in “Ian Kogan Memorial Collection, From Fields to Strings: Circumnavigating Theoretical Physics,” Edited by M. Shifman, A. Vainshtein and J. Wheeler **1** 445 World Scientific (2005).
- [68] R. M. Wald, “General Relativity,” The University of Chicago Press (1984).
- [69] R. Ruffini, Y-B Wu, and S-S. Xue, “Einstein-Euler-Heisenberg Theory and Charged Black Holes,” *Phys. Rev. D* **88** 085004 (2013). Our result for  $r_+$  was anticipated by these authors. As our weak-field analysis shows, however, their  $r_{H-}$  in Eq. (61) is incorrect for realistic black holes. For similar reasons, their conclusion that the horizon radius  $r_H = GM$  is unchanged from the classical case fails to hold: it is not difficult to verify that  $r = GM$  is not a *double* root of  $f(r) = 0$ .
- [70] E. Poisson and W. Israel, “Internal Structure of Black Holes,” *Phys. Rev. D* **41** 1796 (1990).
- [71] S. Carroll, “Spacetime and Geometry: An Introduction to General Relativity,” Pearson Addison Wesley (2004).
- [72] W. Hiscock and L. Weems, “Evolution of Charged Evaporating Black Holes,” *Phys. Rev. D* **41** 1142 (1990).
- [73] M. Casals, A. Fabbri, C. Martinez, and J. Zanelli, “Quantum Backreaction on Three-Dimensional Black Holes and Naked Singularities,” *Phys. Rev. Lett.* **118**, 131102 (2017).
- [74] D. Christodoulou, “Reversible and Irreversible Transformations in Black-Hole Physics,” *Phys. Rev. Lett.* **25** 1596 (1970).
- [75] D. Christodoulou and R. Ruffini, “Reversible Transformations of a Charged Black Hole,” *Phys. Rev. D.* **4** 3552 (1971).

- [76] E. Newman, E. Couch, K. Chinnapared, A. Exton, A. Prakash, R. Torrence, “Metric of a Rotating, Charged Mass,” *J. Math. Phys.* **6** 6 (1965).
- [77] E. Poisson, “A Relativist’s Toolkit, The Mathematics of Black-Hole Mechanics,” Cambridge University Press (2004).
- [78] V.P. Gusynin and I. A. Shovkovy, “Derivative Expansion of the Effective Action for QED in 2+1 and 3+1 dimensions,” *Can. J. Phys.* **74** 282 (1996); *J. Math. Phys.* **40** 5406 (1999).
- [79] R. Ruffini and S. Xue, “Effective Lagrangian of Quantum Electrodynamics,” *J. Korean Phys. Soc.* **49** (2006).
- [80] F. Bastianellia, J. Davilac, and C. Schubert, “Gravitational Corrections to the Euler-Heisenberg Lagrangian,” *JHEP* **03** 086 (2009).
- [81] J. Cresswell, S. vonHausegger, A.D. Jackson, L. Hao, and P. Naselsky, “On the Time Lags of the LIGO Signals,” arXiv:1706.04191v1 [astro-ph.IM] (2017).
- [82] B. Pang and Y. Chen, “Quantum Interactions Between a Laser Interferometer and Gravitational Waves,” *Phys. Rev. D* **98** 124006 (2018).
- [83] S. Bose and L. P. Grishchuk, “Observational determination of squeezing in relic gravitational waves and primordial density perturbations,” *Phys. Rev. D.* **66** 043529 (2002).